EROSION RATES IN SUBTROPICAL, RAPIDLY DEVELOPING COUNTRIES: AN ISOTOPIC APPROACH TO MEASURING BACKGROUND RATES OF EROSION IN BRAZIL AND CHINA

A Dissertation Presented

by

Veronica Sosa-Gonzalez

to

The Faculty of the Graduate College

of

The University of Vermont

In Partial Fulfillment of the Requirements
for the Degree of Doctor of Philosophy
Specializing in Natural Resources

May 2016

Defense Date: March 30, 2016
Dissertation Examination Committee:

Paul R. Bierman, Ph.D., Advisor
Andrea Lini, Ph.D., Chairperson
Walter M. Poleman, Ph.D.
Joshua C. Farley, Ph.D.
Cynthia J. Forehand, Dean of the Graduate College

Abstract

Erosion, a surface process, can be quantified over long-term (assumed to be the natural erosion rate of the landscape) and contemporary (modern) timeframes. My research used the rare cosmogenic isotope ^{10}Be in sand and cobbles collected from rivers in southeastern Brazil (Santa Catarina and Rio de Janeiro states) and southwestern China (Yunnan province) to quantify long-term, background rates of erosion and sediment supply. These measurements will also increase number of such measurements in tropical and subtropical climates. I assessed the relationship between landscape parameters (topographic and climatic) and background erosion rates in order to understand factors related to erosion.

My data from so far unsampled states in Brazil shows that background erosion rates range between 13 and 90 m/Myr. I found that mean basin slope (R^2=0.73) and mean annual precipitation (R^2=0.57) are strongly correlated to erosion rates. Steep, escarpment-draining basins in Brazil erode faster than lower gradient basins draining the highlands. Comparing the isotopic concentration of river sand and cobbles, my data show that these grain sizes are sourced from different parts of the landscape. I compiled all published Brazilian cosmogenic ^{10}Be data, and compared them to erosion rates from similar tectonic settings. While the erosion rates in Brazil are relatively low, they are similar to those in southeastern North America, but faster than rates measured on escarpments in southern Africa.

In China, I tested the human effects on denudation by comparing long-term erosion rates derived from in-situ ^{10}Be concentration and the modern sediment yield of 22 watersheds in Yunnan. Background erosion rates range between 17 and 386 m/Myr; long term sediment yields based on these erosion rates range from 79 to 893 tons km^{-2} yr^{-1}. Modern sediment yields range from 90 to 2,879 tons km^{-2} yr^{-1} (data from Schmidt et al., 2011). In most watersheds, the modern sediment yield is 2-3X higher than long-term rates, likely the effect of a long history of land use in Yunnan. I found a statistically significant, positive relationship between erosion rates and both area (R^2 = 0.60) and mean basin slope (R^2 = 0.42). There is a negative but strong relationship between erosion rates and precipitation in my dataset (R^2 = 0.60). I sampled some places where ^{10}Be samples had been collected before to test the methodological assumption of time-invariant ^{10}Be concentration. Concentrations generally agree on samples taken 6 months apart and in samples from the active channel and from floodplains, but not in samples collected a decade and centuries apart.

Citations

Material from this dissertation has been accepted for publication in Geomorphology on March, 1, 2016 in the following form:

Sosa Gonzalez, V., Bierman, P.R., Fernandes, N.F., Rood, D.H., 2016. Long-term, background denudation rates of southern and southeastern Brazilian watersheds estimated with cosmogenic ^{10}Be. Geomorphology

Dedication

My work, as well as all my achievements, would have not been possible without the unconditional help and love from my family and closest friends.

Carmen (mami) y Junior (papi), ¡esta meta alcanzada es tambien de ustedes y para ustedes!

To my life partner, Paul L. Michael, who got here just in time to help me make it through this journey.

Acknowledgements

I am eternally grateful to Dr. Paul Bierman for his advice and guidance in science, research and life, for the past 6 years. Special thanks go to Dr. Andrea Lini, Dr. Walter Poleman and Dr. Joshua Farley for their help with my research and dissertation.
I want to thank Dr. Amanda H. Schmidt for all of her help with my dissertation, they were a key piece of the puzzle. Thanks to Dr. Dylan H. Rood for his help with the Accelerator Mass Spectrometry Laboratory at SUERC (Scottish Universities Environmental Research Centre) for ^{10}Be measurements.

Big thanks to my family and dearest friends for their support during these 4 years, and for their faith in me. A special thanks go to my sister Noelia and her family for their support. Noa, thanks for keeping your auntie entertained and laughing the stress away.

My research was possible thanks to funding from the US National Science Foundation awarded to Dr. Amanda H. Schmidt (NSF-EAR-1114166), Dr. Paul Bierman (NSF-EAR-1114159), and Dr. Dylan H. Rood (NSF-EAR-1114436).

Table Contents

Abstract i

Citations ii

Dedication iii

Acknowledgements iv

List of Figures vii

List of Tables viii

Chapter 1 - Introduction 1

Objectives: 2

Brazil: 3

China: 3

Dissertation structure: 5

Literature survey 5

Cosmogenic ^{10}Be 5

Erosion Index 7

Sediment yield data 8

Payment for Ecosystem Services 8

Chapter 2 - Long-term, background denudation rates of southern and southeastern Brazilian watersheds estimated with cosmogenic ^{10}Be 10

Abstract 10

Introduction 11

Geologic, tectonic, and climatic setting of Rio de Janeiro and Santa Catarina states 13

Previous work measuring denudation rates in Brazil 15

Methods 16

Results 21

Discussion 26

Conclusions 34

Acknowledgements 35

References 36

Chapter 3 – Spatial and temporal variation of erosion in Yunnan, China measured using ^{10}Be and contemporary sediment yields 41

Abstract 41

Introduction 42

Study Area 45

Methods 49
Results 53
Discussion 62
Temporal replicates 62
Comparison between long-term and modern sediment yields 64
Relationship of erosion rates to topography and climate variables 67
Conclusions 68
Acknowledgements 69
References 70
Chapter 4 – Conclusion 77
References 81
Appendix 1 – Brazil Supplementary Material 93
Appendix 2 – China Supplementary Material 105
Appendix 3 – Brazil Sample catalog 125
Appendix 4 – China Sample catalog 133

List of Figures

Figure 2.1 Topographic and geographic features of Southern and Southeastern Brazil ...13
Figure 2.2 Sampling sites ...17
Figure 2.3 Erosion calculated using different parameters ...19
Figure 2.4 Regression plot of the relationship between erosion and slope ...24
Figure 2.5 Regression plot of the relationship between erosion and precipitation ...24
Figure 2.6 Erosion rates sorted by basin area ...25
Figure 2.7 Histogram of all cosmogenic ^{10}Be-derived erosion rates in Brazil ...26
Figure 2.8 Brazilian erosion rates by predominant basin lithology ...28
Figure 2.9 Summary of previously published cosmogenic ^{10}Be-derived erosion rates in tropical climates and passive margin sites ...31
Figure 3.1 Sampled watersheds in Yunnan, China ...47
Figure 3.2 Spatial variation of error-weighted averaged isotopic activities and erosion rates ...54
Figure 3.3 Relationship between erosion rate and topography variables ...56
Figure 3.4 Temporal variation of $^{10}Be_i$ activity ...58
Figure 3.5 Temporal variation of $^{10}Be_m$ activity ...59
Figure 3.6 Spatial variation of sediment yield ratios and erosion indices ...61
Figure 3.7 Field sites ...66

List of Tables

Table 2.1 Erosion rates and topography variables for Brazilian watersheds 22
Table 2.2 Summarized published ^{10}Be-derived erosion rates for tropical climates and passive margin topography sites 29
Table 3.1 Amount of samples included per analysis 50
Table 3.2 Summarized erosion rate for each major basin.....55
Table 3.3 Summary findings on temporal comparisons of isotopic concentration.....60
Table 3.4 Summarized data on previously published ^{10}Be temporal replicates 62

Chapter 1 - Introduction

Erosion is a natural processes, but its rate has been increased dramatically by humans (Enters, 1998; Hooke, 1994; Hooke, 2000; Reusser et al., 2015). Natural resources and many aspects of our livelihoods can be impacted by erosion including, water quantity and quality (Bilotta and Brazier, 2008), reservoir lifespan (Harden, 2006, Owens et al., 2005), aquatic ecology (Owens et al., 2005), and agriculture (Pimentel et al., 1995; Pimentel, 2006). The magnitude of these effects can be reduced with efficient environmental management. To craft such effective management techniques, knowledge of background erosion rates and dominant landform processes is necessary.

Several terms are associated with the removal of material from hillslopes and its movement through, and out of a watershed. Ritter and others (1995) defined sediment generation as the amount of sediment reaching or given access to a channel and sediment yield as the sediment that exits the basin. Their work also defined erosion rate as the pace at which material is removed from the basin. Although denudation and erosion are often used interchangeably, denudation accounts for the sum of the overall erosive process over long term (Summerfield and Hulton, 1994). Erosion accounts for the mechanical erosive processes that remove solid material, while denudation also accounts for chemical weathering resulting in a dissolved load.

Erosion rates are influenced by natural factors such as geology, slope, and climate but can increase dramatically due to human activities (Ouyang et al., 2010). Averaged long-term (up to 10^4-10^5 years), background erosion rates estimated with cosmogenic ^{10}Be are assumed to be affected only by natural factors (Brown et al., 1995; Bierman and Nichols,

2004; von Blanckenburg, 2005). These erosion rates serve as a benchmark for land management (Vanacker et al., 2007). Contemporary erosion rates can be quantified using several methods, including river gauges (e.g. Clapp et al., 2000; Hewawasam et al., 2003; Reusser et al., 2015) and sedimentation rate of reservoirs (e.g. Vanacker et al., 2007). Comparison of erosion rates over both timeframes, allows for the quantification of the human effects on the environment and surfaces processes.

Objectives:

My field areas are located in tropical and subtropical regions of Brazil and China. Because the objectives for each project are different, I consider the objectives for each project separated by country in this section. Quantifying background erosion rates in both Brazil and China increased the number of cosmogenic nuclide measurements in tropical and subtropical climates. As noted by Portenga and Bierman (2011), although cosmogenic nuclides have been widely used as a method for estimating background erosion rates, their use in tropical environments has been limited. Out of the 1149 samples included in their compilation, only 98 were from tropical watersheds. Studies using cosmogenic nuclides, not included in Portenga and Bierman (2011), with tropical field sites include Puerto Rico (Brocard et al., 2014a; Brocard et al., 2014b), Brazil (Salgado et al., 2006; Salgado et al., 2007; Salgado et al., 2008; Salgado et al., 2013; Cherem et al., 2012a; Cherem et al., 2012b; Barreto et al., 2013, Barreto et al., 2014; Rezende et al., 2013), and the tropical regions of Africa (Hinderer et al., 2013) and Australia (Lal et al., 2012) have been published.

Brazil:

Using *in situ* ^{10}Be concentrations of active channel sediments in Rio de Janeiro and Santa Catarina, Brazil, I constrained background erosion for 14 basins. I assessed the relationship of erosion rates to landscape scale variables. With this information, I placed erosion rates of the Atlantic Forest of Brazil in the context of other tropical places and passive margin areas, where cosmogenic ^{10}Be has been used as an erosion rate monitor. I expect these data to be used to inform the establishment of a payment for ecosystem services (PES) program in Santa Catarina State. This is a novel application of cosmogenic geomorphology to the environmental conservation field.

In order to understand the difference in material sourcing to the river during mass movements and rainy events, I compared the isotopic concentration of river channel sediment and river cobbles in 3 sites in Rio de Janeiro. If the concentrations do not differ greatly, both river sand and cobbles are sourced from similar parts of the landscape.

China:

I measured *in situ* and meteoric ^{10}Be in 70 samples from Yunnan, China; of these samples 40 are from active river channel sediment and 30 are from overbank samples and two were supplied from previous sampling campaigns. My work also included temporal replicates to test the method assumption of time-invariant ^{10}Be concentration. The (original) concentrations I compared to had been analyzed and reported by Neilson (2015) and Schmidt and others (2011).

Using the *in situ* isotopic concentration, I estimated background erosion rates in all the basins we sampled (see Lal, 1991), and assessed the relationship between erosion and

landscape-level variables. We measured meteoric ^{10}Be for these samples, and used these isotopic concentration to calculate the erosion index for each watershed (as per Brown et al., 1988).

I calculated the erosion index and atmospheric deposition rate of meteoric ^{10}Be for each basin using both contemporary sediment yields. I used official data from the Chinese Government which integrates over decades, as the contemporary sediment yields. Water quality parameters, including sediment yield, have been measured daily for at least 5 years in the sampled watersheds, by the Ministry of Hydrology of the People's Republic of China. The sediment yields I used have been calculated from these data and published by Schmidt et al., 2011.

One of the fundamental assumptions of the method that constrains erosion rates using isotopic concentrations was evaluated in my work. ^{10}Be concentration is assumed to be time-invariant, and thus representative of average erosion rates over long periods of time. I compared the isotopic concentration of samples taken at the same site 6 months, and roughly a decade apart. Using radiocarbon ages for charcoal on alluvial terraces, and sand from the same stratum, I compared $^{10}Be_i$ centuries over centennial timescales. To understand if the monsoon dominates sediment sourcing in Yunnan rivers, I compared the isotopic concentration of material in the active channel and material deposited on floodplains. The assumption behind this test is that the active channel material is transported with base flow of the river, and material deposited overbank is deposited during the monsoon season, when the rivers rise.

Dissertation structure:

The remainder of this chapter contains a literature survey, including the most important and relevant sources of information related to my work. Chapters 2 is the manuscript that covers the findings of my research in Brazil. This paper has been accepted for publication in Geomorphology. Chapter 3 is the most recent draft of the manuscript that presents the findings of my research in China. The chapter is formatted according to the guidelines of Earth and Planetary Science Letters, the journal it will be submitted to this spring. Because of this, the erosion rates in chapter 3 are expressed in different units than the rest of the dissertation. Finally, Chapter 4 includes my conclusions and suggestions for future work.

Literature survey

Cosmogenic ^{10}Be

Cosmogenic nuclides were first suggested as a method to determine background basin-scale erosion rates in the 1990's (Brown et al., 1995; Bierman and Steig, 1996; Granger et al., 1996). *In situ* cosmogenic isotopes (I used ^{10}Be) are formed when rocks and sediment are exposed to secondary cosmic rays at and near Earth's surface (Lal and Peters, 1967); such isotopes accumulate over the exposure time. The formation rate of these isotopes decreases with depth, and is generally insignificant below a depth of 2 meters (Lal and Peters, 1967). Because of this formation process, the concentration of ^{10}Be is a good indicator of near-surface residence time, and of denudation rates which are inversely related to isotopic concentrations. The method used to derive denudation rates from cosmogenic isotope concentrations in river sediment assumes that the rate of erosion is

steady over the time period integrated, that sediment sourcing is steady, and that sampled sediment is representative of the erosion of the entire basin (see Brown et al., 1995, Bierman and Steig, 1996 and Granger et al., 1996 for the assumptions of the method). The integration time depends on erosion rate: for fast erosion rates, sediments spend little time in the upper meters of the soil (*in situ* ^{10}Be production zone), whereas in a slowly eroding watershed, sediments spend more time in the nuclide production zone.

Background erosion rates can be used to address issues raised in policy, land management, and ecological economics debates. Considering geologic (background) erosion rates when designing policy and land management regulations will make these approaches more realistic. In terms of agriculture, these erosion rates can be used to plan where the fields will be located or what will be grown. Growing crops that cause less loss of the top soil, and locating fields in areas that are less prone to erosion can save both money and time.

Meteoric ^{10}Be forms in the atmosphere as the result of the spallation (splitting) of nitrogen and oxygen atoms (Lal and Peters, 1967). Once formed in the atmosphere, the isotope adheres to aerosols and is delivered to the surface typically in rainfall, but can also be deposited as dry fall (McHargue and Damon, 1991). The concentration of meteoric ^{10}Be in precipitation is a function of latitude and movement of the isotope from the atmosphere to the troposphere (McHargue and Damon, 1991). Graly and others (2011) published a method to calculate the meteoric ^{10}Be delivery rate, accounting for mean annual precipitation and latitude. Most meteoric ^{10}Be can be found in the upper few meters of soil (Pavich et al., 1984; Pavich et al., 1985). It has been used as a sediment tracer at the

watershed level (see Reusser and Bierman, 2010) and to estimate the rate of soil transport (see Jungers et al., 2009) among other uses.

Erosion Index

Another approach to study surface material transport is to calculate the erosion index of a watershed. Brown and others (1988) defined the erosion index as the ratio of meteoric ^{10}Be leaving the basin to that deposited on it. The equation to calculate erosion index is

$$I = \frac{M\eta'}{Aq}$$

Where M is the annual sediment load, η' is the ^{10}Be concentration in the material leaving the basin, A is the basin area, and q is the atmospheric deposition rate of ^{10}Be in the watershed. I calculate the q value for each watershed, using the equation published by Graly and others (2011):

$$q = P \cdot \left(\frac{1.44}{1 + \frac{EXP(30.7 - L)}{4.36}} + 0.63 \right) \qquad \textit{Equation 2}$$

Where L is the latitude in which the watershed is located and P the mean annual precipitation rate.

If a basin is in steady state (erosion and soil formation), then the amount of ^{10}Be leaving the basin is similar to that being deposited (Brown et al., 1988). If on the other hand, the index has a value over one, it means the basin is eroding more quickly than soil is being produced, in other words, more ^{10}Be is leaving the basin, than it is being deposited by precipitation. The erosion index provides an important piece of information for evaluating land management practices, because it informs us about the balance between soil formation

and erosion. This information is key when considering restoration projects, conservation and future land uses that could tip the erosion index either way (greater or smaller than one).

Sediment yield data

The Ministry of Hydrology of the People's Republic China has been collecting data daily on water quality parameters in the International Rivers of Yunnan and Tibet region since the 1950s (Schmidt et al., 2011). Such a complete record of sediment loading is very rare, and provides a strong underpinning to erosion and water quality research in the region. Two measured parameters are total suspended sediment concentration and water discharge, which can be used to calculate sediment yield at each station. These data were collected from 1953 to 1989, but I use data from up to 1987. Data after 1987 is not publicly available, and some stations have sediment data starting in 1958 or later, so I use the years available for each station. The data were collected from the government documents, translated, and compiled in a database described by Henck et al (2010), and published at: http://www.oberlin.edu/faculty/aschmidt/chdp/index.html. Sediment yields, based on these data, have been calculated and published in Schmidt et al., (2011).

Payment for Ecosystem Services

One approach to environmental conservation adopted in recent years is to share the costs of conserving the land; those who benefit from the ecosystem services rendered by the conserved land pay a fee to the land owner. Pfaff and others (2008) define payment for

ecosystem services as an effective way to induce conservation while compensating those who incur its costs.

The need to shift conservation (and conservation policy) approaches from experience-based to knowledge-based has been discussed by several authors (e.g. Ferraro and Pattanayak, 2006; Pullin and Knight, 2001; Sutherland et al., 2004; Pfaff et al., 2008). They all agree on the need for evaluation and a more scientific (data-based) approach to conservation practices. It is here where geomorphology, through cosmogenic nuclides, can be integrated with conservation. Quantifying background erosion rates for places where a Payment for Ecosystem Services (PES) scheme will be installed, can serve as a benchmark to assess policy effects on contemporary erosion rates. These data will be useful when monitoring the ecosystem and assessing the effects of the PES on the overall health of the ecosystem.

Chapter 2 - Long-term, background denudation rates of southern and southeastern Brazilian watersheds estimated with cosmogenic ^{10}Be

Abstract

In comparison to humid temperate regions of the Northern Hemisphere, less is known about the long-term (millennial scale), background rates of erosion in Southern Hemisphere tropical watersheds. In order to better understand the rate at which watersheds in southern and southeastern Brazil erode, and the relationship of that erosion to climate and landscape characteristics, we made new measurements of *in situ* produced ^{10}Be in river sediment and we compiled all extant measurements from this part of the country.

New data from 14 watersheds in the states of Santa Catarina (n=7) and Rio de Janeiro (n=7) show that erosion rates vary there from 13 to 90 m/My (mean = 32 m/My; median=23 m/My) and that there is no significant difference between erosion rates of basins we sampled in the two states. Sampled basin area ranges between 3 and 14987 km^2, mean basin elevation between 235 and 1606 m, and mean basin slope between 11 and 29°. Basins sampled in Rio de Janeiro, including three that drain the Serra do Mar escarpment, have an average basin slope of 19°, whereas the average slope for the Santa Catarina basins is 14°. Mean basin slope (R^2=0.73) and annual precipitation (R^2=0.57) are most strongly correlated with erosion in the basins we studied. At three sites, where we sampled both river sand and cobbles, the ^{10}Be concentration in river sand was greater than in the cobbles suggesting that these grain sizes are sourced from different parts of the landscape.

Compiling all cosmogenic ^{10}Be-derived erosion rates previously published for southern and southeastern Brazil watersheds to date (n = 76) with our 14 sampled basins, we find that regional erosion rates, though low, are higher than those of watersheds also located on other passive margins including Namibia and the southeastern North America. Brazilian basins erode at a pace similar to escarpments in southeastern North America. Erosion rates in southern and southeastern Brazil are directly and positively related to mean basin slope (R^2 = 0.33), and weakly but significantly to mean annual precipitation (R^2 = 0.05). These relationships are weaker when considering all southern and southeastern Brazil samples, than they are in our smaller, localized dataset. We find that smaller, steeper headwater catchments (many on escarpments) erode faster than the larger, higher-order but lower slope catchments. Erosion in southern and southeastern Brazil appears to be controlled largely by mean basin slope with lesser influence by climate and lithology.

Introduction

Since the mid-1990s, cosmogenic nuclides, most commonly ^{10}Be, have been widely used as a method to measure long-term, background, millennial scale erosion rates (Bierman and Steig, 1996; Brown et al., 1995; Granger et al., 1996). Portenga and Bierman (2011) compiled all published ^{10}Be-derived erosion rates and recalculated the erosion rates using the CRONUS online erosion calculator (http://hess.ess.washington.edu/) to standardize the measurements and allow for comparison of erosion rates among sites worldwide. Although the method has been applied in all climate regimes, its usage in tropical, subtropical, and arctic landscapes is minimal compared to applications in dry and

temperate climates. Out of 1149 samples included in that compilation, only 98 were collected from the tropics.

Studies not included in Portenga and Bierman (2011), with data from tropical areas (such as Puerto Rico, Africa, and Australia), include several from Brazil (Brocard et al., 2014a, Brocard et al., 2014b; Salgado et al., 2006; Salgado et al., 2007; Salgado et al., 2008; Salgado et al., 2013; Cherem et al., 2012; Barreto et al., 2013, Barreto et al., 2014; Rezende et al., 2013; Hinderer et al., 2013; Lal et al., 2012; Nichols et al., 2014). Of the eight papers that have used ^{10}Be to decipher Brazilian landscapes, seven report samples collected from Minas Gerais state and one reports on samples from Paraná state. Erosion rates in these papers are calculated using a variety of different scaling and production parameters and thus are not directly comparable.

In this paper, we both provide new data (from the so-far unsampled Brazilian states of Santa Catarina and Rio de Janeiro) and we compile and reanalyze using a homogeneous approach all extant *in situ* produced ^{10}Be data for southern and southeastern Brazil. The goals of this paper are both to understand better the range and central tendency of erosion rates in southern and southeastern Brazil and to determine whether those rates are related to topographic and climatic variables such as slope and precipitation. Such data are important for land management in rapidly developing, but still agriculturally intensive, nations like Brazil (Martinelli et al., 2010). Long-term, background erosion rates, such as those we provide here, are useful as a benchmark against which to compare contemporary rates of erosion and sediment transport driven by human-induced change (Reusser et al., 2015; Brown et al., 1998; Hewawasam et al., 2003; Vanacker et al., 2007).

Geologic, tectonic, and climatic setting of Rio de Janeiro and Santa Catarina states

Rio de Janeiro and Santa Catarina states are located close to the Atlantic coast in southeastern and southern Brazil and are mostly underlain by high-grade metamorphic rocks (Domínguez, 2009). Both states have escarpment topography parallel to the coast, associated with the South American plate passive margin that separates lower coastal plains from higher interior plateaus (Ollier, 2004; Domínguez, 2009). The state of Rio de Janeiro is mostly mountainous and mainly underlain by gneisses and granites (Heilbron et al., 2008; Fernandes et al., 2010; Silva et al., 2015). The eastern part of Santa Catarina state is occupied by Atlantic lowlands and the southern Brazilian highlands (Behling, 1995) (Figure 2.1).

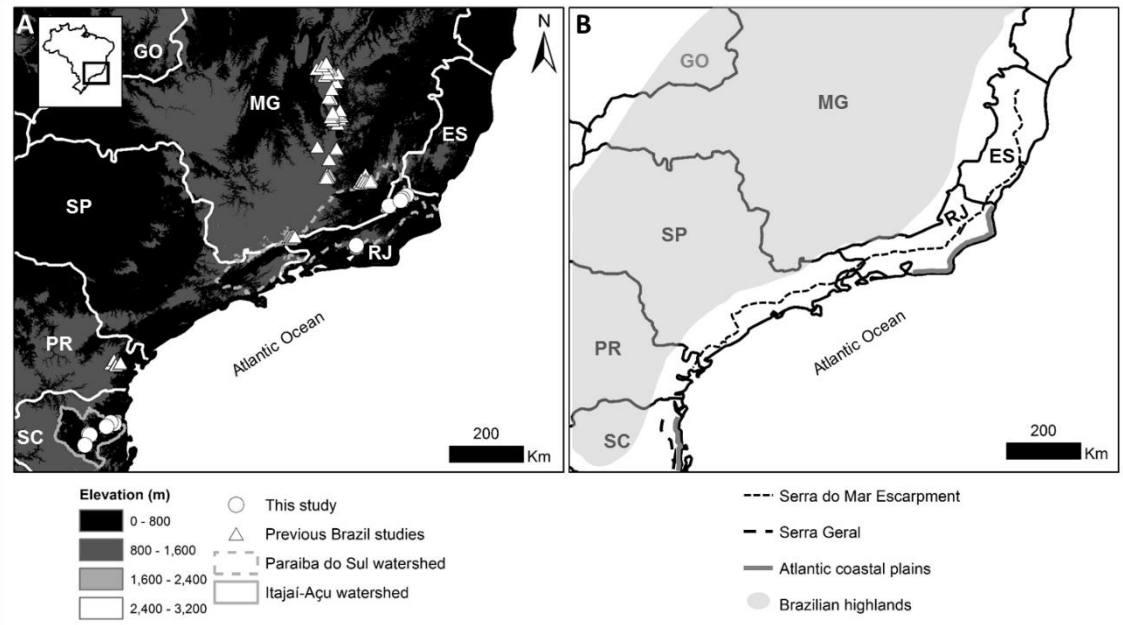

Figure 2.1: Topographic and geographic features of southern and southeastern Brazil. The states of Minas Gerais (MG), Goiás (GO), Espírito Santo (ES), Rio de Janeiro (RJ), São Paulo (SP), Paraná (PR), and Santa Catarina (SC) are shown. (A) Sample locations for this study and previously published cosmogenic studies in Brazil. The escarpment topography can be distinguished along the Atlantic coast by the change in elevation. (B) Approximate location of major geographic and political features of southern and southeastern Brazil.

The Serra do Mar escarpment is mostly composed of gneisses, granites, and migmatites (Heilbron and Machado, 2003; Silva et al., 2015) intruded by Mesozoic diabase dikes (Almeida et al., 2013; Guedes et al., 2005). Normal faults of Mesozoic-Cenozoic age raised and lowered tectonic blocks, topographically partitioning the area (Fernandes et al., 2010). One of these raised blocks, the Serra do Mar escarpment, may represent a Cretaceous South Atlantic rift border (Gallagher et al., 1995; Almeida and Carneiro, 1998) or the retreat of a dissected Cenozoic fault scarp (Asmus and Ferrari, 1978). The dissection increased during Paleogene and Neogene tectonic and thermal reactivations, causing subsidence or uplift of earlier erosional surfaces (Zalan and Oliveira, 2005; Hackspacher et al., 2004). The topography is the result of differential chemical and physical denudation of the gneisses and granites, which are intersected by subvertical faults and fractures that accelerate channel incision; as well as landslides and rock falls along the fractured walls (Fernandes et al., 2010).

Rio de Janeiro and Santa Catarina experience high average humidity and temperatures along the coast, and more stable and lower temperatures in the highlands (Williams, 1962; Nunes et al., 2009). Based on the Köppen-Geiger climate classification, Rio de Janeiro has a tropical climate, with a dry season in the winter (Aw) along the coast, and warm temperatures along with dry winters (Cw) towards the interior (Alvares et al., 2013). Temperatures reach their maximum between January and February (29°C), and minimum in June and July (21°C) (Brickus et al., 1998), with mean annual temperature around 23°C (Nunes et al., 2009). Rio de Janeiro state receives between 1200 and 2000 mm rainfall annually (Alvares et al., 2013; de Sherbinin and Hogan, 2011; Nunes et al.,

2009). Santa Catarina state has a steady warm and moist climate with precipitation in all months (Cfa), and a temperature over 22°C during its warmest month based on the Köppen-Geiger system (Alvares et al., 2013; Behling, 1995). Mean temperatures range from 14°C in the winter to 23°C in the summer (annual mean of 19°C), the relative humidity remains around 85% year round, and precipitation varies between 1250 and 1400 mm annually (Alvares et al., 2013).

Previous work measuring denudation rates in Brazil

There have been eight published studies of erosion rates in southeastern Brazil, some of which report the subsets of the same data using different nomenclature. Salgado et al. (2006) used ^{10}Be to compare chemical weathering and long-term denudation rates in Minas Gerais, Brazil (see Figure DR1 for watershed locations). They found that both chemical weathering and denudation were the highest in marbles, intermediate in schists, phyllites, granites, gneisses and migmatites, and lowest in quartzites. A later study by Salgado et al. (2008) in the same region provided more evidence consistent with differential erosion; watersheds underlain by quartzites and itabirites (banded iron formations) eroded more slowly than those underlain by other lithologies.

Barreto et al. (2013) measured denudation in watersheds draining three different escarpments in Minas Gerais, Brazil and found that they all eroded slowly, from 2 to 6 m/My (Figure DR2). In another study, Salgado et al. (2007) measured erosion rates in sub-basins underlain by schist, phyllite, granite, and gneiss (a subset of the lithologies included in their 2008 publication) and found no difference in erosion due to lithology, but rather

that slope dissection controlled the rate of denudation in Minas Gerais (Figure DR1). Rezende et al. (2013) also found differences in denudation based on lithology; their work measured background erosion rates of nine sub-basins along the drainage divide between the Grande and Paraíba do Sul Rivers in Minas Gerais (Figure DR3). They measured erosion rates between 7 and 28 m/My, with the slowest rates in watersheds underlain by granite (Rezende et al. 2013).

Two studies compared denudation rates of watersheds draining the Serra do Mar (in Paraná state) and the Serra da Mantiqueira (in Minas Gerais state close to the border with Rio de Janeiro) escarpments to watersheds draining the highlands (Salgado et al., 2013; Cherem et al, 2012) (Figure DR1, Figure DR4). Both studies found that escarpment-draining watersheds eroded at a significantly faster pace than the watersheds draining the highlands. Rezende at al. (2013), also working in Serra da Mantiqueira, compared denudation rates at the divide between the Grande (a tributary of the Paraná River) and the Paraíba do Sul river basins at the southern border of Minas Gerais state. Their work found that basins draining the escarpment erode faster than those draining the highlands. Barreto et al. (2014) examined the effects of diamond extraction on denudation rates. They found that drainages overloaded with material resulting from mining saprolite upstream had higher apparent denudation rates than unaffected streams, likely because mining introduced material from well beneath the surface into the streams.

Methods

We collected 14 active channel sediment samples in two different field seasons. Rio de Janeiro watersheds (n=7) were sampled in 2011 and Santa Catarina watersheds

(n=7) in 2012 (Figure 2.2). We also sampled river cobbles at three Rio de Janeiro sites where we sampled active channel sediments (BRA01, 02, 03).

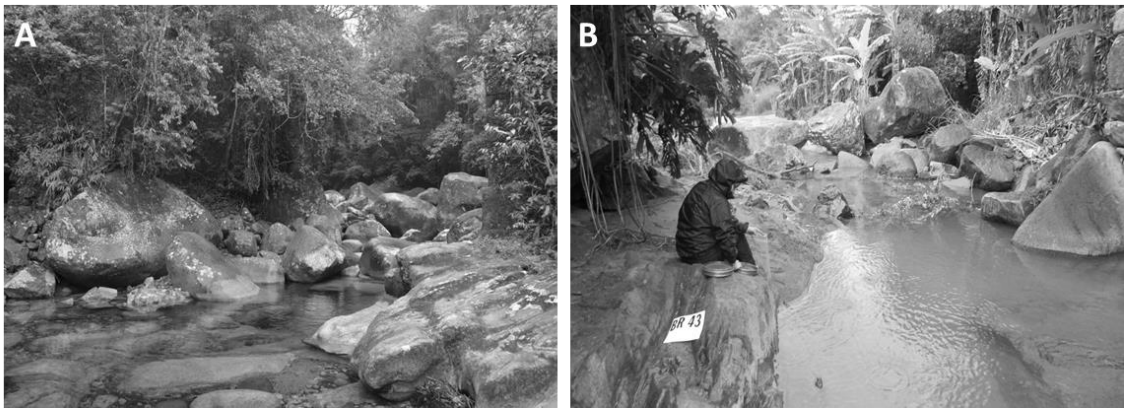

Figure 2.2: Sampling sites. Field photographs of two fluvial sediment sampling sites: (A) BRA02 in Rio de Janeiro state, draining the Serra do Mar escarpment. (B) BRA43 in Santa Catarina state. All samples were field sieved.

All watersheds we sampled in Rio de Janeiro state are sub-basins of the Paraíba do Sul basin (Figure 2.1), with the exceptions of three samples (BRA01, 02, 03) that were collected in coastal watersheds that drain the escarpment of the Serra dos Órgãos (a local name for the Serra do Mar). Four samples (BRA19, 20, 21, 22) come from watersheds where most of the catchment area is located in Minas Gerais state, which drains the Serra da Mantiqueira. Basin area ranges from 3 to 9169 km^2. The watersheds are mostly underlain by deformed and metamorphosed gneiss and granitic rocks. Mean elevation for the Rio de Janeiro basins is between 235 and 1606 m, average basin slope ranged between 12 and 29°, and mean annual precipitation is between 1215 and 1824 mm.

The Santa Catarina watersheds we sampled, all located within the Itajaí-Açu basin, drain the Serra Geral, which extends to the southern part of Santa Catarina state (Figure 2.1). Sampled watersheds have areas between 5 and 14987 km^2, with mean basin elevations

ranging from 293 to 695 m, and mean basin slopes between 11 and 17°. The watersheds receive between 1484 and 1649 mm of precipitation annually. Three of the watersheds are underlain by granite-gneiss-migmatite-granulite complexes, and four are underlain by sedimentary sequences.

Sediments were field-sieved to 250-850 μm and river cobbles were crushed and sieved to the 250-850 μm fraction at the University of Vermont. Quartz from the samples was isolated and purified through a series of hydrochloric, hydrofluoric, and nitric acid etches, a modification of the method of Kohl and Nishiizumi (1992). Clean quartz was dissolved in hydrofluoric acid after the addition of a ^{9}Be carrier created from beryl in the University of Vermont cosmogenic nuclide laboratory. Beryllium was isolated through successive anion and cation exchange extractions, and precipitated as Be hydroxide (Corbett et al., 2016). The hydroxide was dried, burned, and packed into copper cathodes after being mixed with niobium. Samples were analyzed by Accelerator Mass Spectrometry (AMS) at the Scottish Universities Environmental Research Centre (SUERC) in East Kilbride, Scotland (Xu et al., 2010) and normalized to the NIST standard with an assumed ^{10}Be/^{9}Be ratio of 2.79 x 10^{-11} (Nishiizumi et al, 2007). Background correction was done using full process blanks run with each batch of 10 samples; the final uncertainty of the ratio is the uncertainty of the isotopic measurement and the blank propagated in quadrature.

All erosion rates (both for our new data and for data from the literature) were calculated using the CRONUS online calculator version 2.2 (http://hess.ess.washington.edu/), the global production rate, and the time invariant Lal

(1991)/Stone (2000) scaling scheme (see Table DR1 for CRONUS input). The calculator requires an elevation and latitude representative of the basin from which the sediment is sourced. We typically generate these values following the approach of Portenga and Bierman (2011). However, in some cases, despite extensive communication with the authors of other published Brazilian studies, it was not possible to determine precisely their sampling locations; because of this uncertainty, we used the average elevation of each watershed and its centroid latitude and longitude to calculate the erosion rates we report here. As a sensitivity test, we compared CRONUS-calculated erosion rates for the 14 basins we sampled using effective elevation (c.f., Portenga and Bierman, 2011) and mean elevation. We find on average, less than a 10% difference (Figure 2.3). Because of this similarity, we used centroid location and mean basin elevation to calculate the erosion rate of all watersheds considered in this paper.

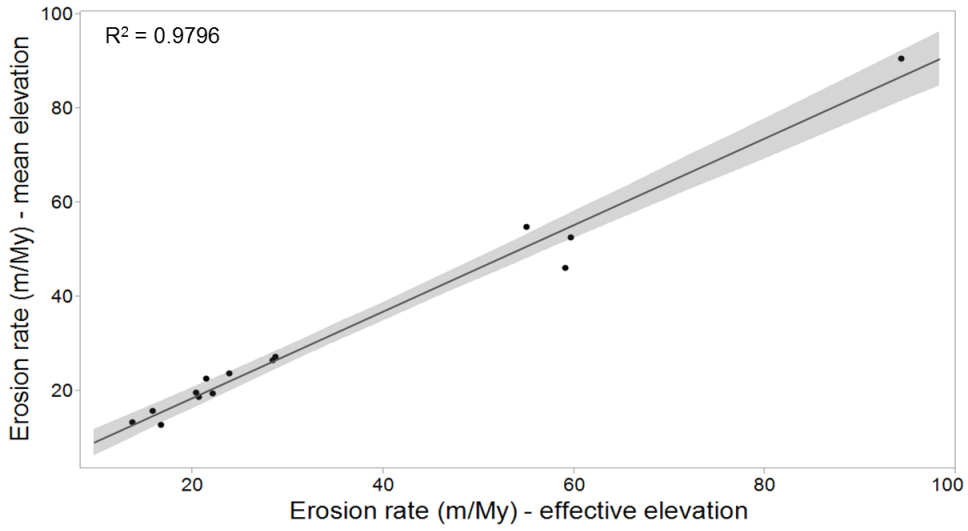

Figure 2.3: Erosion rates calculated using different parameter values. Regression of erosion rates calculated using the basin effective elevation and centroid location (X-axis) and calculated using mean basin elevation and centroid location (Y-axis) are very similar. Shaded zone represents the 95% confidence interval.

Climatic variables were extracted from the WorldClim dataset (Hijmans et al., 2005) available at http://www.worldclim.org/. To calculate area, elevation, and slope for the watersheds, we used the Topodata 30m DEM dataset created and published by the Instituto Nacional de Pesquisas Espaciais, (available at http://www.webmapit.com.br/inpe/topodata/). The lithology dataset we used was published by the Serviço Geológico do Brasil (available at http://geobank.cprm.gov.br/). The lithology dataset is not detailed; hence, the description of lithology in our watersheds is generalized. We analyzed the relationship between erosion rates and a wide array of topographic, climatic, and geologic variables (elevation, slope, area, precipitation, lithology).

In order to compare our results to those previously published for Brazil, we used published locations of sampling points (n=76) to delineate the watersheds and extract the information necessary to obtain erosion rates from CRONUS. We also quantified topographic and climatic variables (mean annual precipitation, basin slope, area and elevation) following the same procedure we used for our sites (see Table DR2).

All of the explanatory (topographic and climatic) variables for each watershed were quantified using ArcGIS 10.3 and entered into JMP 11, a statistical package, for parametric analysis. We performed all statistical analyses assessing significance at the 95% confidence level; therefore, we concluded that tests with p-values greater than 0.05 are not statistically significant.

Results

Erosion rates in the Brazilian drainage basins we sampled vary by a factor of 7, from 13 m/My to 90 m/My (n=14, Table 3.1, Figure DR5, Figure DR6), with an average of 32 m/My and a median of 23 m/My. Erosion for the watersheds in Rio de Janeiro averaged 36±19 m/My and 27±13 m/My for the Santa Catarina watersheds (uncertainties here and elsewhere are one standard deviation). There is no statistically significant difference between the erosion rate of samples collected from Rio de Janeiro and those from Santa Catarina ($t = -0.77$, $p = 0.46$). Both the highest and lowest erosion rates in our study are in Rio de Janeiro watersheds. The highest erosion rate we measured was for a watershed draining the Serra do Mar escarpment (BRA3S).

Table 2.1: Erosion rates and topography variables for river sediment samples from Brazilian states of Rio de Janeiro and Santa Catarina

Sample ID	State	Sample type	Drainage	Latitude	Longitude	^{10}Be concentration (x 10^4 atoms/g)	Erosion rate (m/My)	Elevation (m)	Slope (degrees)	Area (km^2)	Precipitation (mm)	Lithology
BRA 01S	RJ	River sand	E	-22.516	-43.001	8.4 ± 0.3	53 ± 4	708	24.0	8	1744	Granitoid
BRA 01	RJ	River cobbles	-	-22.516	-43.001	3.5 ± 0.3	-	-	-	-	-	-
BRA 02S	RJ	River sand	E	-22.493	-42.998	12.2 ± 0.3	46 ± 3	1351	26.1	18	1824	Granitoid
BRA 02	RJ	River cobbles	-	-22.493	-42.998	2.3 ± 0.3	-	-	-	-	-	-
BRA 03S	RJ	River sand	E	-22.467	-43.003	8.7 ± 0.4	90 ± 7	1606	29.2	3	1808	Granitoid
BRA 03	RJ	River cobbles	-	-22.467	-43.003	6.2 ± 0.3	-	-	-	-	-	-
BRA 19	RJ	River sand	M	-21.506	-42.203	18.5 ± 0.5	23 ± 2	483	12.3	9169	1376	Granite, gneiss
BRA 20	RJ	River sand	M	-21.255	-41.781	24.9 ± 0 .6	16 ± 1	531	13.8	7243	1292	Granite, gneiss
BRA 21	RJ	River sand	M	-21.330	-41.880	24.1 ± 0.5	13 ± 1	235	13.5	247	1223	Granitoid
BRA 22	RJ	River sand	M	-21.380	-41.924	24.2 ± 0.6	13 ± 1	244	14.9	15	1215	Granitoid
BRA 40	SC	River sand	M	-26.808	-48.907	7.6 ± 0.3	55 ± 4	293	16.2	5	1649	Granite, gneiss
BRA 41	SC	River sand	M	-26.775	-48.992	14.4 ± 0.5	27 ± 2	369	16.8	9	1646	Granite, gneiss
BRA 43	SC	River sand	M	-26.778	-48.993	14.6 ± 0.4	27 ± 2	377	16.5	8	1644	Granite, gneiss
BRA 44	SC	River sand	M	-26.881	-49.099	19.6 ± 0.5	24 ± 2	596	11.7	14987	1533	Consolidated sedimentary
BRA 45	SC	River sand	M	-27.061	-49.527	22.6 ± 0.6	20 ± 1	612	12.1	4167	1484	Consolidated sedimentary
BRA 46	SC	River sand	M	-27.080	-49.498	21.4 ± 0.5	20 ± 1	628	11.0	6931	1543	Consolidated sedimentary
BRA 47	SC	River sand	M	-27.334	-49.619	23.8 ± 0.5	19 ± 1	695	11.6	2335	1578	Consolidated sedimentary

Notes: Sampling locations are based in WGS1984. CRONUS Earth Calculator Version 2.2 was used to calculate erosion rates, we used the scaling of Lal (1991) and Stone (2000). The external uncertainty calculated by CRONUS is expressed as the uncertainty of each erosion rate. Isotopic data standardized to NIST_27900 with assumed ratio of 2.79 × 10-11. Data have been blank corrected.

Mean basin elevation is reported as the elevation of each basin. Slope and area were calculated using the slope and calculate area ArcGIS 10.3 tools, respectively. We used the Topodata30m DEM from the Instituto Nacional de Pesquisas Espaciais. Precipitation data extracted from the WorldClim dataset (Hijmans et al., 2005).

Drainage refers to the terrain each basin drains: escarpment (E), or a mixed terrain of escarpment and highlands (M).

Based on lithology, our sampled watersheds can be divided into granitoid (n=5), granite and gneiss (n=5) and consolidated sedimentary lithologies (n=4). There is no statistically significant difference in erosion rates as a function of these three lithologies ($F= 1.29$, $p = 0.31$). Basins underlain by consolidated sedimentary rocks in our study erode at an average rate of 20 ± 2 m/My, whereas the basins underlain by granite and gneiss are eroding at an average rate of 29 ± 15 m/My; watersheds underlain by granitoids erode at 43 ± 32 m/My on average.

Erosion rates in our dataset are proportional to mean basin slope ($R^2 = 0.73$, $p < 0.001$, (Figure 2.4). The highest average basin slopes in our study (24 to 29°) are in watersheds that drain the Serra do Mar escarpment, where three of the four highest erosion rates are found. The relationship between erosion and mean annual precipitation (MAP) was also significant ($R^2 = 0.57$, $p = 0.002$, Figure 2.5). If precipitation and slope are combined as predictive variables, the relationship with erosion improves slightly ($R^2 = 0.78$, $p = 0.0002$). While there is no significant bivariate relationship between erosion and watershed area ($R^2 = 0.13$, $p=0.20$), smaller watersheds in general erode faster than larger ones (Figure 2.6A, inset). Based on the area distribution of our watersheds, we can divide the samples by quartiles into the following groups: 2-9, 9-150, 150-7010, and 7010-15000 km^2. Comparing the means (Figure 2.6B), we find that the smaller watersheds (2-9 km^2) erode significantly faster than the larger basins ($t = 2.23$, $p = 0.05$; Figure 2.6A), most likely because small headwaters watersheds on average have steeper hillslopes (21°) than larger watersheds (12°).

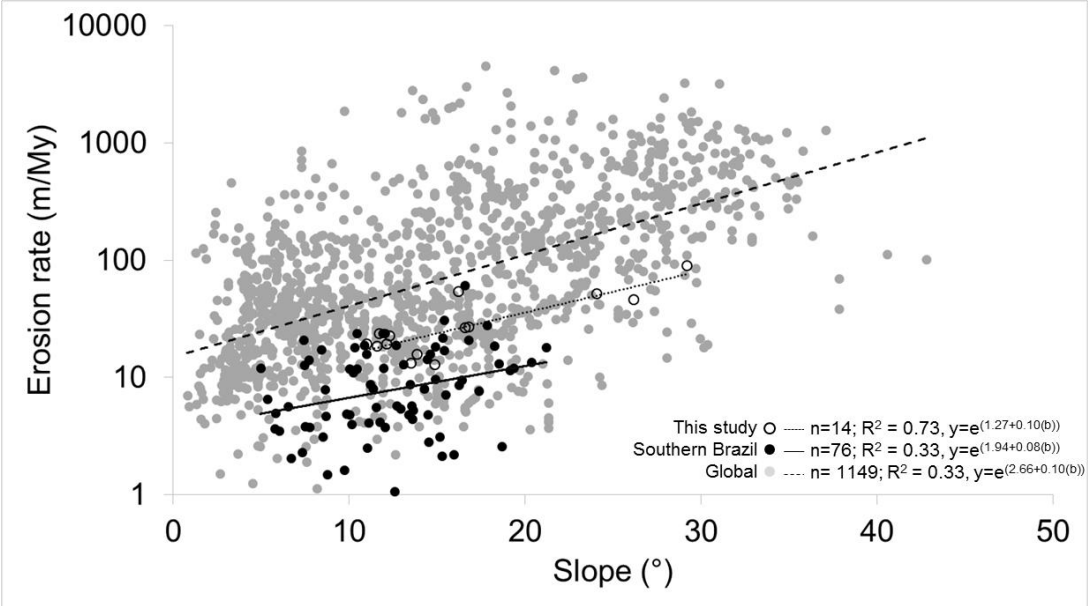

Figure 2.4: Regression plot of the relationship between erosion rate and mean basin slope. The strongest relationship in our dataset (open circles) was found between erosion and basin slope. The relationship is still significant but weaker in the entire southern and southeastern Brazilian dataset (filled black circles). Portenga and Bierman (2011) found slope to be the strongest predictor of erosion in their global dataset (filled grey circles).

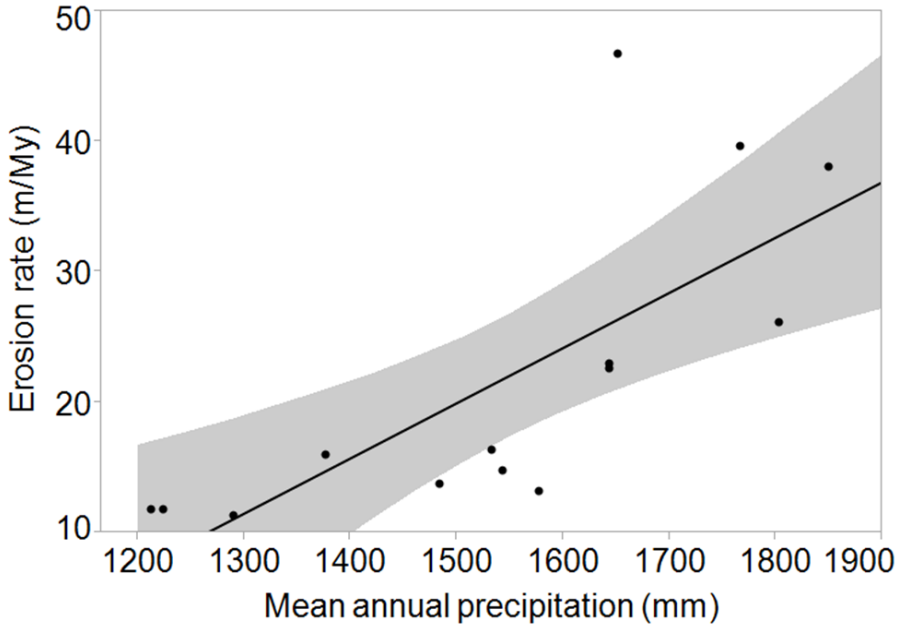

Figure 2.5: Regression plot of the relationship between erosion rate and mean annual precipitation. The shaded zone represents the confidence interval of the linear fit at the 95% level.

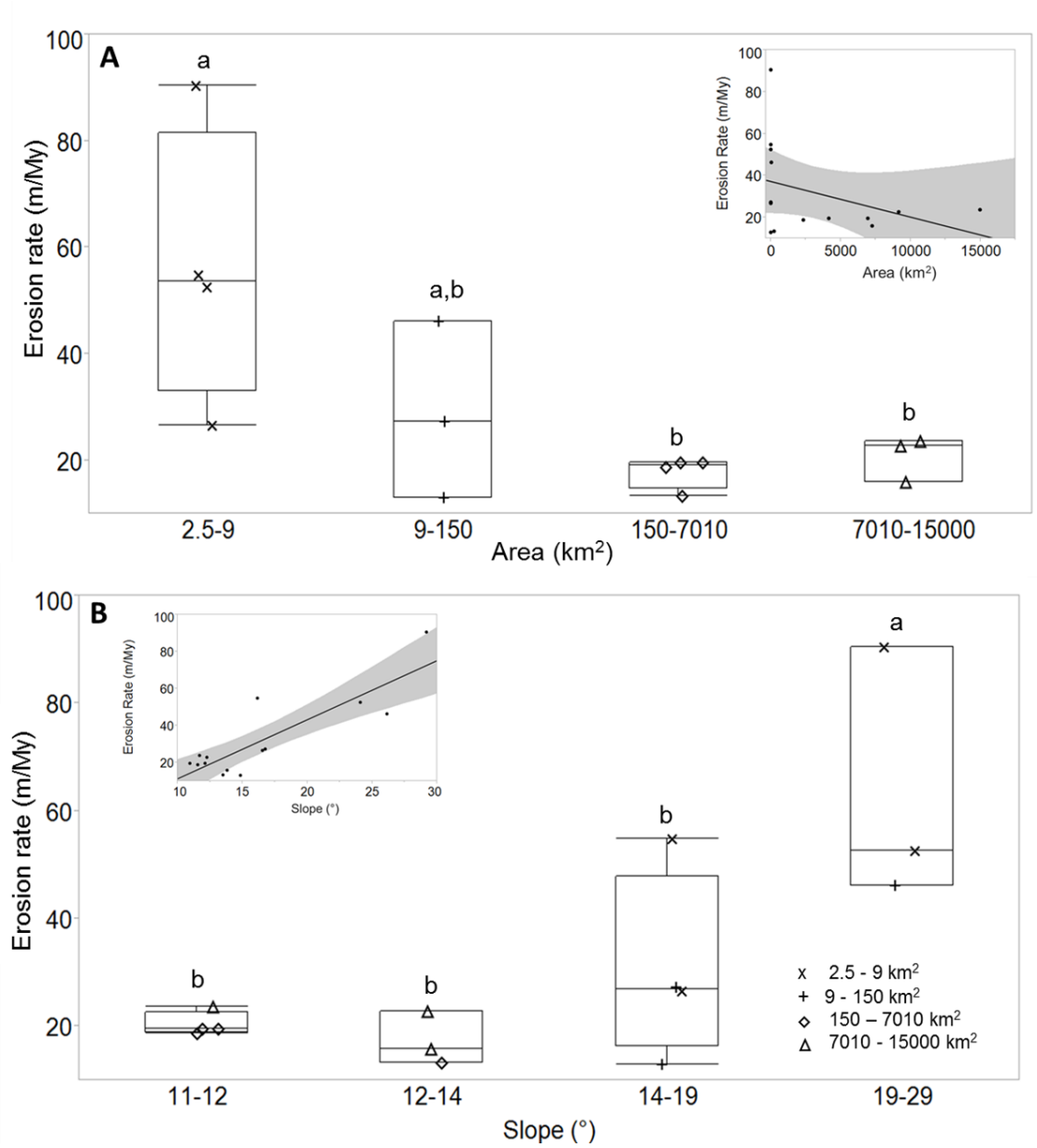

Figure 2.6: (A) Erosion rates sorted by basin area. Although erosion rates are not linearly related to basin area (inset), there is a statistically significant difference in erosion rates by basin area category. Categories not connected by the same letter are significantly different. (B) Erosion rate by mean basin slope subgroup. The positive relationship between erosion and slope in our dataset (inset), can be further explained by the correlation between area and slope. Steep headwater basins have a higher mean slope than larger basins with extensive lowlands. Categories not connected by the same letter are significantly different. Categories for area and slope were selected based on the quartiles of the values distribution. In both insets, the shaded zone represents the 95% confidence interval. The bottom and top limits of boxplots represent the first and third quartile of the data respectively. The line across the boxes is the median of each category. The whiskers represent the minimum and maximum value of each category.

Comparing the isotopic concentration of cobbles and sand transported as bed load in three Rio de Janeiro channels (BRA01, 02, 03), the concentration of ^{10}Be in cobbles is lower than in sand for all three sites (see Table 2.1). At one of the sites (BRA02), the isotopic concentration differs by over an order of magnitude between river sand (1.22 x10^5 atoms/g) and cobbles (2.26 x10^4 atoms/g).

Discussion

New erosion rate data, many of which are from samples collected from the steep continental margin of southern and southeastern Brazil, are broadly consistent with, although generally higher than, rates measured elsewhere in Brazil. Combining our new data for 14 watersheds with those for which data have already been published, we find that erosion rates in southern Brazil range between 1 and 90 m/My, with an average of 14 m/My (Figure 2.7).

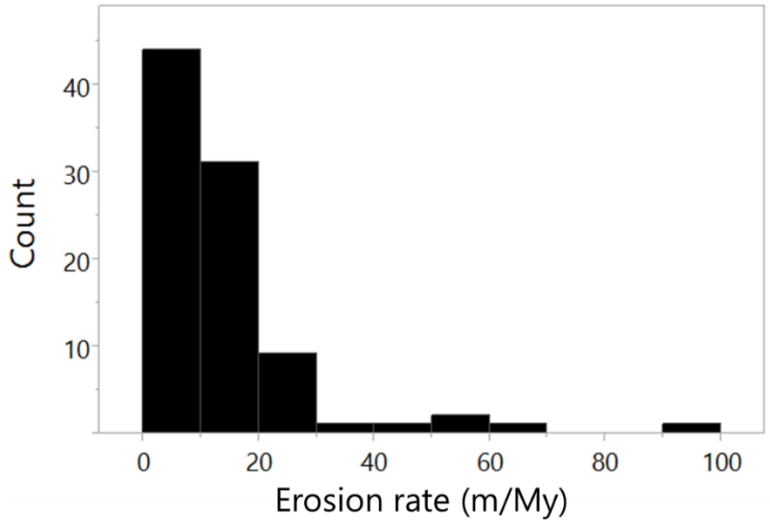

Figure 2.7: Histogram of all cosmogenic ^{10}Be-derived erosion rates published for southern Brazil. Erosion rates range from 1 to 90 m/My, with an average erosion rate of 14 m/My. Most watersheds are eroding at < 30 m/My.

Considering all southern Brazil samples, there are topographic and climatologic correlations on erosion. We find in Brazil, as others (e.g., Brown et al., 1998) have found in steep, tropical regions, that coarser fluvial sediment has less ^{10}Be than sand-sized sediment, either the result of landslides delivering coarser material once at depth to the stream (Brown et al., 1998) or because of the sourcing of coarser sediment from lower elevations (Matmon et al., 2003).

The relationship between mean basin slope and erosion is the strongest one in the compiled dataset of Brazilian erosion rates (R^2 = 0.33, $p < 0.001$). However, the relationship is weaker than it is when we consider only our spatially limited dataset (Figure 2.4). Portenga and Bierman (2011) note that as the scale of analysis grows (from local to regional to global), the relationship between topographic variables and erosion rate decreases presumably as other factors such as lithology, tectonics, and climate influence erosion rates. Similarly, there is a relationship between precipitation and erosion at the regional scale in Brazil ($R^2 = 0.05$, $p = 0.03$), but it is much weaker than the relationship shown by our 14 samples collected in a smaller area ($R^2 = 0.57$; Figure 2.4). Considering all Brazilian data, basin area is not related to erosion ($R^2 = 0.01$, $p = 0.30$) although regional studies, including ours, find that erosion is more rapid in smaller, steeper headwater sub-basins in Brazil than in larger, lower-slope basins (Salgado et al., 2006, 2007).

Considering all Brazilian studies, we find that there is a significant difference in erosion rate as a function of lithology ($F=10.9$, $p <0.01$). Basins underlain by granite, granitoid, and consolidated sedimentary material erode significantly faster than those underlain by quartzite, schist, and phyllite (Figure 2.8). Lithologic effects on erosion rate

has been noted in other, smaller-scale Brazilian studies. Similar to our findings at the large scale, Barreto et al. (2013) found that basins underlain by schist and phyllite erode more slowly than watersheds underlain by granite and quartzite and Salgado et al. (2008) measured the fastest erosion rates in watersheds underlain by granite, and the slowest in those underlain by quartzite. Salgado et al. in another study (2013), show that watersheds in Paraná state underlain by granite erode more slowly than watersheds underlain by migmatites and gneisses. In Brazil, only Rezende et al. (2013) reported that granite-bearing watersheds eroded more slowly than watersheds underlain by other lithologies.

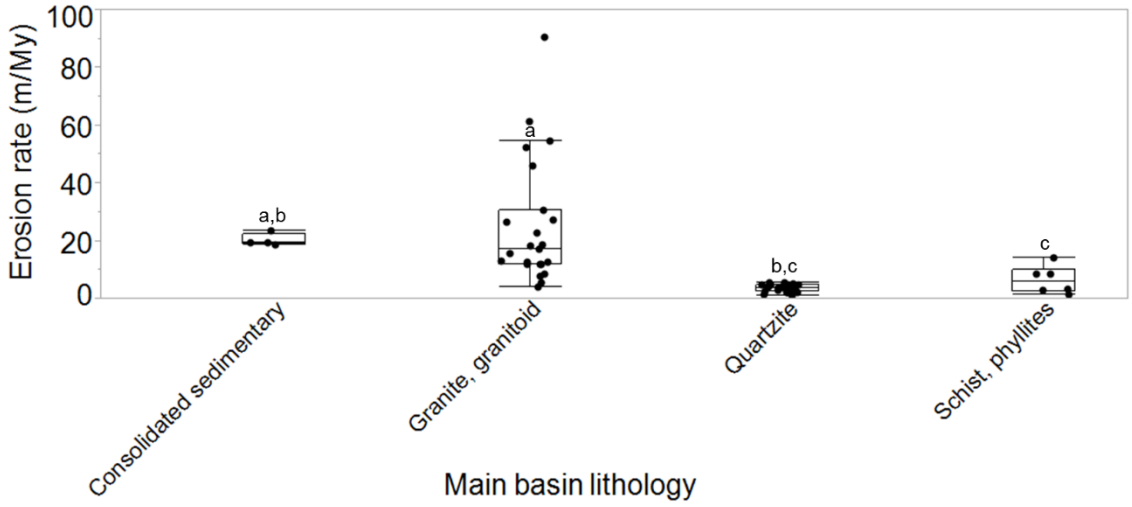

Figure 2.8: Brazilian erosion rates by predominant basin lithology. The compiled Brazilian dataset shows differences in average erosion rates as a function of dominant lithology in each samples basin. Basins underlained by granite and granitoids erode significantly faster than those underlain by quartzite, schist, and phyllites consistent with findings from smaller scale studies in Brazil. The bottom and top limits of boxplots represent the first and third quartile of the data respectively. The line across the boxes is the median of each category. The whiskers represent the minimum and maxim value of each category. Categories not connected by the same letter are significantly different.

Comparing our data to other cosmogenic ^{10}Be-derived erosion rates for watersheds in southern and southeastern in Brazil, we find that some of our 14 watersheds are among the most rapidly eroding (Table 2.2, See Portenga and Bierman for data). For example, the

coastal portions of Rio de Janeiro and Paraná states have similar geologic settings, with the Serra do Mar escarpment crossing both states. Previously published denudation rates for watersheds draining the escarpment in Paraná state (Salgado et al., 2013) range between 8 and 62 m/My, with an average of 20 m/My. This is considerably slower than the average erosion rate of the escarpment-draining watersheds in our small dataset (n=4), 63 m/My. In all Brazilian studies, steep escarpment-draining watersheds have the highest erosion rates.

Table 2.2 : Summarized published cosmogenic ^{10}Be-derived erosion rates for tropical climates and passive margin topography sites

Country	Publications	Samples	Erosion rates (m/Myr)			Comparison type
			Range	Average	Median	
Australia	Heimsath et al., 2009[1]	14	8.3 - 51.9	18	20.8	Tropical
	Nichols et al., 2014[2]					
Bolivia	Insel et al., 2010[1]	12	33.6 - 907	360	260	
	Wittmann et al., 2009[1]					
Madagascar	Cox et al., 2009[1]	7	5.8 - 22.3	13	11.8	
Panama	Nichols et al., 2005[1]	17	88.3 - 218	158	160.5	
Puerto Rico	Brown et al., 1995[1]	27	17.6 - 144	61	51.5	
	Brown et al., 1998[1]					
	Riebe et al., 2003[1]					
Sri Lanka	Hewawasam et al., 2003[1]	16	3.81 - 28.2	22	18.5	
	von Blanckenburg et al., 2004[1]					
Namibia	Bierman and Caffee, 2001[1]	46	1.51 - 14.6	9	8.7	Passive margin
	Bierman et al., 2007[1]					
Southeastern USA	Duxbury et al., 2015[2]	136	3.02 - 48.7	13	10.6	
	Sullivan, 2007[1]					
	Reusser et al., 2015[2]					
Australia	Heimsath et al., 2006[1]	17	6.49 - 119.4	43	45.7	Tropical passive margin
	Nichols et al., 2014[2]					
Sri Lanka	Vanacker et al., 2007[1]	19	1.92 - 69.4	23	12.2	
Brazil - escarpment	Barreto et al., 2013, 2014[3]	57	1.49 - 61.5	10	5.3	Brazil studies[5]
	Cherem et al., 2012[3]					
	Rezende et al., 2013[3]					
	Salgado et al., 2013[3]					
Brazil - highland	Cherem et al., 2012[3]	19	1.07 - 21.9	11	11	
	Salgado et al., 2006, 2007, 2008[4]					

[1] Erosion rates re-calculated using CRONUS and published by Portenga and Bierman (2011)
[2] Erosion rates from the original publication, calculated using CRONUS
[3] Erosion rates recalculated using CRONUS
[4] Samples in Salgado et al., 2006, 2007, and 2008 are from the same locations but were processed using different AMS standards. We used the most complete dataset of all three, the 2008 publication, for our comparison
[5] Data from this study are not included in this table, see Table 1

At a global scale, in comparison with erosion rates derived from cosmogenic ^{10}Be measured in river sand collected from other passive margin locations, Brazilian erosion rates have a wider range than those in Africa (Namibia) and North America (Table 2.2, Figure 2.9, See Portenga and Bierman for data). A one-way ANOVA comparing the erosion rate of basins in these three passive margins shows a statistically significant difference in at least two of the groups ($F = 4.81$, $p < 0.01$). Basins sampled in Brazil and North America, are eroding at a similar pace. In contrast, the escarpment-draining watersheds sampled in Namibia are eroding at a slower pace, significantly different to Brazil and North America, perhaps because Namibia is far drier than both Brazil and North America. The average erosion rate for passive margin watersheds in Namibia is 9±3 m/My (n=46; Bierman and Caffee, 2001; Bierman et al., 2007). Several studies have measured erosion rates for watersheds draining the southeastern United States passive margin. Published cosmogenic-derived erosion rates for Virginia watersheds average 11±8 m/My (n=69; Duxbury et al., 2015; Reusser et al., 2015). Samples from other sites in southeastern USA (North Carolina, South Carolina, Georgia and Alabama) also suggest an average erosion rate of 11±5 m/My (n=19; Reusser et al., 2015). The Blue Ridge Escarpment in North Carolina and Virginia, USA is eroding more rapidly, 17±9 m/My (Sullivan, 2007).

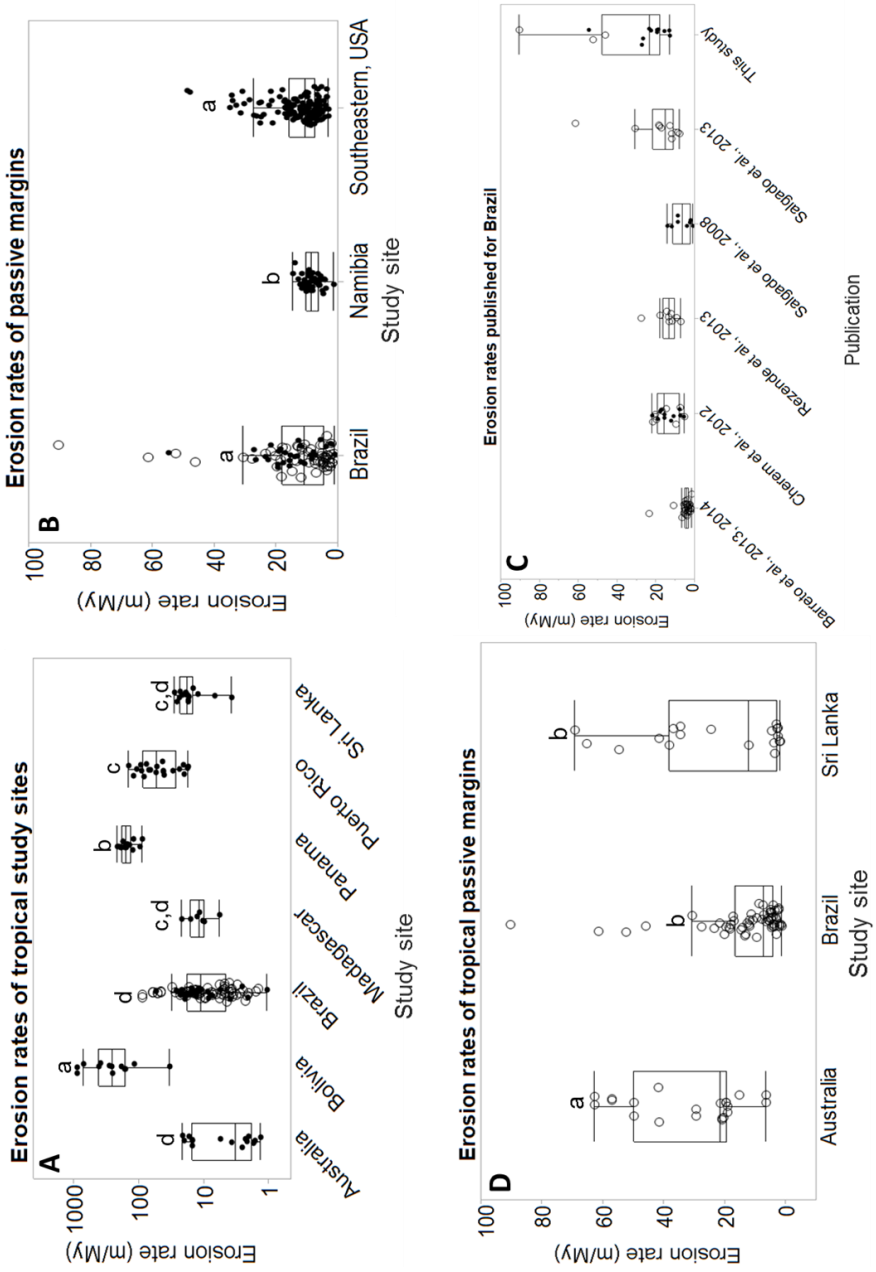

Figure 2.9: Summary of previously published cosmogenic ^{10}Be-derived erosion rates in (A) tropical climates (note the Y-axis scale), (B) passive margin, (C) Brazil and (D) tropical escarpments. Hollow circles represent escarpment draining watersheds. In all the boxplots the compiled Brazil data is included for reference. For this comparisons we used the CRONUS calculated erosion rates published by Portenga and Bierman (2011), except when otherwise noted (see Table 2). For the previous Brazil studies, we calculated the erosion rates using CRONUS and used that for comparisons. Table DR1 includes the CRONUS input table for these studies. Categories not connected by the same letter are significantly different.

Comparing the erosion rates of our sampled watersheds with other tropical regions where cosmogenic ^{10}Be has been measured in river sediments, we found that areas of Brazil

sampled so far are eroding considerably slower than areas sampled in Puerto Rico, Panama, Sri Lanka and Bolivia but faster than tropical regions of Madagascar and at a similar pace to Australian basins (Table 2.2, Figure 2.9, See Portenga and Bierman for data). Madagascar is the mostly slowly eroding with an average erosion rate of 13±5 m/My (n=7; Cox et al., 2009). The tropical regions in Australia erode on average at 18±12 m/My (n = 14; Heimsath et al., 2009; Nichols et al., 2014). Tropical watersheds in Sri Lanka erode at an average pace of 22±11 m/My (n=16; Hewawasam et al., 2003; von Blanckenburg et al., 2004). The average erosion rate for watersheds in Puerto Rico is 61±34 m/My (n=27; Brown et al., 1995; Brown et al., 1998; Riebe et al., 2003). Panama is eroding significantly faster than Brazil at an average erosion rate of 158±35 m/My (n=17; Nichols et al., 2005). Cosmogenically derived erosion rates measured in the tropical region of Bolivia average 360±296 m/My (n=12; Insel et al., 2010; Wittmann et al., 2009). Erosion rates in Brazil are significantly different only from those in Bolivia, Panama, Puerto Rico ($F = 38.7$, $p<0.01$).

Some of the basins sampled in Bolivia, Panama, and Puerto Rico record a greater mean annual rainfall than the Brazilian ones we studied, which may explain in part the higher erosion rates. However, tectonic activity appears to be the major controlling factor for rates of erosion at a basin scale in tropical region studies. Bolivian erosion rate samples were collected in a tectonically active region of the Andes; Puerto Rico and Panama are also tectonically active, which contrasts with the passive margin setting of southern and southeastern Brazil.

The influence of tectonic setting can be quantified using expected Peak Ground Acceleration (PGA) from earthquake activity where PGA is defined as the magnitude of ground motion with a 10% chance of being exceeded within 50 years, and expressed as a fraction of the acceleration due to gravity (*g)* in soil (Giardini, 1999). PGA maps, a proxy for tectonic activity, from the Global Seismic Hazard Assessment Program (Giardini, 1999; http://www.seismo.ethz.ch/static/GSHAP/) show that Brazilian sample sites have PGA values well below 1*g*. Watersheds in Puerto Rico average 1.88*g*, whereas Bolivia and Panama record a lower average PGA of 1.55 and 1.43*g*, respectively. Tectonic activity has been linked to accelerated rates of erosion (Dedkov and Moszherin, 1992), perhaps because repeated shaking fractures and weakens the rocks (Young et al., 2000). Furthermore, Milliman and Syvitski (1992) suggest that a complex relationship between fractured rocks, steep slopes, seismic and volcanic activity, rather than relief alone, controls erosion in active orogenic belts. This may be the case for Puerto Rico, Bolivia, and Panama.

Cosmogenic ^{10}Be has been used as an erosion proxy in tropical regions with escarpment topography in Sri Lanka and Australia (see Table 2.2 and Figure 2.9). Considering all published data, Brazilian escarpments are eroding at an average rate of 13±16 m/My (n=60; Barreto et al., 2013, 2014; Cherem et al. 2012; Rezende et al., 2013; Salgado et at., 2006, 2007, 2008, 2013; this study; Table DR2). This rate is considerably slower than the average rate for Sri Lanka, where the published data suggest that escarpment watersheds erode at an average of 23±23 m/My (n=19; Vanacker et al., 2007). Australian escarpment basins erode even more quickly, at an average rate of 43±30 m/My (n=17; Heimsath et al., 2006; Nichols et al., 2014). A One-way ANOVA comparing the

erosion rates of escarpment watersheds in Australia, Sri Lanka and Brazil shows differences between at least two of the countries ($F = 16.4$, $p < 0.01$). The Australian escarpment is eroding significantly faster than the Brazilian and Sri Lankan escarpments. The main lithology of the sampled watersheds in the Australian escarpment is sedimentary, in contrast with those watersheds sampled on the Brazilian escarpment, which are mostly underlain by crystalline rock. If the relationship between lithology and erosion rate in Brazilian watersheds is similar in Australia, this might explain why the Australian escarpment erodes more quickly than escarpments in Brazil and Sri Lanka. Precipitation could also be driving the increased rates of erosion on the Australian escarpment. Mean annual precipitation in the sampled Australian watersheds is up to 2500 mm/yr, greater than rainfall in the Brazilian watersheds we sampled.

Conclusions

The first ^{10}Be-based, drainage-basin scale erosion rate estimates from Rio de Janeiro and Santa Catarina states in Brazil are broadly consistent with other cosmogenic erosion rate data from southern and southeastern Brazil, and indicate that erosion rates in this tectonically inactive environment are mostly a few tens of meters per million years. Drainage basins in southern and southeastern regions of the country are eroding between 1 and 90 m/My with an average rate of 14 m/My. Erosion rates are greater in basins draining escarpments than in basins draining lower-relief highlands. Similar to other cosmogenic studies in Brazil, we found that the smaller, steeper headwater catchments erode faster than the larger, higher-order but lower slope catchments. Erosion in Brazil is mostly controlled by mean basin slope with lesser influence of climate and lithology.

Acknowledgements

Research supported by the US National Science Foundation (NSF-EAR-1114159) and by the Rio de Janeiro state Research Foundation (FAPERJ E-26/110.724/2012). The authors thank Silvio B. Bhering, Ana Carolina Santos, Maria Naíse de O. Peixoto, João Paulo Araújo and Marcel R. Lopes for field assistance during sampling in Rio de Janeiro watersheds. We thank Joshua Farley, João Carlos Gre, Janele Abreu, and Jose Abreu for their assistance in sampling Santa Catarina watersheds. The authors thanks Miguel Tupinambá, Telma Mendes da Silva, Lúcia Maria da Silva and an anonymous reviewer for improving the manuscript.

References

Almeida, F.F.M., Carneiro, C.D.R., 1998. Origem e Evolução da Serra do Mar. Revista Brasileira de Geociências 28(2), 135-150.

Almeida, J.C.H,; Dios, F., Mohriak, W., Valeriano, C.M., Heilbron, M, Eirado, L.G., Tomazzoli, E.,2013. Pre-rift tectonic scenario of the Eo-Cretaceous Gondwana break-up along SE Brazil-SW Africa: insights from tholeiitic mafic dike swarms. Geological Society Special Publications, 369, SP369.24-40.

Alvares, C. A., Stape, J.L., Sentelhas, P.C., Gonçalves, J.L.M., Sparovek, G., 2013. Köppen's climate classification map for Brazil. Meteorologische Zeitschrift, 22(6), 711-728.

Asmus, H.E., Ferrari, A.L., 1978. Hipótese Sobre a Causa do Tecnonismo Cenozóico na Região Sudeste do Brasil. In: Petrobrás (Ed.), Aspectos Estruturais da Margem Continental Leste e Sudeste do Brasil, Rio de Janeiro, Brazil, pp. 75-88.

Barreto, H.N., Varajão, C.A.C., Braucher, R., Bourlès, D.L., Salgado, A.A.R., Varajão, A.F.D.C., 2013. Denudation rates of the Southern Espinhaço Range, Minas Gerais, Brazil, determined by in situ-produced cosmogenic beryllium-10. Geomorphology, 191, 1-13.

Barreto, H.N., Varajão, C.A.C., Braucher, R., Bourlès, D.L., Salgado, A.A.R., Varajão, A.F.D.C., 2014. The impact of diamond extraction on natural denudation rates in the Diamantina Plateau (Minas Gerais, Brazil). Journal of South American Earth Sciences, 56, 357-364.

Behling, H., 1995. Investigations into the Late Pleistocene and Holocene history of vegetation and climate in Santa Catarina (S Brazil). Vegetation History and Archaeobotany, 4(3), 127-152.

Bierman, P., Steig, E.J., 1996. Estimating rates of denudation using cosmogenic isotope abundaces in sediment. Earth Surface Processes and Landforms, 21, 125-139.

Bierman, P.R., Caffee, M., 2001. Slow rates of rock surface erosion and sediment production accross the Namib dessert and escarpment, Southern Africa. American Journal of Sciences, 301, 326-358.

Bierman, P.R., Nichols, K.K., Matmon, A., Enzel, Y., Larsen, J., Finkel, R., 2007. 10-Be shows that Namibian drainage basins are slowly, steadily and uniformly eroding. Quaternary International, 167-168, 33.

Brickus, L.S.R., Cardoso, J.N., Neto, F.R.d.A., 1998. Distributions of indoor and outdoor air pollutants in Rio de Janeiro, Brazil: Implications to indoor air quality in bayside offices. Environmental Science and Technology, 32, 3485-3490.

Brocard, G., Willenbring, J., Johnson, A., Scatena, F., 2014a. Migration of a slow wave of erosion and its effects on nutrient availability in a tropical rainforest: detrital ^{10}Be signature and soil mineralogy, Luquillo, CZO, Puerto Rico, EGU General Assembly 2014, Vienna, Austria.

Brocard, G., Willenbring, J., Scatena, F., 2014b. Long-term increase in local relief enforced by forest competition: detrital ^{10}Be and LiDar topographic evidence in the tropical rainforest of Puerto Rico, Luquillo, CZO, EGU General Assembly 2014, Vienna, Austria.

Brown, E.T., Stallard, R.F., Larsen, M.C., Bourlés, D., Raisbeck, G.M., Yiou, F., 1998. Determination of predevelopment denudation rates of an agricultural watershed (Cayaguás River, Puerto Rico) using in-situ produced ^{10}Be in river-borne quartz. Earth and Planetary Science Letters, 160, 723-728.

Brown, E.T., Stallard, R.F., Larsen, M.C., Raisbeck, G.M., Yiou, F., 1995. Denudation rates determined from the accumulation of in-situ produced ^{10}Be in the Luquillo Experimental Forest, Puerto Rico. Earth and Planetary Science Letters, 129, 193-202.

Cherem, L.F.S., Varajão, C.A.C., Braucher, R., Bourlés, D., Salgado, A.A.R., Varajão, A.C., 2012. Long-term evolution of denudational escarpments in southeastern Brazil. Geomorphology, 173-174, 118-127.

Corbett, L. B., Bierman, P. R., Rood, D,H., 2016. An approach for optimizing in situ cosmogenic ^{10}Be sample preparation, Quaternary Geochronology, http://dx.doi.org/10.1016/j.quageo.2016.02.001.

Cox, R., Bierman, P., Jungers, Matthew C., Rakotondrazafy, A.F.M., 2009. Erosion rates and sediment sources in Madagascar inferred from ^{10}Be analysis of lavaka, slope, and river sediment. The Journal of Geology, 117(4), 363-376.

de Sherbinin, S., Hogan, D., 2011. Climate proofing Rio de Janeiro, Brazil. In: C. Rosenzweig, W.D. Solecki, S.A. Hammer, S. Mehrotra (Eds.), Climate change and cities: First assessment report of the urban climate change research network. Cambridge University Press.

Dedkov, A.P., Moszherin, V.I., 1992. Erosion and sediment yield in mountain regions of the world, Proceedings of the Chengdu Symposium. IAHS Publications, Chengdu, China.

Domínguez, J.M.L., 2009. The coastal zone of Brazil. In: S. Dillenburg, P. Hesp (Eds.), Geology and geomorphology of Holocene coastal barriers of Brazil. Springer, Berlin, Germany.

Duxbury, J., Bierman, P.R., Portenga, E.W., Pavich, M., Southworth, S., Freeman, S.P., 2015. Erosion rates in and around Shenandoah National Park, Virginia, determined using analysis of cosmogenic ^{10}Be. American Journal of Science, 315(1), 46-76.

Fernandes, N.F., Tupinambá, M., Mello, C.L., Peixoto, M.N.O., 2010. Rio de Janeiro: A Metropolis between granite-gneiss massifs. In: M. Migon (Ed.), Great Geomorphological Landscapes of the World, New York, USA, pp. 89-100.

Gallagher, K., Hawkesworth, C.J., Mantovani, M.S.M., 1995. Denudation, fission track analysis and the long-term evolution of passive margin topography: an application to the southeast Brazilian margin. Journal of South American Earth Sciences, 8(1), 65-77.

Giardini, D., 1999. The global seismic hazard assessment program (GSHAP) - 1992/1999. Annali di Geofisica, 42(6), 957-974.

Granger, D.E., Kirchner, J.W., Finkel, R., 1996. Spatially averaged long-term erosion rates measured from in-situ produced cosmogenic nuclides in alluvial sediments. The Journal of Geology, 104, 249-257.

Guedes, E.; Heilbron, M.; Vasconcelos, P.; Valeriano, C.; Almeida, J.; Teixeira, W.; Thomaz Filho, A., 2005. K-Ar and Ar-Ar ages of dikes emplaced in the onshore

basement of Santos Basin, Resende Area, SE, Brazil: Implications for the South Atlantic opening and a tertiary reactivation. Journal of South American Earth Sciences, 18(3), 371-382.

Hackspacher, P.C., Ribeiro, L.F.B., Ribeiro, M.C.S., Fetter, A.H., Hadler Neto, J.C., Tello, C.E.S., Dantas, E.L., 2004. Consolidation and Break-up of the South American Platform in Southeastern Brazil: Tectonothermal and Denudation Histories. Gondwana Research 7(1), 91-101.

Heilbron M., Machado, N., 2003. Timing of terrane accretion in the Neoproterozoic-Eopaleozoic Ribeira Orogen (SE Brazil). Precambrian Research, 125, 87–112.

Heilbron, M., Valeriano, C.M., Tassinari, C.C.G., Almeida, J.C.H., Tupinambá, M., Siga Jr., O., Truow, R.A.J., 2008. Correlation of Neoproterozoic terranes between the Ribeira Belt, SE Brazil and its African counterpart: comparative tectonic evolution and open questions. Geological Society Special Publications, 294, 211-237.

Heimsath, A.M., Chappell, J., Finkel, R.C., Fifield, K., Alimanovic, A., 2006. Escarpment erosion and landscape evolution in southeastern Australia. Geological Society of America, Special Paper 398, 173-190.

Heimsath, A.M., Fink, D., Hancock, G.R., 2009. The 'humped' soil production function: eroding Arnhem Land, Australia. Earth Surface Processes and Landforms, 34(12), 1674-1684.

Hewawasam, T., von Blanckenburg, F., Schaller, M., Kubik, P.W., 2003. Increase of human over natural erosion rates in tropical highlands constrained by cosmogenic nuclides. Geology, 31(7), 597-600.

Hijmans, R.J., Cameron, S.E., Parra, J.L., Jones, P.G., Jarvis, A., 2005. Very high resolution interpolated climate surfaces for global land areas. International Journal of Climatology, 25(15), 1965-1978.

Hinderer, M., Pflanz, D., Schneider, S., 2013. Chemical denudation rates in the humid tropics of east Africa and comparison with ^{10}Be-derived erosion rates. Procedia Earth and Planetary Science, 7, 360-364.

Insel, N., Ehlers, T.A., Schaller, M., Barnes, J.B., Tawackoli, S., Poulsen, C.J., 2010. Spatial and temporal variability in denudation across the Bolivian Andes from multiple geochronometers. Geomorphology, 122, 65-77.

Kohl, C.P., Nishiizumi, K., 1992. Chemical isolation of quartz for measurement of in-situ produced cosmogenic nuclides. Geochimica et Cosmochimica Acta, 56, 3583-3587.

Lal, D., 1991. Cosmic ray labeling of erosion surfaces: *in situ* nuclide production rates and erosion models. Earth and Planetary Science Letters, 104, 424-439.

Lal, R., Fifield, L.K., Tims, S.G., Wasson, R.J., Howe, D., 2012. A study of soil formation rates using ^{10}Be in the wet-dry tropics of northern Australia. EPJ Web of Conferences, 35, 01001.

Martinelli, L.A., Naylor, R., Vitousek, P.M., Moutinho, P., 2010. Agriculture in Brazil: impacts, costs, and opportunities for a sustainable future. Current Opinion in Environmental Sustainability, 2(5-6), 431-438.

Matmon, A., Bierman, P.R., Larsen, J., Southworth, S., Pavich, M., Finkel, R., Caffee, M., 2003. Erosion of an ancient mountain range, the Great Smoky Mountains, North Carolina and Tennessee. American Journal of Science, 303, 817-855.

Milliman, J.D., Syvitski, P.M., 1992. Geomorphic/tectonic control of sediment discharge to the ocean: the importance of small mountainous rivers. The Journal of Geology, 100, 525-544.

Nichols, K.K., Bierman, P., Finkel, R., C., Larsen, J., 2005. Long-term sediment generation rates for the Upper Río Chagres Basin: Evidence from cosmogenic ^{10}Be. In: R.S. Harmon (Ed.), The Río Chagres, Panama: A multidisciplinary profile of a tropical watershed. Springer, The Netherlands, 297-313.

Nichols, K.K., Bierman, P., Rood, D.H., 2014. ^{10}Be constrains the sediment sources and sediment yields to the Great Barrier Reef from the tropical Barron River catchment, Queensland, Australia. Geomorphology, 224, 102-110.

Nishiizumi, K., Imamura, M., Caffee, M.W., Southon, J.R., Finkel, R.C., McAninch, J., 2007. Absolute calibration of ^{10}Be AMS standards. Nuclear Instruments and Methods B, 258(2), 403-413.

Nunes, L.H., Vicente, A.K., Candido, D.H., 2009. Clima da Região Sudeste do Brasil. In: I.F.A. Cavalcanti, N.J. Ferreira, M.G.A.J. Silva, M.A.F.S. Dias, (Eds.), Tempo e Clima no Brasil. Oficina de Textos, São Paulo, pp. 243-259.

Ollier, C., 2004. The evolution of mountains on passive continental margins. In: P.N. Owens, O. Slaymaker (Eds.), Mountain Geomorphology. Arnold, New York, USA.

Portenga, E., Bierman, P.R., 2011. Understanding Earth's eroding surface with ^{10}Be. Geology, 21(8), 4-10.

Reusser, L., Bierman, P., Rood, D., 2015. Quantifying human impacts on rates of erosion and sediment transport at a landscape scale. Geology, 43(2), 171-174.

Rezende, E.A., Salgado, A.A.R., da Silva, J.R., Bourlés, D., Leánni, L., 2013. Factores controladores da evolução do relevo no flanco NNW do rift continental do sudeste do Brasil: Uma análise baseada na mensuração dos processos denudacionais de longo-termo. Revista Brasileira de Geomorfologia, 14(2), 221-234.

Riebe, C.S., Kirchner, J.W., Finkel, R.C., 2003. Long-term rates of chemical weathering and physical erosion from cosmogenic nuclides and geochemical mass balance. Geochimica et Cosmochimica Acta, 67(22), 4411-4427.

Salgado, A., Varajão, C., Colin, F., Braucher, R., Varajão, A., Nalini Jr, H., 2007. Study of the erosion rates in the upper Maracujá Basin (Quadrilátero Ferrífero/MG, Brazil) by the in situ produced cosmogenic ^{10}Be method. Earth Surface Processes and Landforms, 32(6), 905-911.

Salgado, A.A.R., Braucher, R., Colin, F., Nalini, H.A., Varajão, A.F.D.C., Varajão, C.A.C., 2006. Denudation rates of the Quadrilátero Ferrífero (Minas Gerais, Brazil): Preliminary results from measurements of solute fluxes in rivers and in situ-produced cosmogenic ^{10}Be. Journal of Geochemical Exploration, 88(1-3), 313-317.

Salgado, A.A.R., Braucher, R., Varajão, A.C., Colin, F., Varajão, A.F.D.C., Nalini, J.H.A., 2008. Relief evolution of the Quadrilátero Ferrífero (Minas Gerais, Brazil) by means of ^{10}Be cosmogenic nuclei. Zeitschrift für Geomorphologie, 52(3), 317-323.

Salgado, A.A.R., Marent, B.R., Cherem, L.F.S., Bourlès, D., Santos, L.J.C., Braucher, R., Barreto, H.N., 2013. Denudation and retreat of the Serra do Mar escarpment in southern Brazil derived from in situ-produced ^{10}Be concentration in river sediment. Earth Surface Processes and Landforms, 39(3), 311-319.

Silva, T.M., Ferrari, A.L., Tupinambá, M., Fernandes, N.F., 2015. The Guanabara Bay. In: B.C. Vieira, A.A.R. Salgado, L.J.C. Santos (Eds.), Landscapes and landforms of Brazil. Springer, New York, USA, pp. 1-16.

Stone, J.O., 2000. Air pressure and cosmogenic isotope production. Journal of Geophysical Research, 105(B10), 23,753-23,759

Sullivan, C.L., 2007. ^{10}Be erosion rates and landscape evolution of the Blue Ridge Escarpment, southern Appalachian Mountains. M.Sc., University of Vermont, Burlington, VT, 76 pp.

Vanacker, V., von Blanckenburg, F., Govers, G., Molina, A., Poesen, J., Deckers, J., Kubik, P., 2007. Restoring dense vegetation can slow mountain erosion to near natural benchmark levels. Geology, 35(4), 303.

von Blanckenburg, F., Hewawasam, T., Kubik, P.W., 2004. Cosmogenic nuclide evidence for low weathering and denudation in the wet, tropical highlands of Sri Lanka. Journal of Geophysical Research, 109(F3).

Williams, L., 1962. South Brazil: its vegetation, natural resources, research centers, and other economic aspects. Economic Botany, 16(3), 143-160.

Wittmann, H., von Blanckenburg, F., Guyot, J.L., Maurice, L., Kubik, P.W. 2009. Cosmogenic nuclide budgeting of floodplain sediment transfer. Geomorphology, 109(3-4), 246-256.

Xu, S., Dougans, A.B., Freeman, S.P.H.T., Schnabel, C., Wilcken, K.M., 2010. Improved Be-10 and Al-26 AMS with a 5 MV spectrometer. Nuclear Instruments and Methods B, 268, 736-738.

Young, R.P., Hazzard, J.F., Pettitt, W.S., 2000. Seismic and micromechanical studies of rock fracture. Geophysical Research Letters, 27(12), 1767-1770.

Zalan P.V., Oliveira J.A.B., 2005. Origem e evolução estrutural do Sistema de Riftes Cenozóicos do Sudeste do Brasil. Boletim de Geociências da Petrobrás, 13(2), 269-300.

Chapter 3 – Spatial and temporal variation of erosion in Yunnan, China measured using ^{10}Be and contemporary sediment yields

Abstract

^{10}Be, both *in situ* and meteoric, is measured in river sediment to quantify background erosion rates and as a tracer of surface processes. Applications of this method are based on the rarely-tested assumption of time-invariant ^{10}Be concentration. We analyzed 103 samples for temporal variations in ^{10}Be concentration over timeframes from months to millennia. While the central tendencies of temporal comparisons are similar, there is variability beyond analytical uncertainty. Our data show similar concentrations in samples taken 6 months apart and paired in-channel and overbank samples, suggesting that the monsoon does not systematically alter sediment sourcing to rivers in Yunnan. ^{10}Be concentrations vary more over longer time frames, though not in a systematic way.

We assess the effects of land use on sediment yields, using sediment yield data from the mid-1980's when deforestation was widespread. Comparing long-term, cosmogenically-determined erosion rates with contemporary sediment yield data, we find that in 15 out of 20 basins the contemporary sediment yield is higher than long-term rates of sediment generation, by an average factor of 3. This discrepancy likely reflects deforestation and agriculture promoted by the Chinese government in the later 20th century. Using the same sediment yield data, along with measurements of meteoric ^{10}Be, we calculate the erosion index for each watershed, an approach for understanding whether watersheds are in steady state in regard to fluxes of meteoric ^{10}Be and the sediment to

which it is adhered. Only four basins show a balance between soil formation and erosion, the remaining basins are split between samples that export sediment at a faster rate than it is produced, and basins that store sediment.

Long-term erosion rates, derived from in situ-produced ^{10}Be, range from 0.02 to 0.39 mm/yr, and are strongly and positively related to mean basin relief, slope, and normalized channel steepness. Our results suggest that topography exerts a first-order control on erosion.

Introduction

Cosmogenic isotopes, including ^{3}He, ^{21}Ne, ^{26}Al, ^{14}C, ^{36}Cl and ^{10}Be, have many applications in the Earth Sciences, including geomorphology (Strobl et al., 2012), hydrology (Sültenfuβ et al., 2010), and landscape dynamics (Mackey et al., 2014). Following the development of accelerator mass spectrometry (AMS) in the early 1980's (Turekian et al., 1979; Elmore and Phillips, 1987), with the capability of quantifying very low concentrations of these isotopes in rock and near-surface materials, cosmogenic isotopes have been widely used to study surface processes (e.g., von Blanckenburg and Willenbring, 2014; Dunai and Lifton, 2014). Two ^{10}Be systems have been used for geomorphic applications – meteoric and *in situ*.

In situ produced ^{10}Be (^{10}Be$_i$) is the most widely used cosmogenic isotope (Portenga and Bierman, 2011; Heyman et al., 2011) because it accumulates in a common mineral (quartz), is easily measured, and there is only one primary production pathway (Lal, 2000). It has been used since the 1990's to study erosion and sediment transport (e.g., Nishiizumi et al., 1993; McKean et al., 1993; Monagahan et al., 1992; von Blanckenburg, 2005;

Willenbring and von Blanckenburg, 2010). *In situ* ^{10}Be forms in the crystal lattice of quartz as the result of spallation reactions between secondary cosmic rays (primarily neutrons) and the oxygen and silicon nuclei in quartz. This reaction occurs primarily near Earth's surface and is inconsequential at depths greater than ~ 2 meters (Lal and Peters, 1967). Because of this, $^{10}Be_i$ is a good indicator of near-surface residence time of rock and regolith, and thus of denudation rates at both the outcrop and basin scale, which are inversely related to isotopic concentration (Brown et al., 1995; Bierman and Steig, 1996; Granger et al., 1996).

Meteoric ^{10}Be ($^{10}Be_m$) forms in the atmosphere through cosmic-ray induced spallation of nitrogen and oxygen nuclei (Lal and Peters, 1967; Graly et al., 2011). Once formed in the atmosphere, the isotope adheres to aerosols and is delivered to the surface by either precipitation or dry deposition (McHargue and Damon, 1991). The delivery of $^{10}Be_m$ is a function of latitude, precipitation, and the movement of the isotope within the atmosphere (Graly et al., 2011; Willenbring and von Blanckenburg, 2010). Most $^{10}Be_m$ resides in the upper few meters of soil and regolith (Graly et al., 2010). Although $^{10}Be_m$ has been used less than $^{10}Be_i$ for geomorphology (Willenbring and von Blanckenburg, 2010), $^{10}Be_m$ has been used as a sediment tracer at the watershed level (e.g., Reusser and Bierman, 2010) and to estimate rates of sediment transport (Jungers et al., 2009; Wittmann and von Blanckenburg, 2009; Wittmann et al., 2009, 2011a, 2011b; West et al., 2011, 2013, 2014; Campforts et al., 2016). $^{10}Be_m$ can also be used to calculate the erosion index (EI) of a watershed, which reflects the balance between delivery and export of the isotope, a function of erosion and sediment transport efficiency (Brown et al., 1988).

Accurately interpreting basin-scale geomorphic behavior from both $^{10}Be_i$ and $^{10}Be_m$ in river sediment assumes both that the rate of erosion is steady over the time period integrated and that sampled sediment is representative of the entire basin (Brown et al., 1995; Bierman and Steig, 1996; Granger et al., 1996) – assumptions that have rarely been tested. Variations of $^{10}Be_i$ and $^{10}Be_m$ concentrations over time and space beyond analytical precision have been found in a few watersheds (Reusser and Bierman, 2010). Small watersheds, like some included in temporal ^{10}Be comparisons, are influenced by stochastic events, such as landslides (Niemi et al., 2005), bank collapses, and debris flows that have the potential to change the isotopic concentration of sediment over both time and space. Measurements of the temporal variations of $^{10}Be_i$ and $^{10}Be_m$ in the mainstem of large river basins (>1,000 km^2) basins are scarce (Wittmann et al., 2009, 2011c) but variability at larger scales may be less than at smaller scales (Matmon et al., 2003; Niemi et al., 2005; Reusser and Bierman, 2010). To the best of our knowledge, there is only one temporal replicate published for a large river basin (Lupker et al., 2012). Temporal variation of $^{10}Be_i$ over millennial timescales has been assessed by comparing isotopic activity of river terraces and active channel sediments in France, the Netherlands, and Madagascar (Schaller et al., 2002; Cox et al., 2009).

The goal of this paper is to measure the variability of both $^{10}Be_i$ and $^{10}Be_m$ concentrations in river sediment over different time and spatial scales for the Mekong, Salween, Irrawaddy, and Red Rivers in China. We then compare these data to unusually long and complete records of contemporary sediment yield (Henck et al., 2010) on the same rivers while considering the relationship between measured ^{10}Be and topographic and

climatic metrics for each drainage basin. This comparison allows us to understand whether erosion has been similar over time and space, and speculate on what controls rates of erosion in this region.

Study Area

Yunnan province is located in southwestern China. The province is a mostly mountainous region connecting with the Tibetan highlands in the northwest and descending into a broad plateau toward the east (Leloup et al., 1995). Climate in Yunnan is controlled largely by elevation (ranging from 76 to 6740 m, exceeding 4000 m in most mountainous areas), with mean annual temperatures ranging between 7 and 22°C; between 800 and 1100 mm of precipitation falls annually (Hui et al., 2013; Leloup et al., 1995). Yunnan's climate is dominated by the interaction between the East Asian summer monsoon and the Indian summer monsoon, as well as by surface orography (Hui et al., 2013). During the monsoon season (June to September), 85% of the annual precipitation falls and the rivers transport 62% of the annual discharge and 86% of their annual suspended sediment (Henck et al., 2010). Soil erosion is intensified during the monsoon months by flooding and runoff (Zisheng et al., 2010).

The geology of Yunnan is the result of a long history of the interactions between tectonism, surface uplift, and regional climate (Schoenbohm et al., 2004). Twelve geologic units underlie the watersheds sampled for this study (Figure 3.1A). There are four geologic units that each underlie at least a portion of each of the four major basins we study (Mekong, Red, Irrawaddy and Red). These geologic units are the: Tenasserim-Shan block, Lhasa terrane, Qiangtang terrane, and the Lanping Simao basin (USGS, 2000). The Lhasa

unit is characterized by three distinctive belts of rocks: a northeast belt of Mesozoic sedimentary rocks; a central belt dominated by Upper Paleozoic sedimentary and sedimentary rocks; and a southern belt of Mesozoic and Cenozoic plutonic rocks (Burchfiel and Chen, 2012a). The Lanping-Simao basin is mostly composed of sedimentary rocks, with some volcanic rocks of Triassic age (Burchfiel et al., 2008). The Qiangtang unit is composed of Paleozoic and Mesozoic rocks overlain by an Upper Triassic to late Mesozoic sedimentary cover (Burchfiel and Chen, 2012b). Field observations and a geologic map of the region (Geology of Sanjiang, 1986) indicate that granite, limestone, and sandstone underlie most of our studied watersheds. Monzonitic granite underlies the basins we sampled within the Mekong River (Geology of Sanjiang, 1986). The Lancang and Gaoligongshan groups stretch over portions the main channel of the Mekong and Salween rivers, and are composed mostly of schist, gneiss, marble and quartzite (Geology of Sanjiang, 1986). Sandstones, limestones, and slates of Cambrian and Triassic ages underlain a significant portion of our field area (Geology of Sanjiang, 1986).

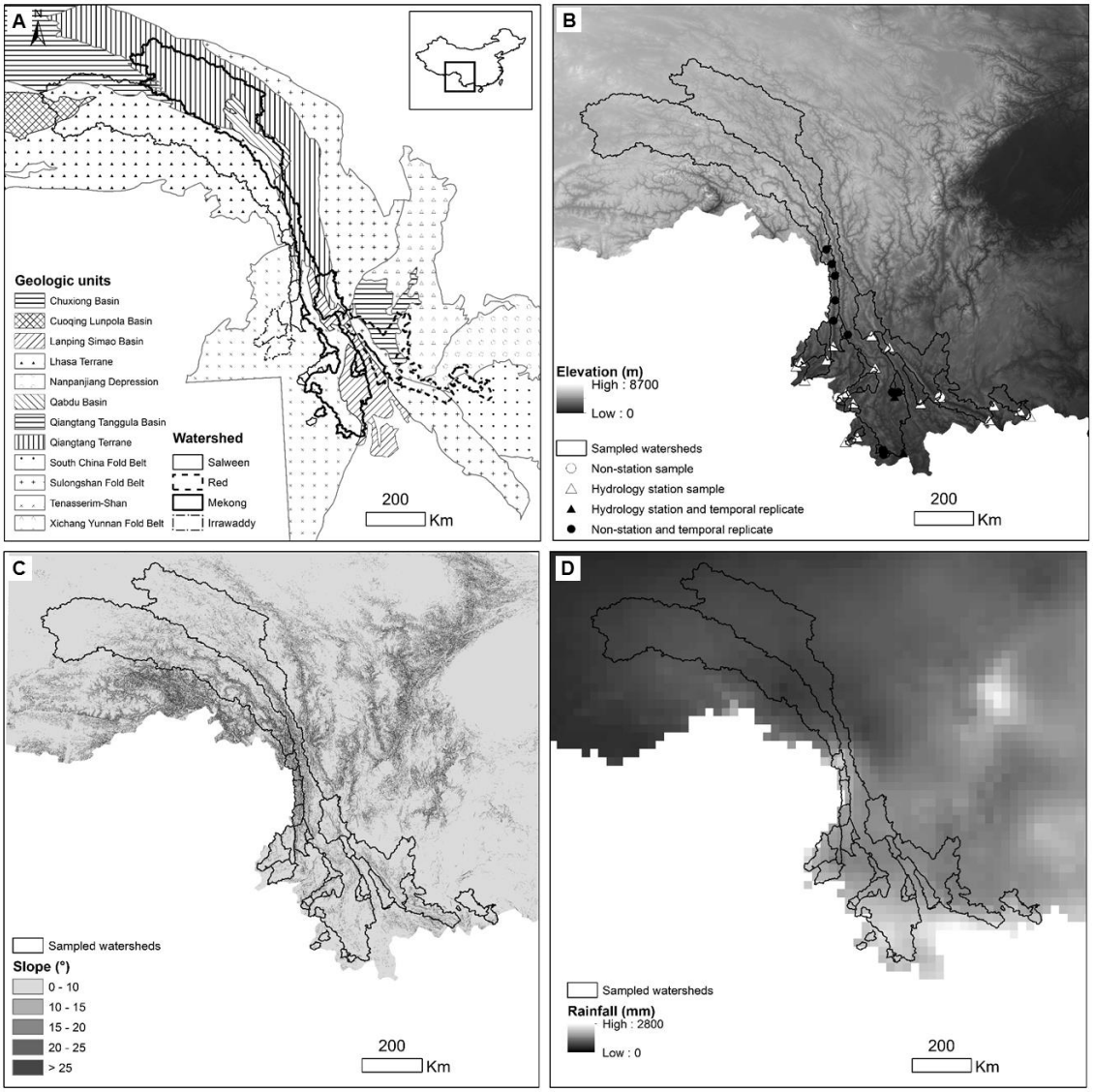

Figure 3.1: Sampled watersheds. Watersheds included in this study are parallel to the southwestern border of China, Yunnan Province. Several geologic units underlie our study area (A). Map data from USGS (2000). Each of our four major basins have least a portion in one of these four units: Lhasa terrane, Lanping-Simao basin, Tenasserim-Shan block and Qiangtang terrane. Our samples include hydrology stations, and some sites were sampled multiple times (B). Mean basin slope in our studied watersheds range from 9 to 20° (C). Data from NASA 30-m GDEM. Mean annual rainfall in our watersheds range between 511 and 1349 mm (D). Data from APHRODITE (Yatagai et al., 2012).

Western China, including Yunnan, experienced extensive deforestation during the 20th century, when forests were cleared for fuel, cropland, or private economic benefit (Trac et al., 2007; Fang and Xie, 1994; Rozelle et al., 1997; Shapiro, 2000). Forest coverage

in Yunnan ranged from 10 to 20% between 1940 and 1980 (He et al., 2015). The severe droughts China faced in 1997 followed by massive floods along the middle and lower Yangtze in 1998 triggered the implementation of two nationwide programs to increase and protect forested areas: the Natural Forest Protection Program and the Returning Farmland to Forest Program (sometimes referred to as the Sloping Land Conversion Plan or Grain to Green Program) (Trac et al., 2013; Xu et al., 2006; Zhang et al., 2014; Weyerheuser et al., 2005). By 2003, both of these programs were implemented in Yunnan (Zhang et al., 2014). Increase in cropland and decrease in forested land were recorded before the programs were begun; as a result of the programs, forest cover has increased, and cropland has decreased in the decade following the implementation (Zhang et al., 2014). There is controversy about the effectiveness of these programs in southwest China (Brandt et al., 2012; Trac et al., 2007, 2013). While an increase in sediment flux is generally associated with extensive deforestation and agriculture, sediment exported from Chinese rivers decreased between the years 1993 and 2000, likely due to the construction and operation of hydropower dams (Kummu and Varis, 2007, Lu and Siew, 2006).

China is the ideal location to compare long-term erosion rates calculated from $^{10}Be_i$ concentration with contemporary sediment yield because of unusually detailed and complete river sediment yield and discharge records. The Chinese Hydrology Bureau has collected data, including discharge and suspended sediment, in Yunnan since 1949, but the records are not publicly available after 1987 (Henck et al., 2010). Data available from the sediment records coincides with the period of massive deforestation in China (1950s to 1990s). The sediment data were compiled, published, and analyzed by Schmidt et al.

(2011). Their work found that sediment yield for rivers in Yunnan correlates with upstream area, rainfall, cropland and population density (Schmidt et al., 2011). The relationship with area is negative, while the others are positive.

Methods

We collected 64 sand-size (250-850 μm) sediment samples from active river channels and floodplains to analyze for both $^{10}Be_i$ and $^{10}Be_m$ (Figure 3.1B). Our erosion rate calculations also include two laboratory processed replicates (CH-137(A) and CH-148(A)), and a sample collected by Devin McPhillips (Y-13-01-DM), collected approximately 2 kilometers downstream from our CH-113 sample. Including these three samples, our erosion calculations consider a total of 67 samples (Table 3.1; Table DR3).

For most watersheds, we have samples from tributaries and the mainstem, except for the Irrawaddy River, from which we have no mainstem samples. Eleven sites were sampled in May - June 2013 just as the monsoon was beginning (series CH-0XX), and resampled in January 2014 during the dry season (series CH-1XX). We also resampled seven sites first sampled by Henck et al. (2011) in 2005 (series TRR-XX). These samples had been analyzed for $^{10}Be_i$ but not $^{10}Be_m$; we analyzed the seven TRR samples for $^{10}Be_m$. Sample TRR-14b was not analyzed for $^{10}Be_i$ due to a high content of native ^{9}Be in the sample. To test for seasonal bias of sediment sourcing, we sampled sediment from the active channel during dry season base flow and adjacent overbank sediment deposited during monsoon floods. When alluvial terraces alongside the river contained charcoal, we sampled charcoal and sand-size material deposited in the same stratum. We radiocarbon

dated the charcoal at the W.M. Keck Carbon Cycle Accelerator Mass Spectrometry Laboratory, California (Santos et al., 2007; Table DR4).

Table 3.1: Number of samples included per category

Analysis	Isotope analyzed	Amount of samples included	Sample year
Erosion rates and topography[1]	$^{10}Be_i$	67	2014
Temporal replicates - 6 months	$^{10}Be_i$	22	2013/2014
	$^{10}Be_m$	18	2013/2014
Temporal replicates - in channel/overbank	$^{10}Be_i$	64	2013/2014
	$^{10}Be_m$	58	2013/2014
Temporal replicates - decade	$^{10}Be_i$	12	2005/2014
	$^{10}Be_m$	12	2005/2014
Temporal replicates - millenial	$^{10}Be_i$	18	2013/2014

[1] We used the error-weighted average isotopic concentration of in channel and overbank sediment for erosion rates calculation and regression analysis, when both data were available. We used 35 sites for regression analysis.
[2] Temporal replicates include both samples included in each temporal analysis

Quartz from the samples was isolated and purified through a series of acid etches, a modification of the method of Kohl and Nishiizumi (1992). $^{10}Be_i$ was extracted from quartz following the method of Corbett et al. (2016). Once the quartz was dissolved in hydrofluoric acid, aliquots were removed and analyzed by inductively coupled plasma-optical emission spectroscopy (ICP-OES) to measure Be and Al content (Portenga et al., 2015; Corbett et al., 2016). 21 samples had Be recovery >100% (range: 106.2 – 198.1%) (based on the Be carrier added), indicating the presence of native Be in those samples. Samples analyzed for $^{10}Be_m$ were milled in preparation for isotopic analysis. A small (~0.5g) of pulverized material was used for isotopic extraction. We used a modification of the flux fusion method of Stone (1998) to extract $^{10}Be_m$.

Isotopic ratios were measured using Accelerator Mass Spectrometry (AMS) at the Scottish Universities Environmental Research Centre in East Kilbride, Scotland (Xu et al., 2010) and normalized to the NIST standard with an assumed $^{10}Be/^{9}Be$ ratio of 2.79×10^{-11}

(Nishiizumi et al, 2007; Table DR3). Background correction was done using full process blanks, one of which was run with each batch of 10 samples. For samples with native ^{9}Be, we used the total Be from ICP measurements to calculate ^{10}Be concentration, rather than the amount of Be added as carrier (c.f., Portenga et al., 2015). The final uncertainty of the blank-corrected ratio is the uncertainty of the isotopic measurement and the blank propagated in quadrature.

We used the 30m GDEM (NASA LP-DAAC, 2012), to calculate area, mean elevation, mean basin slope (Figure 1C), and normalized channel steepeness (ksn) for each watershed. We calculated mean basin relief using a 5-km radius. We calculated ksn as per Wobus et al., (2006). Two outliers on the ksn data (values of 8085 and 13406) were not considered for analysis. Erosion rates, which we consider as long-term sediment yields, were calculated from $^{10}Be_i$ concentrations using the CRONUS Earth Calculator Version 2.2 (http://hess.ess.washington.edu/) (Balco et al., 2008). In order to estimate erosion rates, we calculated the effective elevation of each watershed using the approach of Portenga and Bierman (2011) (see Table DR5 for CRONUS input). We used the error weighted-average of the isotopic concentration of active channel and overbank material at a site to calculate erosion rates and for consequent statistical analysis. In places where we sampled both active channel and overbank sediment in 2013 and 2014, the error-weighted average of all four concentrations is used. We used the scaling scheme of Lal (1991) and Stone (2000) and the global production rate of $^{10}Be_i$. Climatic data were extracted from the APHRODITE program dataset (Yatagai et al., 2012) (Figure 3.1D). Though this dataset has a coarser resolution than others available, it is the most accurate for Asia (Andermann

et al., 2011). Land cover data were extracted from the GlobeLand30 dataset (Chen et al., 2015; http://globallandcover.com). We quantify peak ground acceleration (PGA), a proxy for tectonic activity in our watersheds, using the dataset from Giardini (1999).

We use the modern sediment yield for 22 rivers as calculated and published by Schmidt et al. (2011), based on discharge data from the Chinese Ministry of Hydrology (http://www.oberlin.edu/faculty/aschmidt/chdp/index.html). We compared long term erosion rates deduced from $^{10}Be_i$ concentration to modern sediment yield data to quantify changes in sediment flux over time. We divided the modern sediment yield by the long-term sediment yield to obtain the ratio of yields, and discuss our findings in terms of this ratio. At one site (CH-133), the modern sediment yield is greater than the long-term by a factor of 121, this outlier is not included in our analysis.

To calculate erosion indices, we used the equation of Brown et al. (1988):

$$I = M\eta'/Aq, \quad (1)$$

where M is the annual sediment load (g/yr), η' is the $^{10}Be_m$ concentration (atoms/g) in the material leaving the basin, A is the basin area (cm^2), and q is the atmospheric deposition rate of $^{10}Be_m$ in the watershed (atoms cm^{-2} yr^{-1}). The value of q for each watershed was calculated as per Graly et al. (2011). We calculated M using measured contemporary sediment load (Schmidt et al., 2011). One EI value of 54.4 (CH-133) is an outlier, and is not considered for analysis.

To quantify temporal variations in isotopic concentrations, we subtracted the isotopic concentration of the replicate from the concentration of the original sample (or in

channel from overbank for interannual replicates), and divided by the average of the measurements. We express the result as a percentage. Samples with differences greater than 10% are not considered to be within error.

Topographic metrics for each watershed were quantified using ArcGIS 10.3 and entered into JMP 11, a statistical package, for parametric analysis. To test for differences in isotopic activity over time, we used the Wilcoxon test. We performed all statistical analyses assessing significance at the 95% confidence level and thus concluded that tests with p-values greater than 0.05 are not statistically significant.

Results

Measured $^{10}Be_i$ activities for in-channel and overbank samples range from $2.72x10^4$ to $5.21x10^5$ atoms/g (Table DR3). Error weighted-average in-channel and overbank $^{10}Be_i$ concentrations, used for erosion calculations and regressions with topography variables, range from $3.72x10^4$ to $5.0x10^5$ atoms/g (Figure 3.2A). Erosion rates (calculated from error-weighted average $^{10}Be_i$ concentrations) range between 0.02 and 0.39 mm/yr, with an average and a median of 0.16 and 0.13 mm/yr, respectively (Table DR6). While there is no distinct spatial pattern in the long-term erosion rates (Figure 3.2B), an ANOVA test shows a significant difference in the erosion rate by basin ($F= 3.6$, $p = 0.02$, Table 3.2).

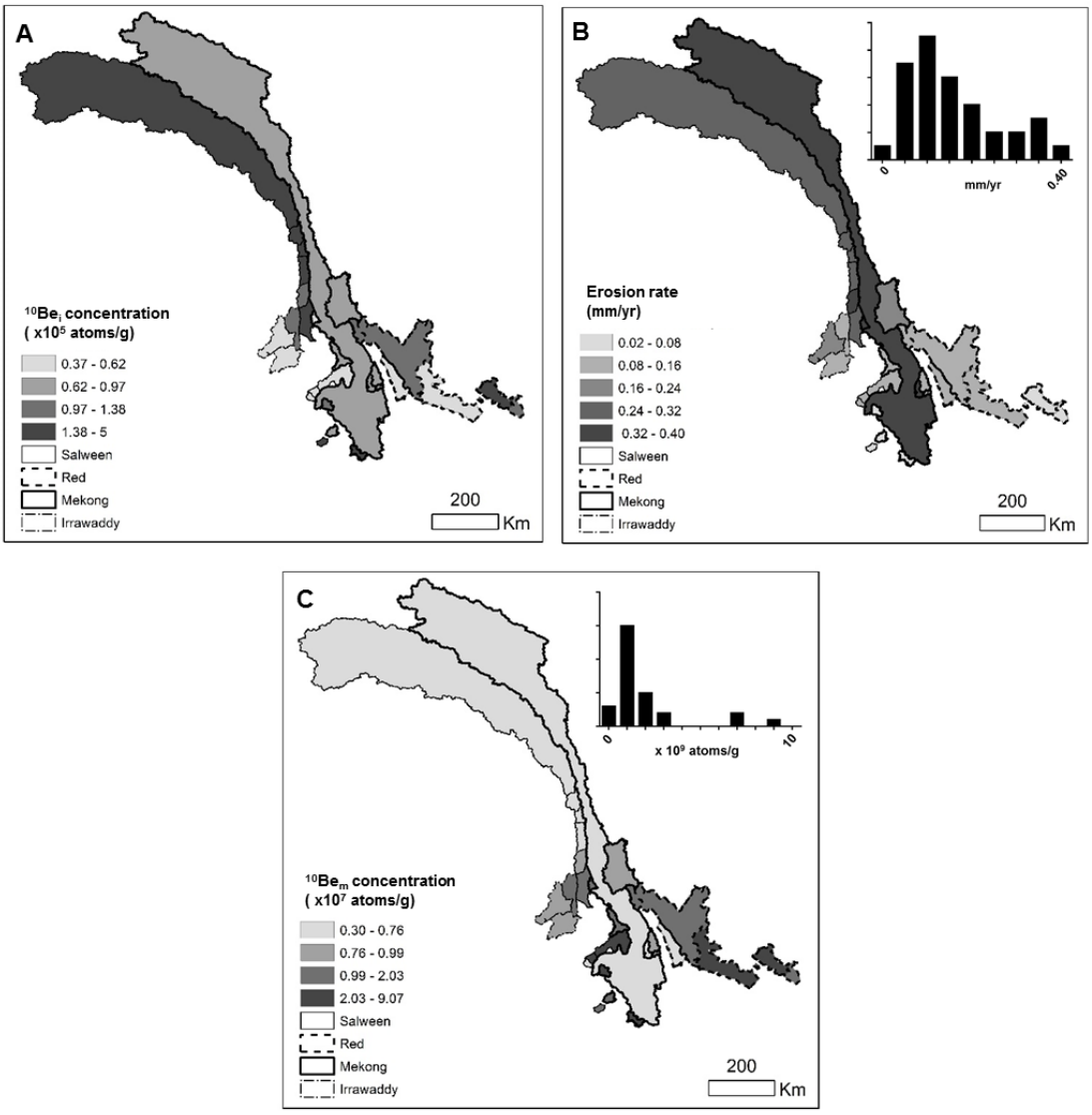

Figure 3.2: Spatial variation of error-weighted averaged isotopic activities and erosion rates. Categories for the isotopic concentration maps are determined by the quantiles in the data, because the concentrations are highly skewed. Our data shows no spatial pattern on the distribution of $^{10}Be_i$ concentrations (A). Erosion rates derived from $^{10}Be_i$ range from 0.02 and 0.39 mm/yr (B). Erosion rates calculated from $^{10}Be_i$ concentration at the outlet are representative of the entire upstream area of each watershed. No spatial pattern can be distinguished in the distribution of $^{10}Be_m$ activities (C). Insets show the distribution of ^{10}Be concentrations in our dataset.

Table 3.2: Summarized erosion rate for each major basin

River	Samples analyzed[1]	Erosion rates (mm/yr)			ANOVA[2]
		Range	Mean	SD	
Mekong	12	0.04 - 0.37	0.14	0.11	B
Salween	11	0.14 - 0.39	0.22	0.10	A
Irrawaddy	4	0.12 - 0.18	0.15	0.03	A, B
Red	8	0.02 - 0.16	0.09	0.05	B

[1] To calculate erosion rates, we used the error-weighted average of in channel and overbank sample at each site.
[2] Summary of ANOVA results. Categories not connected by the same letter are eroding at significantly different rates ($p < 0.05$).

Agricultural land use ($R^2 = 0.60$, $p < 0.01$), mean basin relief ($R^2 = 0.61$, $p < 0.01$) and basin area ($R^2 = 0.60$, $p < 0.01$), are significantly related to erosion rates in our dataset (Figure 3.3). The relationship between erosion and agricultural land use is inverse, whereas the relationships with area and relief are positive. We find that mean ksn (normalized channel steepness) ($R^2 = 0.55$, $p < 0.01$) and slope ($R^2 = 0.51$, $p < 0.01$) are strongly and positively correlated with erosion rates (Figure 3.3). Combining area and slope slightly increases the relationship with erosion rates ($R^2 = 0.72$, $p < 0.01$). There is no statistically significant relationship between erosion rates and peak ground acceleration in our dataset ($R^2 = 0.06$, $p= 0.14$). Our dataset shows a strong and inverse relationship between erosion rate and mean annual rainfall ($R^2 = 0.60$, $p < 0.01$). Evaluating the relationship between erosion rate and mean annual rainfall in each of the four major basins, we find that the relationship is inverse in all basins, but only significant for the Mekong and Salween. Similarly, area is significantly related to erosion rate in only the Mekong and Salween rivers, and positive in all watersheds. Slope and relief are significantly and positively related to erosion rate in the Mekong and Red watersheds only (see Table DR7 for regression information).

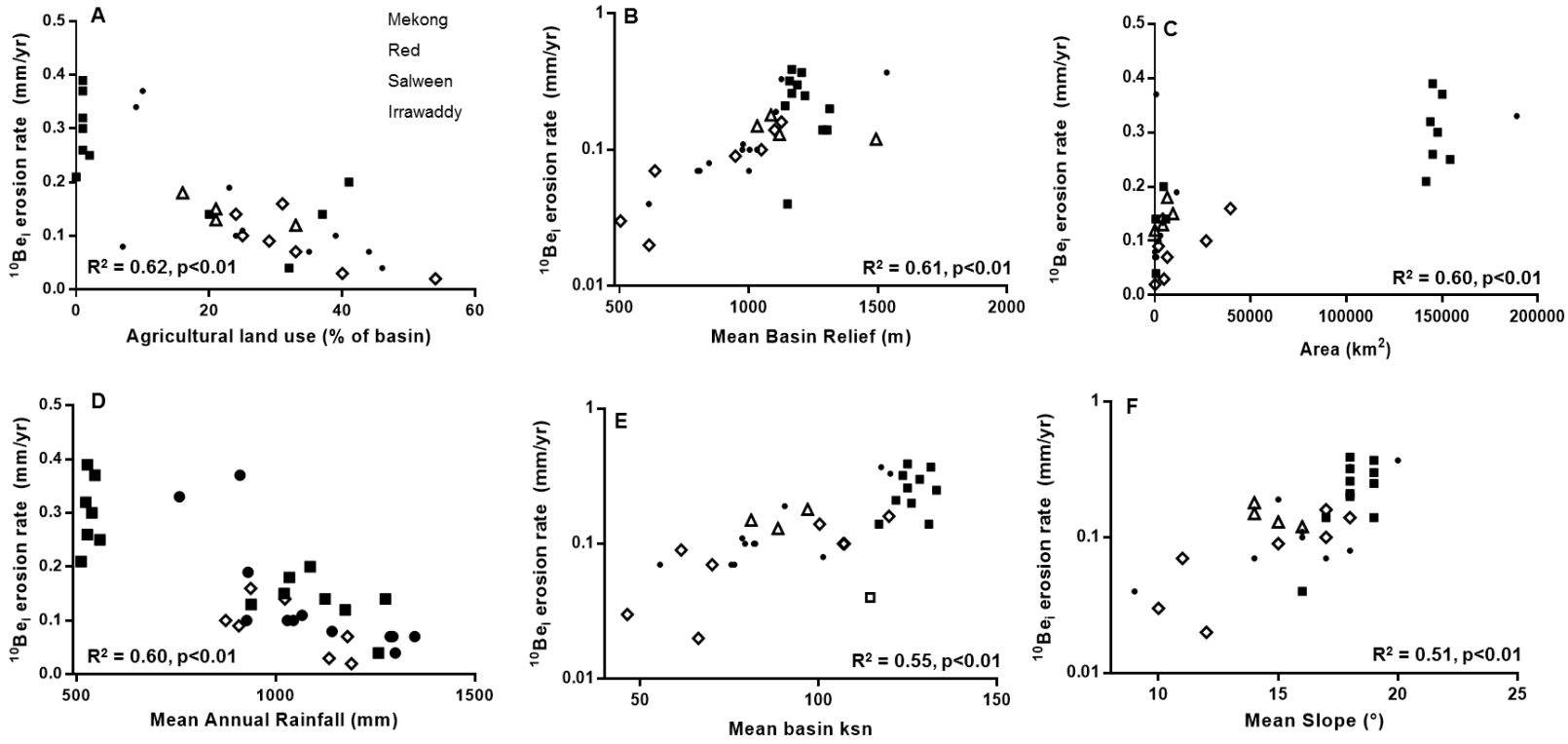

Figure 3.3: Relationship between erosion rate and topographic variables. Agricultural land use (A) and mean basin relief (B) have the strongest relationship with erosion in sampled watersheds in Yunnan.. Basin area (C) and mean annual rainfall (D) are also strongly related to erosion rates. Mean basin ksn (E) and slope (F) are positively related. Two outliers were removed in the regression plot for erosion rates and ksn, when considering those values, the relationship is not significant. Note the logarithmic Y-axis on panels (B), (E), and (F).

$^{10}Be_m$ concentration ranges from 0.30 to $9.07x10^7$ atoms/g. All samples from the Irrawaddy and most from the Salween River have isotopic activities in the order of 10^6 atoms/g (Figure 3.2C). Most samples from the Mekong and Red Rivers have activities on the order of 10^7 atoms/g. We found a significant, positive relationship between $^{10}Be_m$ concentrations and $^{10}Be_i$ concentration ($R^2 = 0.51$, $p = 0.01$) and agricultural land use ($R^2 = 0.21$, $p < 0.01$). $^{10}Be_m$ is inversely related to mean basin slope ($R^2 = 0.31$, $p = 0.01$) and relief ($R^2 = 0.32$, $p < 0.01$). $^{10}Be_m$ is not significantly related to area ($R^2 = 0.02$, $p = 0.46$), rainfall ($R^2 = 0.05$, $p = 0.19$), or ksn ($R^2 = 0.01$, $p = 0.50$).

Isotopic activity of $^{10}Be_i$ and $^{10}Be_m$ exhibits temporal variation over some of the timeframes we studied (Figure 3.4, Figure 3.5, Table 3.3; Table DR8). Comparing $^{10}Be_i$ over a 6-month period, we find 7 out of the 11 analyzed samples are within 10%. Only one sample (out of 6) is in agreement over a 6-month period for $^{10}Be_m$. The concentration of $^{10}Be_i$ and $^{10}Be_m$ varies when comparing in channel and overbank samples (interannual variation). For $^{10}Be_i$, 11 (out of 32) samples are within 10% of each other, $^{10}Be_m$ concentrations are within 10% in 10 out of the 29 samples. For both isotopes, the isotopic concentrations of in-channel samples are not significantly different from overbank samples. Over a decade, the concentration of $^{10}Be_m$ is only within 10% in one of 6 samples, while none are within 10% for $^{10}Be_i$. In 4 of the 11 samples we analyzed, $^{10}Be_i$ concentrations are within 10% over a millennial timeframe. The only statistically significant difference in our temporal comparisons is for $^{10}Be_i$ over a decade. Temporal comparisons exhibit a considerable amount of noise beyond analytical uncertainty, with

samples exceeding 100% difference in some cases although central tendencies of sample populations are similar.

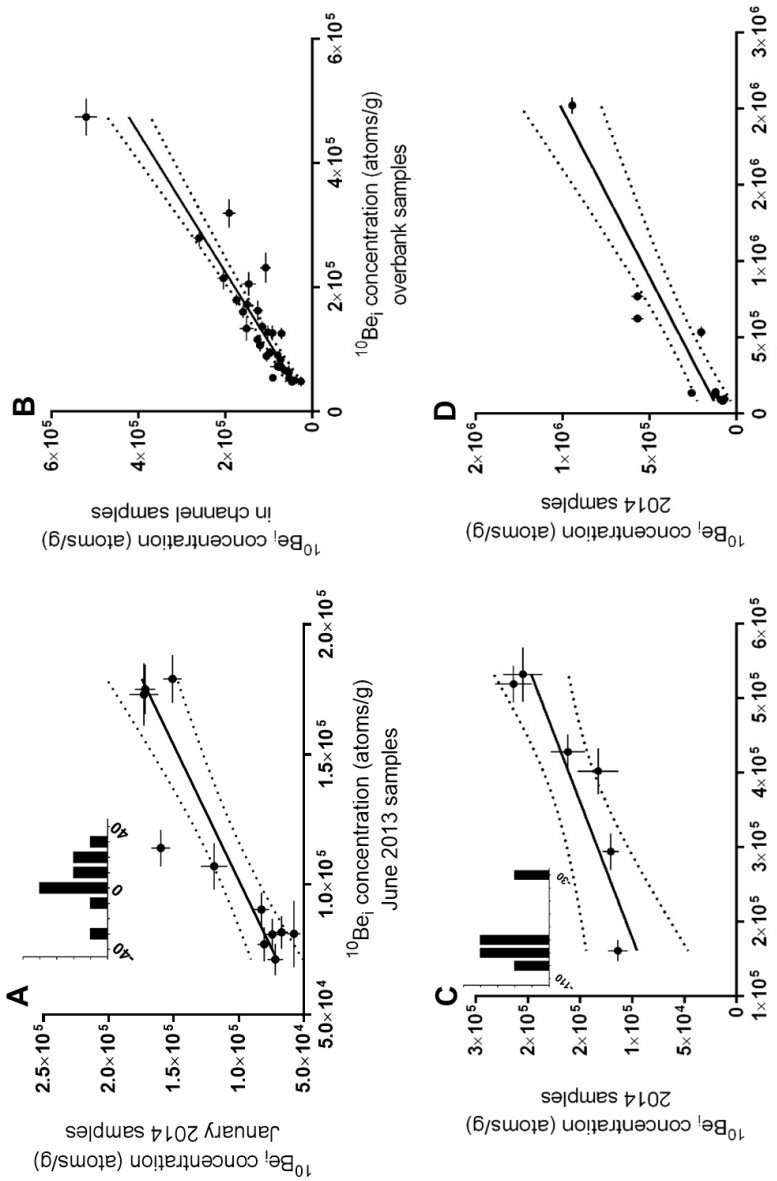

Figure 3.4: Temporal variation of $^{10}Be_i$ activity. $^{10}Be_i$ concentration does not change significantly in samples taken six months apart (A), or when comparing in channel and overbank samples (B). Similarities in concentration over a year suggest that there is no seasonal bias in sediment sourcing. Variations in isotopic activity are found when comparing concentrations of samples taken a decade apart (C). There is no significant difference in isotopic activity of sands from the active channel and terraces (D). In all plots, the dotted lines represent the 95% confidence interval of the regression between the temporal replicates, represented by the solid line. The error bars on the data are the 2σ of each measurement. Inset (histograms) show the distribution of percent difference between both isotopic measurements taken at one place of each temporal comparison.

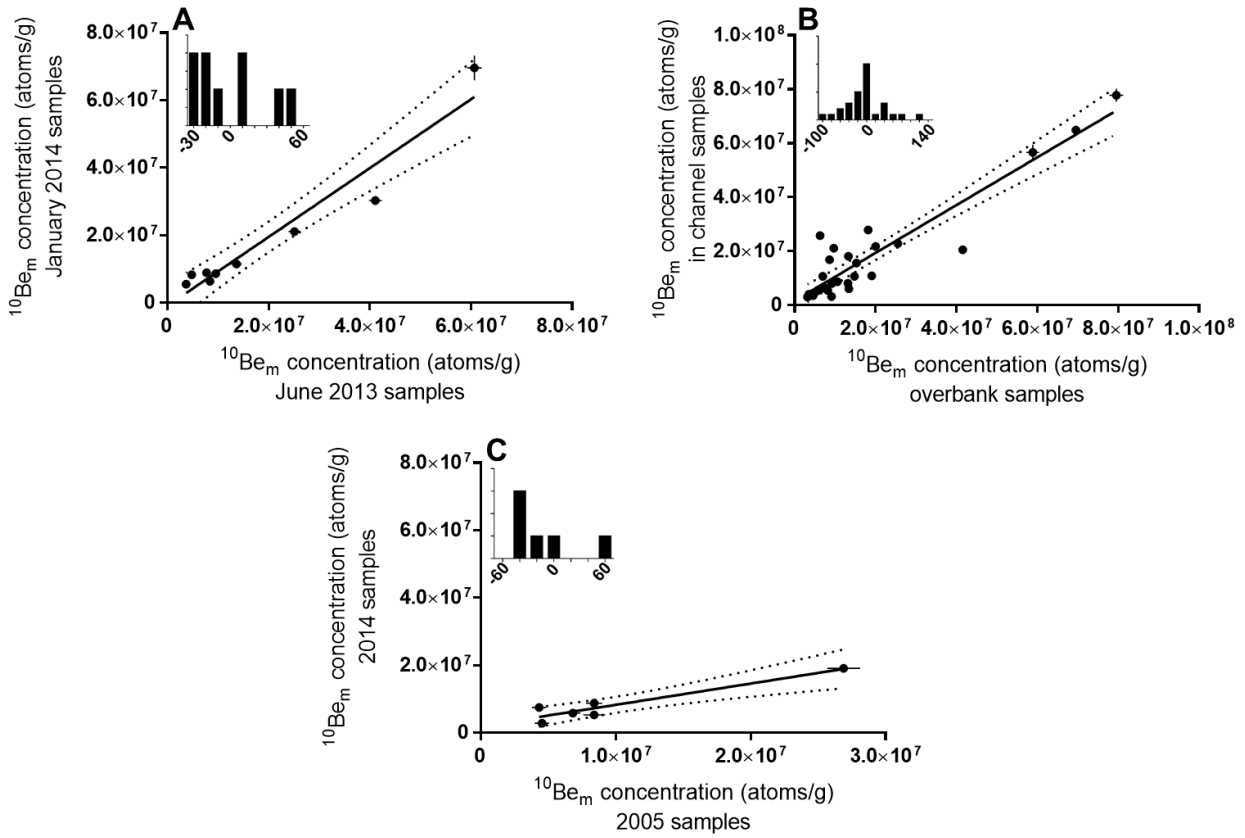

Figure 3.5: Temporal variation of $^{10}Be_m$ concentration. $^{10}Be_m$ activity reproduces well over a six month period (A). Our data suggest that seasonal differences in sediment sourcing do not affect $^{10}Be_m$ activity (B). We found no significant difference in $^{10}Be_m$ activity in samples taken roughly a decade apart (C). In all plots, the dotted lines represent the 95% confidence interval of the regression between the temporal replicates, represented by the solid line. The error bars on the data are the 2σ of the measurement. Inset (histograms) show the distribution of percent difference between both isotopic measurements taken at one place of each temporal comparison.

Table 3.3: Summary findings on temporal comparisons of isotopic concentrations

Temporal comparison	Isotope	Samples		Wilcoxon test results[2]		Percent difference		
		Included in analysis	Within error of each other[1]	t	p	Range	Mean	SD
6 months	$^{10}Be_i$	11	7	-7.50	0.49	- 34 to 33	4	0.17
	$^{10}Be_m$	9	1	-3.50	0.73	-30 to 54	2	0.30
Interannual	$^{10}Be_i$	32	11	-90.5	0.06	-72 to 52	-9	0.24
	$^{10}Be_m$	29	10	50.0	0.29	-97 to 121	-5	0.45
Decade	$^{10}Be_i$	6	0	-10.5	0.03	-101 to -34	-80	21
	$^{10}Be_m$	6	1	-4.50	0.44	-46 to 54	-14	0.35
Millennia	$^{10}Be_i$	11	4	-9.50	0.30	-72 to 77	6	0.43

[1] Samples that are within 10% of their temporal replicate are considered within error.
[2] When the value of the Wilcoxon test statistic is < 0.05, we reject the hypothesis that samples are from the same population.

Long-term sediment yields calculated from $^{10}Be_i$ data range between 45 and 930 tons km^{-2} yr^{-1}, assuming a rock density of 2.7 g/cm^3. Modern sediment yields calculated from hydrology station data vary between 21 and 2,879 tons km^{-2} yr^{-1} (Schmidt et al., 2011) (Table DR9). There is a statistically significant difference between the modern and long term sediment yields when considering the population of all stations ($n = 21$, $t = -94.5$, $p < 0.01$). In most sites that we compared (15 out of 21), the contemporary sediment yield is higher than the long-term (ratios range from 1.5 to 24). There are four sites that have a higher long-term sediment yield (ratios range from 0.3 to 0.8), and two sites where the sediment yields are similar (ratios from 0.9 to 1.2). Although there are no statistically significant differences in sediment yield ratios between samples in all four basins ($F= 1.7$, $p= 0.21$), the ratios in the Salween river are higher than in other basins (average ratio = 9.1), although this is due to one high ratio of 24. If the ratio of 24 is removed, the difference in ratios by watershed becomes significant ($F= 3.75$, $p= 0.04$), but the results are not statistically representative, since there are only two samples from the Salween basin. Therefore, we keep the ratio of 24 in our analysis. Ratios from the Irrawaddy ($\mu=1.7$), and

Mekong (μ=1.7) rivers are significantly different than ratios in the Salween basin. Ratios in the Red (μ=3.3) River basin are not significantly different from those in any other river (Figure 3.6A).

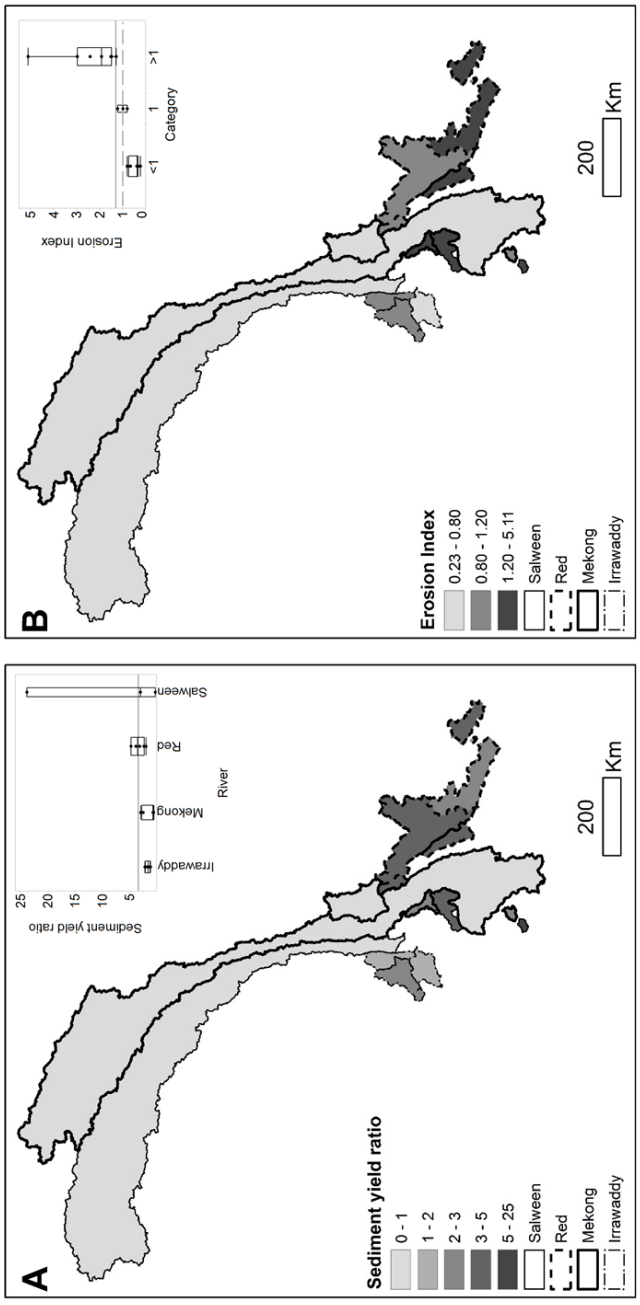

Figure 3.6: Spatial variation of sediment yield ratios and erosion indices. Sediment yields (A) represent the ratio of modern (hydrology stations data) to long-term yield (cosmogenically-determined erosion rates). Inset shows the distribution of sediment yield ratios per watershed. Erosion indices show no spatial pattern (B). Inset shows the distribution of erosion indices in our dataset. Solid line shows the mean of our dataset. Dashed line represents an erosion index of 1, a basin with balanced soil erosion and formation

Erosion indices calculated from modern sediment data range between 0.2 and 5.1, averaging 1.3 (Table DR10). There is no statistically significant difference in erosion indices by major watershed (F= 2.68, p = 0.09). There are seven sites with an erosion index greater than one, and six sites with erosion index below one. Five sites have an erosion index close to one (0.8 – 1.2) (Figure 3.6B).

Discussion

Temporal replicates

The temporal variability of cosmogenic ^{10}Be concentration in river sediment has been infrequently studied (Matmon et al., 2003; Reusser and Bierman, 2010; Lupker et al., 2012; Granger and Riebe, 2007, Sosa Gonzalez, 2012; Cox et al., 2009) (Table 3.4). Our work adds 44 $^{10}Be_m$ and 59 $^{10}Be_i$ pairs of replicates to previously published temporal analyses.

Table 3.4: Summarized data on previously published ^{10}Be temporal replicates

Publication	Study sites	Isotope analyzed	Basin area (km^2)	Samples	
				Included in analysis	Within error
Schaller et al., 2002	France, Netherlands	$^{10}Be_i$	Not reported	14	14
Matmon et al., 2003	Great Smoky Mountains	$^{10}Be_i$	330	1	1
Granger and Riebe, 2007	Fort Sage Mountains	$^{10}Be_i$	0.132	1	1
Cox et al., 2009	Madagascar	$^{10}Be_i$	134 to 209	2	2
Reusser and Bierman, 2010	New Zealand	$^{10}Be_m$	130 to 1560	3	2
Lupker et al., 2012	Himalayas	$^{10}Be_i$	873,240	1	1
Sosa Gonzalez, 2012	Panama	$^{10}Be_i$	57 to 59	2	2

Increased precipitation during the monsoon season increases suspended sediment delivery and river discharge (Henck et al., 2010). Our paired in channel/overbank sediments, as well as samples taken six months apart, allow us to test for differences in sediment sourcing as a function of seasonal changes, primarily, the monsoon. Our replicate

samples show non-systematic noise above the analytic uncertainty (Figure 3.4, Figure 3.5, Table 3.3, Table DR8). For example, for a series of 6 nested samples along the mainstem of the Salween River, 1 sample is within 10% for $^{10}Be_m$ temporal replicates, while 5 samples are not. Furthermore, the sample that agrees is nested among samples that are not within 10%. None of the samples are within 10% for $^{10}Be_i$ in these nested samples. In general, at any given site where both isotopes were measured over time, $^{10}Be_i$ concentration reproduced better than $^{10}Be_m$. The agreement in both $^{10}Be_i$ and $^{10}Be_m$ concentrations of in channel and overbank samples suggest that while the monsoon increases water discharge and sediment delivery, it does not alter sediment sourcing in any systematic way.

Although there is no statistically significant difference between the isotopic concentration of active channel and terrace sands, most of the samples are not within 10% of each other. Of all our terrace replicate samples (n=11), only four have $^{10}Be_i$ concentrations within 10% of contemporary channel sediment. One of these terraces (CH-040) is modern (0 ± 20 ^{14}C ybp), two are about a century in age (CH-019, 115 ± 15 ^{14}C ybp; CH-038, 130 ± 20 ^{14}C ybp), and the other is older (CH-124, 2570 ± 20 ^{14}C ybp).

Our data show poor reproducibility in samples taken roughly a decade apart. Only one site (out of 6) shows $^{10}Be_m$ concentrations within 10% of each other (CH-170). $^{10}Be_i$ concentration varies by more than 10% in all 6 sites we compared over a decadal timeframe. We attribute these differences, at least in part, to analytical differences. The quartz isolation and $^{10}Be_i$ extraction took place in two different laboratory facilities, with slight variations in the methodological approach. The isotopic ratios were also measured at different AMS facilities.

Comparison between long-term and modern sediment yields

Long-term $^{10}Be_i$-based and contemporary sediment yields have been compared before, with varying results (e.g., Hewawasam et al., 2003; Vanacker et al., 2007; Reusser et al., 2015). In some cases, the landscape appears to be in a steady state, where the contemporary and long-term sediment yields are similar (Matmon et al., 2003; Gellis et al., 2004; Nichols et al., 2005; Vanacker et al., 2007; Cyr and Granger, 2008; Bellin et al 2012; Nichols et al., 2014). In regions where contemporary sediment yields are lower than the $^{10}Be_i$-based erosion rates, it is possible that the contemporary measurements are not capturing stochastic events (mass wasting or extreme precipitation events), thereby lowering the calculated contemporary sediment yield (Bierman et al., 2001; Kirchner et al., 2001; Schaller et al., 2001; Humphreys et al., 2006). Previous work has found contemporary sediment yields significantly higher than long-term yields in regions with a long history of human activity, such as deforestation and intensive agriculture (Brown et al., 1998; Clapp et al., 2000; Hewawasam et al., 2003; Bierman et al., 2005; Reusser et al., 2014).

We find that in most sites (15 of 21), contemporary sediment yields surpass long-term rates of sediment generation determined from $^{10}Be_i$ (average ratio = 3.5). This may be a function of the relatively short period considered for contemporary sediment yield measurements compared to $^{10}Be_i$-based sediment generation rates or could be related to human land use. The contemporary sediment yield data we used spans the years (1950s-1980s) when deforestation was widespread across Yunnan. It is possible that this is driving the difference we measure. Contemporary sediment yield measurements are easily biased

by extreme events such as landslides or a high-intensity precipitation (Kirchner et al., 2001). However, this seems unlikely in our study area as a change in monsoon intensity would affect the entire study area. Thus, it seems more likely that agriculture and deforestation have elevated sediment yield (e.g., Hooke, 2000). We find that the watersheds with contemporary sediment yield, higher than long-term rates have on average 35% agricultural land, compared to an average agricultural land use of 18% in watersheds where the contemporary sediment yield is similar or lower than long-term erosion rates. This suggests that using the land for agriculture can significantly increase sediment delivery. Field observations of monocultures on steep slopes, agriculture in floodplains, in many cases reaching the river banks, and slash and burn practices support this hypothesis (Figure 3.7). Riverbed material dredging is very common in our field area. It is possible that scouring sediments from the river channel as a result of sand mining also increases contemporary sediment yields.

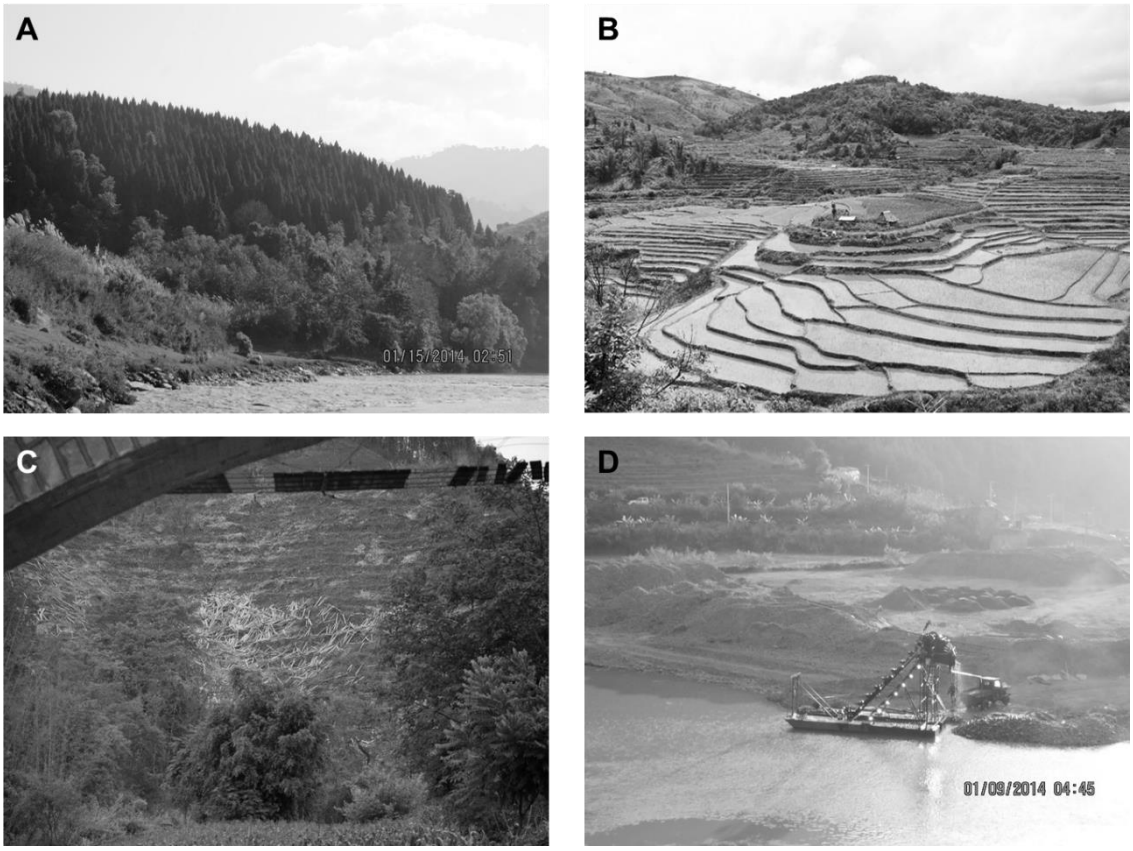

Figure 3.7: Field photographs documenting landuse impacts. Reforestation projects have established monocultures along steep slopes in Yunnan (A) (site of CH-142/CH-143). Rice paddies are common in the field area (B). Agricultural practices include slash and burn (site of CH-114) (C). River sand mining is also common in some of the rivers we sampled (site of CH-117/CH-118) (D). Photographs by Thomas B. Neilson and Adrian Singleton.

In addition to increasing modern sediment yield, human activity can also decrease sediment yield. For example, dams and reservoirs trap sediment before it exits the basin, reducing the sediment yield (Reusser et al., 2014). Dams in our study area post-date the available sediment data (ending in 1987) (FAO, 2015). In the four basins (CH-119, CH-121, CH-147, CH-155) where the modern sediment yield is lower than the long-term, terraced rice paddies are a common agricultural practice. Field observations and satellite

imagery confirm that rice paddies comprise a significant part of these four basins. We suspect that the rice paddies are efficient sediment traps, similar to dams.

Our erosion index data also provide insight of the impact of humans on the landscape. Although it is not statistically significant, the average percentage of agricultural land use is greater in basins that are exporting sediment at a faster rate than it is being produced (μ = 35% cultivated land, n = 7). The basins exporting sediment at a rate slower than it is produced, therefore suggesting sediment storage, average 20% cultivated land (n = 7). The difference in these rates further shows the impact of human activities on surface processes. Because erosion indices are derived directly from sediment yield data, our EI data reflects in part spatial trends of sediment yield.

Relationship of erosion rates to topography and climate variables

A relationship between erosion rates and topography has been found at the regional and global scale (Portenga and Bierman, 2011). While our long-term erosion rate data show a statistically significant relationship with slope, other topographic variables (relief and ksn) are also strongly related to erosion rates in our dataset. Previously published studies have found a direct relationship between ksn and erosion rates in tectonically active regions (e.g. Safran et al., 2005; Ouimet et al., 2009; DiBiase et al., 2010; Vanacker et al., 2015). The lack of relationship between erosion and PGA in our dataset suggest that while our study area is tectonically active and similar to settings where ksn has been related to erosion, tectonism is not driving the relationship between erosion and ksn. Our findings suggest that topography is the strongest control of erosion rates in our study area.

The effects of climate on erosion rates has been debated, with some studies finding a strong relationship (e.g. Montgomery et al., 2001), whereas others have found a minimal climatic control on erosion (e.g. Riebe et al., 2001). Although rainfall is significantly and negatively related to erosion in our dataset, there is also a significant and inverse relationship between rainfall and slope in our data (R^2 = 0.67, p <0.01). Similarly, agricultural land use is significant and inversely related to erosion (R^2 = 0.62, p <0.01) and to slope (R^2 = 0.44, p <0.01). There is also a positive relationship between agriculture and rainfall in our dataset (R^2 = 0.67, p <0.01). It is likely that the co-variance between slope, rainfall, and agriculture is driving the inverse relationships we find in our analyses.

Our results suggest that topography controls long-term rates of erosion in our study area. Steepness of the hillslopes decreases towards the south of our study area, which is farther from the Tibetan plateau and the active India-Eurasia plate collision zone. Southerly parts of our field area have more monsoon-related precipitation. Agriculture is more prevalent in the less steep portions of the landscape, where it is wetter. However, erosion is faster on steeper, drier hillslopes in our study area.

Conclusions

We present an extensive dataset of replicate samples, spanning time intervals of 6 months to millennia, in which we measured ^{10}Be concentrations. While there is noise beyond analytical uncertainty, the central tendencies are similar in most comparisons, suggesting that the time-invariant ^{10}Be concentration is a valid assumption. Furthermore, our data show that the monsoon does not alter sediment sourcing to rivers in Yunnan. This

is a very important finding for cosmogenic studies, since we now know that the time of the year when rivers are sampled does not change the resulting numbers.

Our analysis of denudation in Yunnan shows that topography exerts a first-order control on long-term erosion rates, while climate exerts a second-order control. Human alterations of the landscape have increased contemporary sediment yields in our study area, compared to long-term erosion rates. Erosion index data from our basins further demonstrate human impacts on surface processes, since most sites show a net export of meteoric ^{10}Be. Background, long-term erosion rates presented here serve as a benchmark to compare future alterations of the landscape. These background erosion rate data are important because many dams, which will undoubtedly change sediment yields, are proposed or already operating in the Salween and Mekong Rivers (Lu and Siew, 2006; Magee, 2006).

Acknowledgements

This work was supported by funding from the US National Science Foundation awarded to A. H. Schmidt (NSF-EAR-1114166), P. Bierman (NSF-EAR-1114159), and D. H. Rood (NSF-EAR-1114436). We thank L. Corbett, A. Lubeck, and J. Southon for the ^{14}C analyses of the charcoal samples. The authors thank D. McPhillips for collecting and providing sample Y13-01-DM. We thank T. Neilson, C.M. Zhang, R.J. Wei, J.A. Bower, A. Singleton, and Y. Qiu for their field assistance.

References

Andermann, C., Bonnet, S., Gloaguen, R., 2011. Evaluation of precipitation data sets along the Himalayan front. Geochemistry, Geophysics, Geosystems 12.

Balco, G., Briner, J., Finkel, R.C., Rayburn, J.A., Ridge, J.C., Schefer, J.M., 2009. Regional beryllium-10 production rate calibration for late-glacial northeastern North American. Quaternary Geology 4, 93-107.

Balco, G., Stone, J.O., Lifton, N.A., Dunai, T.J., 2008. A complete and easily accessible means of calculating surface exposure ages or erosion rates from ^{10}Be and ^{26}Al measurements. Quaternary Geology 3, 174-195.

Bellin, N., Vanacker, V., Kubik, P., 2012. Contrasting modern and ^{10}Be-derived erosion rates for the Southern Betic Cordillera, Spain, EGU General Assembly 2012

Bierman, P.R., Clapp, E.M., Nichols, K., Gillespie, A., Caffee, M.W., 2001. Using cosmogenic nuclide measurements in sediments to understand background rates of erosion and sediment transport, in: Harmon, R.S., Doe, W.M. (Eds.), Landscape erosion and evolution modeling Kluwer, New York, pp. 89-116.

Bierman, P.R., Reuter, J.M., Pavich, M.J., Gellis, A.C., Caffee, M.W., Larsen, J., 2005. Using cosmogenic nuclides to contrast rates of erosion and sediment yield in a semi-arid, arroyo-dominated landscape, Rio Puerco Basin, New Mexico. Earth Surface Processes and Landforms 30, 935-953.

Bierman, P.R., Steig, E.J., 1996. Estimating rates of denudation using cosmogenic isotope abundances in sediment. Earth Surface Processes and Landforms 21, 125-139.

Brandt, J., Kuemmerle, T., Li, H., Ren, G., Zhu, J., Radeloff, V.C., 2012. Using Landsat imagery to map forest change in southwest China in response to the national logging ban and ecotourism development. Remote Sensing of Environment 121, 358-369.

Brown, E.T., Stallard, R.F., Larsen, M.C., Bourlès, D., Raisbeck, G.M., Yiou, F., 1998. Determination of predevelopment denudation rates of an agricultural watershed (Cayaguás River, Puerto Rico) using in-situ produced ^{10}Be in river-born quartz. Earth and Planetary Science Letters 160, 723-728.

Brown, E.T., Stallard, R.F., Larsen, M.C., Raisbeck, G.M., Yiou, F., 1995. Denudation rates determined from the accumulation of in-situ produced ^{10}Be in the Luquillo Experimental Forest, Puerto Rico. Earth and Planetary Science Letters 129, 193-202.

Brown, L., Pavich, M.J., Hickman, R.E., Klein, J., Middleton, R., 1988. Erosion of the Eastern United States observed with ^{10}Be. Earth Surface Processes and Landforms 13, 441-457.

Burchfiel, B.C., Chen, L., Wang, E., Swanson, E., 2008. Preliminary investigation into the complexities of the Ailao Shan and Day Nui Con Voi shear zones of SE Yunnan and Vietnam. Geological Society of America Special Paper 444.

Burchfiel, B.C., Chen, Z., 2012a. Lhasa Unit, in: Condie, K., Harvey, F.E. (Eds.), Tectonics of the Southeastern Tibetan Plateau and its adjacent foreland. The Geological Society of America, Boulder, CO, pp. 117-126.

Burchfiel, B.C., Chen, Z., 2012b. Qiangtang Unit, in: Condie, K., Harvey, F.E. (Eds.), Tectonics of the Southeastern Tibetan Plateau and its adjacent foreland. The Geological Society of America, Boulder, CO, pp. 77-96.

Campforts, B., Vanacker, V., Vanderborght, J., Baken, S., Smolders, E., Govers, G., 2016. Simulating the mobility of meteoric ^{10}Be in the landscape through a coupled soil-hillslope (Be2D). Earth and Planetary Science Letters 439, 143-157.

Chen, J., Chen, J., Liao, A., Cao, X., Chen, L., He, C., Han, G., Peng, S., Lu, M., Zhang, W., Tong, X., Mills, J., 2015. Global land cover mapping at 30 m resolution: A POK-based operational approach. ISPRS Journal of Photogrammetry and Remote Sensing 103, 7-27.

Clapp, E.M., Bierman, P.R., Schick, A., P., Lekach, J., Enzel, Y., Caffee, M.W., 2000. Sediment yield exceeds sediment production in arid region drainage basins. Geology 28, 995-998.

Corbett, L.B., Bierman, P.R., Rood, D.H., 2016. An approach for optimizing in situ cosmogenic ^{10}Be sample preparation. Quaternary Geology 33, 24-34.

Cox, R., Bierman, P.R., Jungers, M.C., Rakotondrazafy, A.F.M., 2009. Erosion rates and sediment sources in Madagascar inferred from ^{10}Be Analysis of lavaka, slope, and river sediment Journal of Geology 117, 363-376.

Cyr, A.J., Granger, D.E., 2008. Dynamic equilibrium among erosion, river incision, and coastal uplift in the northern and central Apennines, Italy. Geology 36, 103-106.

DiBiase, R.A., Whipple, K.X., Heimsath, A.M., Ouimet, W.B., 2010. Landscape form and millennial erosion rates in the San Gabriel Mountains, CA. Earth and Planetary Science Letters 289, 134-144.

Dunai, T.J., Lifton, N.A., 2014. The Nuts and Bolts of Cosmogenic Nuclide Production. Elements 10, 347-350.

Elmore, D., Phillips, F.M., 1987. Accelerator mass spectrometry for measurement of long-lived radioisotopes. Science 236, 543-550.

Fang, J., Xie, Z., 1994. Deforestation in preindustrial China: The Loess plateau region as an example. Chemosphere 29, 983-999.

FAO, 2015. Georeferenced dams database, in: Nations, Food and Agriculture Organization of the United Nations (Ed.).

Gellis, A.C., Pavich, M.J., Bierman, P.R., Clapp, E.M., Ellevein, A., Aby, S., 2004. Modern sediment yield compared to geologic rates of sediment production in a semi-arid basin, New Mexico: Assessing the human impact. Earth Surface Processes and Landforms 29, 1359-1372.

Giardini, D., 1999. The Global Seismic Hazard Assessment Program (GSHAP) - 1992/1999. Annals of Geophysics 42, 957-974.

Graly, J.A., Bierman, P.R., Reusser, L.J., Pavich, M.J., 2010. Meteoric ^{10}Be in soil profiles - A global meta-analysis. Geochimica et Cosmochimica Acta 74, 6814-6829.

Graly, J.A., Reusser, L.J., Bierman, P.R., 2011. Short and long-term delivery rates of meteoric ^{10}Be to terrestrial soils. Earth and Planetary Science Letters 302, 329-336.

Granger, D.E., Kirchner, J.W., Finkel, R.C., 1996. Spatially averaged long-term erosion rates measured from in-situ produced cosmogenic nuclides in alluvial sediment. The Journal of Geology 104, 249-257.

Granger, D.E., Riebe, C.S., 2007. Cosmogenic nuclides in weathering and erosion, in: Drever, J.I. (Ed.), Treatise on geochemistry. Elsevier, London, UK.
He, F., Li, S., Zhang, X., 2015. A spatially explicity reconstruction of forest cover in China over 1700-2000. Global and Planetary Change 131, 73-81.
Henck, A.C., Huntington, K.W., Stone, J.O., Montgomery, D.R., Hallet, B., 2011. Spatial controls on erosion in the Three Rivers Region, southeastern Tibet and southwestern China. Earth and Planetary Science Letters 303, 71-83.
Henck, A.C., Montgomery, D.R., Huntington, K.W., Liang, C., 2010. Monsoon control of effective discharge, Yunnan and Tibet. Geology 38, 975-978.
Hewawasam, T., Von Blanckenburg, F., Schaller, M., Kubik, P.W., 2003. Increase of human over natural erosion rates in tropical highlands constrained by cosmogenic nuclides. Geology 33, 597-600.
Heyman, J., Stroeven, A.P., Harbor, J.M., Caffee, M.W., 2011. Too young or too old: Evaluating cosmogenic exposure dating based on an analysis of compiled boulder exposure ages. Earth and Planetary Science Letters 203, 71-80.
Hooke, R.L., 2000. On the history of humans as geomorphic agents. Geology 28, 843-846.
Hui, F., Jinming, H., Daming, H., 2013. Trends in precipitation over the low latitude highlands of Yunnan, China. Journal of Geographical Sciences 23, 1107-1122.
Humphreys, G.S., Tomkins, K.M., Wilkinson, M.T., Fink, D., Shakesby, R.A., Doerr, S.H., Walbrink, P.J., Blake, W.H., 2006. Longer-term and contemporary denudation rates, and the role of extreme events along a passive margin, Australia, Goldschmidt Conference Melbourne, Australia.
Jungers, M.C., Bierman, P.R., Matmon, A., Nichols, K., Larsen, J., Finkel, R., 2009. Tracing hillslope sediment production and transport with in situ and meteoric ^{10}Be. Journal of Geophysical Research 114.
Kirchner, J.W., Finkel, R., C., Riebe, C.S., Granger, D.E., Clayton, J.L., King, J.G., Megahan, W.F., 2001. Mountain erosion over 10 yr, 10 k.y., and 10 m.y. time scales. Geology 29, 591-594.
Kohl, C.P., Nishiizumi, K., 1992. Chemical isolation of quartz for measurement of in-situ produced cosmogenic nuclides. Geochimica et Cosmochimica Acta 56, 3583-3587.
Kummu, M., Varis, O., 2007. Sediment-related impacts due to upstream reservoir trapping, the Lower Mekong River. Geomorphology 85, 275-293.
Lal, D., 1991. Cosmic ray labeling of erosion surfaces: in situ nuclide production rates and erosion models. Earth and Planetary Science Letters 104, 424-439.
Lal, D., 2000. Cosmogenic ^{10}Be: A critical view on its widespread dominion in geosciences. Journal of Earth System Science 109, 181-186.
Lal, D., Peters, B., 1967. Cosmic ray produced radioactivity on the earth. Springer, Berlin, pp. 551-612.
Leloup, P.H., Lacassin, R., Tapponnier, P., Schärer, U., Dalai, Z., Xiaohan, L., Liangshang, Z., Schaocheng, J., Trinh, P.T., 1995. The Ailao Shan-Red River shear zone (Yunnan, China), Tertiary transform boundary of Indochina. Tectonophysics 251, 3-84.

Lu, X.X., Siew, R.Y., 2006. Water discharge and sediment flux changes over the past decades in the Lower Mekong River: possible impacts of the Chinese dams. Hydrology and Earth System Sciences 10, 181-195.

Lupker, M., Blard, P.-H., Lavé, J., France-Lanord, C., Leanni, L., Puchol, N., Charreau, J., Bourlès, D., 2012. ^{10}Be-derived Himalayan denudation rates and sediment budgets in the Ganga basin. Earth and Planetary Science Letters 333-334, 146-156.

Mackey, B.H., Scheingross, J.S., Lamb, M.P., Farley, K.A., 2014. Knickpoint formation, rapid propagation, and landscape response following coastal cliff retreat at the last interglacial sea-level highstand: Kaua'i, Hawai'i. Geological Society of America Bulletin 126, 925-942.

Magee, D., 2006. Powershed politics: Yunnan hydropower under Great Western development. The China Quarterly 185, 23-41.

Matmon, A., Bierman, P.R., Larsen, J., Southworth, S., Pavich, M.J., Finkel, R.C., Caffee, M.W., 2003. Erosion of an ancient mountain range, the Great Smoky Mountains, North Carolina and Tennessee. American Journal of Science 303, 517-855.

McHargue, L.R., Damon, P.E., 1991. The global beryllium-10 cycle. Reviews of Geophysics 29, 141-158.

McKean, J.A., Dietrich, W.E., Finkel, R.C., Southon, J.R., Caffee, M.W., 1993. Quantification of soil production and downslope creep rates from cosmogenic ^{10}Be accumulations on a hillslope profile. Geology 21, 343-346.

Monaghan, M.C., McKean, J.A., Dietrich, W.E., Klein, J., 1992. ^{10}Be chronometry of bedrock-to-toil conversion rates. Earth and Planetary Science Letters 111, 483-492.

Montgomery, D.R., Balco, G., Willett, S.D., 2001. Climate, tectonics and the morphology of the Andes. Geology 29, 579-582.

NASA LP-DAAC, 2012. ASTER GDEM.

Nichols, K., Bierman, P.R., Rood, D.H., 2014. ^{10}Be constrains the sediment sources and sediment yields to the Great Barrier Reef from the tropical Barron River catchment, Queenslad, Australia. Geomorphology 224, 102-110.

Nichols, K.K., Bierman, P., Finkel, R., C., Larsen, J., 2005. Long-term sediment generation rates for the Upper Río Chagres Basin: Evidence from cosmogenic ^{10}Be, in: Harmon, R.S. (Ed.), The Río Chagres, Panama: A multidisciplinary profile of a tropical watershed. Springer, The Netherlands.

Nichols, K.K., Bierman, P., Rood, D.H., 2014. ^{10}Be constrains the sediment sources and sediment yields to the Great Barrier Reef from the tropical Barron River catchment, Queensland, Austrlia. Geomorphology 224, 102-110.

Niemi, N.A., Oskin, M., Burbank, D.W., Heimsath, A.M., Gabet, E.J., 2005. Effects of bedrock landslides on cosmogenically determined erosion rates. Earth and Planetary Science Letters 237, 480-498.

Nishiizumi, K., Imamura, M., Caffee, M.W., Southon, J.R., Finkel, R.C., McAninch, J., 2007. Absolute calibration of ^{10}Be AMS standards. Nuclear Instruments and Methods B 258, 403-413.

Nishiizumi, K., Kohl, C.P., Arnold, J.R., Dorn, R., Klein, J., Fink, D., Middleton, R., Lal, D., 1993. Role of in situ cosmogenic nuclides ^{10}Be and ^{26}Al in the study of diverse geomorphic processes. Earth Surface Processes and Landforms 18, 407-425.

Ouimet, W.B., Whipple, K.X., Granger, D.E., 2009. Beyond threshold hillslopes: Channel adjustment to base-level fall in tectonically active mountain ranges. Geology 37, 579-582.

Portenga, E.W., Bierman, P.R., 2011. Understanding Earth's eroding surface with ^{10}Be. GSA Today 21, 4-10.

Portenga, E.W., Bierman, P.R., Duncan, C., Corbett, L.B., Kehrwald, N.M., Rood, D.H., 2015. Erosion rate of the Bhutanese Himalaya determined using in situ-produced ^{10}Be. Geomorphology 233, 112-126.

Reusser, L.J., Bierman, P.R., 2010. Using meteoric ^{10}Be to track fluvial sand through the Waipaoa River basin, New Zealand. Geology 38, 47-50.

Reusser, L.J., Bierman, P.R., Rood, D.H., 2014. Quantifying human impacts on rates of erosion and sediment transport at a landscape scale. Geology 43, 171-174.

Riebe, C.S., Kirchner, J.W., Granger, D.E., Finkel, R., C., 2001. Minimal climatic control on erosion rates in the Sierra Nevada, California. Geology 29, 447-450.

Rozelle, S., Huang, J., Zhang, L., 1997. Poverty, population and environmental degradation in China. Food Policy 22, 229-251.

Safran, E.B., Bierman, P.R., Aalto, R., Dunne, T., Whipple, K.X., Caffee, M.W., 2005. Erosion rates driven by channel network incision in the Bolivian Andes. Earth Surface Processes and Landforms 30, 1007-1024.

Sanjiang, Geology of., 1986. Geological map of Nujiang, Lancang, and Jinsha Rivers area, in: Resources, M.o.G.a.M. (Ed.). Geological Publishing House.

Santos, G.M., Moore, R.B., Southon, J.R., Griffin, S., Hinger, E., Zhang, D., 2007. AMS 14C sample preparation at the KCCAMS/UCI facility: Statys report and performance of small samples. Radiocarbon 49, 255-269.

Schaller, M., von Blanckenburg, F., Veldkamp, A., Tebbens, L.A., Hovius, N., Kubik, P.W., 2002. A 30 000 yr record of erosion rates from cosmogenic ^{10}Be in Middle European river terraes. Earth and Planetary Science Letters 204, 307-320.

Schmidt, A.H., Montgomery, D.R., Huntington, K.W., Liang, C., 2011. The question of communist land degradation: New evidence from local erosion and basin-wide sediment yield in Southwest China and Southeast Tibet. Annals of the Association of American Geographers 101, 1-20.

Schoenbohm, L.M., Whipple, K.X., Burchfiel, B.C., Chen, L., 2004. Geomorphic constraints on surface uplift, exhumation, and plateau growth in Red River region, Yunnan Province, China. GSA Bulletin 116, 895-909.

Shapiro, J., 2008. Mao's war against Nature: Politics and the Environment in Revolutionary China. Cambridge University Press, Cambridge, UK.

Sosa-Gonzalez, V., 2012. Determining long-term erosion rates in Panama: An application of ^{10}Be, The Rubenstein School of Environment and Natural Resources. University of Vermont, Burlington, VT, USA, p. 114.

Stone, J., 1998. A rapid fusion method for separation of beryllium-10 from soils and silicates. Geochimica et Cosmochimica Acta 62, 555-561.

Stone, J.O., 2000. Air pressure and cosmogenic isotope production. Journal of Geophysical Research 105, 23,573-523,579.

Strobl, M., Hetzel, R., Niedermann, S., Ding, L., Zhang, L., 2012. Landscape evolution of a bedrock peneplain on the southern Tibetan Plateau revealed by in situ-produced cosmogenic ^{10}Be and 21Ne. Geomorphology 153-154, 192-204.

Sültenfuβ, J., Purtschert, R., Führböter, J.E., 2010. Age structure and recharge conditions of a coastal aquifer (northern Germany) investigated with 39Ar, 14C, 3H, He, isotopes and Ne. Hydrogeology Journal 19, 221-236.

Trac, C.J., Harrell, S., Hinckley, T.M., Henck, A.C., 2007. Reforestation programs in Southwest China: Reported success, observed failures, and the reasons why. Journal of Mountain Science 4, 275-292.

Trac, C.J., Schmidt, A.H., Harrell, S., Hinckley, T.M., 2013. Is the returning farmland to forest program a success? Three case studies from Sichuan. Environmental Practice 15, 350-366.

Turekian, K.K., Cochran, J.K., Krishnaswami, S., Lanford, W.A., Parker, P.D., Bauer, K.A., 1979. The measurement of ^{10}Be in manganese nodules using a tandem Van de Graaff accelerator. Geophysical Research Letters 6, 417-420.

USGS, 2000. Geologic Provinces of the Far East.

Vanacker, V., Von Blanckenburg, F., Govers, G., Molina, A., Campforts, B., Kubik, P., 2015. Transient river response, captured by channel steepness and its concavity. Geomorphology 228, 234-243.

Vanacker, V., Von Blanckenburg, F., Govers, G., Molina, A., Poesen, J., Deckers, J., Kubik, P., 2007. Restoring dense vegetation can slow mountain erosion to near natural benchmark levels. Geology 35, 303-306.

von Blanckenburg, F., 2005. The control mechanisms of erosion and weathering at basin scale from cosmogenic nuclides in river sediment. Earth and Planetary Science Letters 237, 462-479.

von Blanckenburg, F., Willenbring, J.K., 2014. Cosmogenic Nuclides: Dates and Rates of Earth-Surface Change. Elements 10, 341-346.

Weyerhaeuser, H., Wilkes, A., Kahrl, F., 2005. Local impacts and responses to regional forest conservation and rehabilitation programs in China's northwest Yunnan province. Agricultural Systems 85, 234-253.

Willenbring, J.K., von Blanckenburg, F., 2010. Meteoric cosmogenic Beryllium-10 adsorbed to river sediment and soil: Applications for Earth-surface dynamics. Earth-Science Reviews 98, 105-122.

Wittmann, H., von Blanckenburg, F., 2009. Cosmogenic nuclide budgetng of floodplain sediment transfer. Geomorphology 109, 246-256.

Wittmann, H., von Blanckenburg, F., Guyot, J.L., Maurice, L., Kubik, P.W., 2011c. Quantifying sediment discharge from the Bolivian Andes into the Beni foreland basin from cosmogenic ^{10}Be-derived denudation rates. Brazilian Journal of Geology 41, 629-641.

Wittmann, H., von Blanckenburg, F., Maurice, L., Guyot, J.L., Filizola, N., Kubik, P.W., 2011a. Sediment production and delivery in the Amazon River basin quantified by in situ-produced cosmogenic nuclides and recent river loads. Geological Society of America Bulletin 123, 934-950.

Wittmann, H., von Blanckenburg, F., Maurice, L., Guyot, J.L., Kubik, P.W., 2011b. Recycling of Amazon floodplain sediment quantified by cosmogenic ^{26}Al and ^{10}Be. Geology 39, 467-470.

Wobus, C., Whipple, K.X., Kirby, E., Snyder, N., Johnson, J., Spyropolou, K., Crosby, B., Sheehan, D., 2006. Tectonics from topography: Procedures, promise and pitfalls. Geological Society of America Special Paper 398.

Xu, J., Yin, R., Li, Z., Liu, C., 2006. China's ecological rehabilitation: Unprecedented efforts, dramatic impacts, and requisite policies. Ecological Economics 57, 595-607.

Xu, S., Dougans, A.B., Freeman, S.P.H.T., Schnabel, C., Wilcken, K.M., 2010. Improved Be-10 and Al-26 AMS with a 5 MV spectrometer. Nuclear Instruments and Methods B 268.

Yatagai, A., Kamiguchi, K., Arakawa, O., Hamada, A., Yasutomi, N., Kitoh, A., 2012. APHRODITE: Constructing a long-term daily gridded precipitation dataset for Asia based on a dense network of rain gauges. Bulleting of the American Meteorological Society 39, 1401-1415.

Zhang, J., Pham, T., Kalacska, M., Turner, S., 2014. Using Landsat Thematic Mapper records to map land cover change and the impacts of reforestation programmes in the borderlands of southeast Yunnan, China: 1990-2010. International Journal of Applied Earth Observation and Geoinformation 31, 25-36.

Zisheng, Y., Longfei, Y., Bosheng, Z., 2010. Soil erosion and its basinc characteristics at karst rocky-desertified land consolidation area: a case study at Muzhe Village of Xichou couny in Southeast Yunnan, China. Journal of Mountain Science 7, 55-72.

Chapter 4 – Conclusion

This work presents the first compilation of published long-term erosion rates in southern and southeastern Brazil, as well as constrain the first long-term erosion rates for two unsampled states: Rio de Janeiro and Santa Catarina. I present the biggest dataset for cosmogenic studies in China. I test an important assumption of the method to derive long-term erosion rates from cosmogenic measurements: the time-invariant ^{10}Be concentration assumption.

My work presents the first cosmogenically-derived erosion rates for the Brazilian states of Santa Catarina and Rio de Janeiro. Erosion rates, in the basins I studied, range from 13 to 90 m/My. They are broadly consistent with cosmogenic erosion rates published by others for southern Brazil. I also compiled all previously published cosmogenic nuclide measurements for southern and southeastern Brazilian watersheds. This region is eroding at a pace similar to other passive margins, but significantly slower than other tropical watersheds where cosmogenic erosion rates have been calculated. Topography is the main control on erosion in Brazil, with lesser influence from climate and lithology. In the compiled Brazilian dataset, I found that basins draining the escarpment erode faster than their counterpart basins, draining the highlands, regardless of the lithology that underlie the basins. This finding strongly suggests that topography controls erosion in this region.

The erosion data for Santa Catarina watersheds were measured as baseline data prior to the establishment of a Payment for Ecosystem Services (PES) program. My hope is that my data can now be used as a benchmark to compare the effects of the management program, but also as a quantification of the ecosystem dynamics. In order to quantify

changes to the landscape as a function of the PES, contemporary sediment yield measurements are needed. To the best of my knowledge, such data are not publicly available for Brazil.

In China, I created what is the biggest cosmogenic nuclide dataset for the region, with over 100 samples. Among the strengths of the dataset, is the vast amount of temporal replicates to test for the (cosmogenic) method assumption of time-invariant ^{10}Be concentration. While the central tendency in the replicate analyses is similar in most of the timeframes we studied, there is noise beyond analytical uncertainty in our data. The greatest discrepancy in the temporal replicates is between 2005 and 2014 samples. My collaborators discovered an error with the original cosmogenic data (published in Henck et al., 2011). As a result of this, the lack of correlation seen in my data is not scientifically meaningful. Future work includes correcting these data, and re-assessing the differences in isotopic concentration. More temporal replicate analysis work is needed, in order to put my dataset in context. With more data, it would be possible to assess whether my dataset has higher errors than expected, or if the samples are reproducing better than expected. Because little work has been done on temporal replicate, I can only compare my data to studies that have one or two replicates, which makes it hard to find trends in the datasets. Based on the temporal replicate data, I found that the monsoon does not change sediment sourcing to the rivers. This is a very important finding for cosmogenic studies, since we now know that the time of the year when rivers are sampled does not change the resulting numbers.

I found erosion rates in Yunnan range from 17 and 386 m/Myr. Topography exerts a first-order control on erosion in the watersheds I studied, with a lesser control from

climate and no tectonic control. Slope, a topography metric, co-varies with rainfall and agricultural land use in my dataset. This is further proof that topography is the strongest control of erosion in this region. Perhaps the most interesting finding in this dataset is the lack of relationship between tectonic activity and erosion. It is common for tectonic activity to drive erosion in places where there is active tectonism. An example of this is the Panama dataset I generated for my Master's thesis, where tectonic activity was the strongest control of erosion (Sosa-Gonzalez, 2012).

I found that modern sediment yields are higher than long-term yields by a factor of as much as 24X, in most of the sites I studied. This is not a surprising finding, given the long-history of human activity and landscape modification in Western China. However, I find such an increase comparing long-term erosion rates to sediment yield data that dates back to the 1960s – 1980s. I can confidently hypothesize that the sediment yields today are at least as high as they were back then, if not higher, based on the constant changes to the landscape, and widespread agriculture. However, sediment yields today can give the impression of being lower, because sediments can be trapped behind dams and in rice paddies. In order to understand which of these human activities is driving the sediment yields, a fine-scale network of sediment monitoring is needed in this region. This network would need to measure sediments exported from end-member basins in a watershed, including all forested, all agriculture, all urban, and some mixed basins. This would allow geomorphologists to understand which land uses are generating sediment, and which are trapping it.

A potential use of the China dataset is to serve as a benchmark to quantify future impacts of dams. With the increase in dams and reservoirs this region will face in the next decade (Kummu et al., 2010), having a baseline to compare changes in sediment yields will be invaluable. For this comparison to be possible and effective, an active sediment data monitoring program is needed. The best approach would be to have sediment yield data from the rivers a few years prior to the dam construction, as well as data collected after the dam is built and functioning. Ideally, this monitoring can be done long-term to examine the effects of sediment releases from the dam. As reservoirs fill up, it is necessary to release water, and dredge sediments in order to keep the reservoir operational.

My work in both Brazil and China has increased the number of cosmogenic samples in tropical and subtropical watersheds. Samples from these sites have shown that topography is the strongest control of erosion in these places, regardless of tectonic activity in western China. Future work includes integrating my Brazilian data to the establishment of a Payment for Ecosystem Services program. In doing so, my work would apply geomorphology to environmental conservation, a novel approach. In China, future work includes incorporating short-lived isotope data from my samples, measured by undergraduate collaborators at Oberlin College. This new information, will give us an insight of short-term surfaces processes, and allow us to compare to long-term processes. Further work in China includes quantification of sediment yield measurements after dams are built and operating. Comparing these new yields to our long-term data would allow us to understand the changes on sediment exported from basins as a result of dams.

References

Almeida, F.F.M., Carneiro, C.D.R., 1998. Origem e Evolução da Serra do Mar. Revista Brasileira de Geociências 28(2), 135-150.

Almeida, J.C.H,; Dios, F., Mohriak, W., Valeriano, C.M., Heilbron, M, Eirado, L.G., Tomazzoli, E.,2013. Pre-rift tectonic scenario of the Eo-Cretaceous Gondwana break-up along SE Brazil-SW Africa: insights from tholeiitic mafic dike swarms. Geological Society Special Publications, 369, SP369.24-40.

Alvares, C. A., Stape, J.L., Sentelhas, P.C., Gonçalves, J.L.M., Sparovek, G., 2013. Köppen's climate classification map for Brazil. Meteorologische Zeitschrift, 22(6), 711-728.

Andermann, C., Bonnet, S., Gloaguen, R., 2011. Evaluation of precipitation data sets along the Himalayan front. Geochemistry, Geophysics, Geosystems, 12(7).

Asmus, H.E., Ferrari, A.L., 1978. Hipótese Sobre a Causa do Tecnonismo Cenozóico na Região Sudeste do Brasil. In: Petrobrás (Ed.), Aspectos Estruturais da Margem Continental Leste e Sudeste do Brasil, Rio de Janeiro, Brazil, pp. 75-88.

Balco, G., Briner, J., Finkel, R.C., Rayburn, J.A., Ridge, J.C., Schefer, J.M., 2009. Regional beryllium-10 production rate calibration for late-glacial northeastern North American. Quaternary Geology, 4, 93-107.

Balco, G., Stone, J.O., Lifton, N.A., Dunai, T.J., 2008. A complete and easily accessible means of calculating surface exposure ages or erosion rates from ^{10}Be and ^{26}Al measurements. Quaternary Geology, 3, 174-195.

Barreto, H.N., Varajão, C.A.C., Braucher, R., Bourlès, D.L., Salgado, A.A.R., Varajão, A.F.D.C., 2013. Denudation rates of the Southern Espinhaço Range, Minas Gerais, Brazil, determined by in situ-produced cosmogenic beryllium-10. Geomorphology, 191, 1-13.

Barreto, H.N., Varajão, C.A.C., Braucher, R., Bourlès, D.L., Salgado, A.A.R., Varajão, A.F.D.C., 2014. The impact of diamond extraction on natural denudation rates in the Diamantina Plateau (Minas Gerais, Brazil). Journal of South American Earth Sciences, 56, 357-364.

Behling, H., 1995. Investigations into the Late Pleistocene and Holocene history of vegetation and climate in Santa Catarina (S Brazil). Vegetation History and Archaeobotany, 4(3), 127-152.

Bellin, N., Vanacker, V., Kubik, P., 2012. Contrasting modern and ^{10}Be-derived erosion rates for the Southern Betic Cordillera, Spain, EGU General Assembly 2012

Bierman, P., Steig, E.J., 1996. Estimating rates of denudation using cosmogenic isotope abundaces in sediment. Earth Surface Processes and Landforms, 21, 125-139.

Bierman, P.R., Caffee, M., 2001. Slow rates of rock surface erosion and sediment production accross the Namib dessert and escarpment, Southern Africa. American Journal of Sciences, 301, 326-358.

Bierman, P.R., Clapp, E.M., Nichols, K., Gillespie, A., Caffee, M.W., 2001. Using cosmogenic nuclide measurements in sediments to understand background rates of erosion and sediment transport. In: R.S. Harmon, W.M. Doe (Eds.), Landscape erosion and evolution modeling Kluwer, New York, pp. 89-116.

Bierman, P.R., Nichols, K.K., 2004. Rock to sediment - slope to sea with ^{10}Be - rates of landscape change. Annual Review of Earth and Planetary Sciences, 32, 215-255.

Bierman, P.R., Nichols, K.K., Matmon, A., Enzel, Y., Larsen, J., Finkel, R., 2007. 10-Be shows that Namibian drainage basins are slowly, steadily and uniformly eroding. Quaternary International, 167-168, 33.

Bierman, P.R., Reuter, J.M., Pavich, M.J., Gellis, A.C., Caffee, M.W., Larsen, J., 2005. Using cosmogenic nuclides to contrast rates of erosion and sediment yield in a semi-arid, arroyo-dominated landscape, Rio Puerco Basin, New Mexico. Earth Surface Processes and Landforms, 30, 935-953.

Bierman, P.R., Steig, E.J., 1996. Estimating rates of denudation using cosmogenic isotope abundances in sediment. Earth Surface Processes and Landforms, 21, 125-139.

Bilotta, G.S., Brazier, R.E., 2008. Understanding the influence of suspended solids on water quality and aquatic biota. Water research, 42(12), 2849-2861.

Brandt, J., Kuemmerle, T., Li, H., Ren, G., Zhu, J., Radeloff, V.C., 2012. Using Landsat imagery to map forest change in southwest China in response to the national logging ban and ecotourism development. Remote Sensing of Environment, 121, 358-369.

Brickus, L.S.R., Cardoso, J.N., Neto, F.R.d.A., 1998. Distributions of indoor and outdoor air pollutants in Rio de Janeiro, Brazil: Implications to indoor air quality in bayside offices. Environmental Science and Technology, 32, 3485-3490.

Brocard, G., Willengring, J., Johnson, A., Scatena, F., 2014b. Migration of a slow wave of erosion and its effects on nutrient availability in a tropical rainfores: detrital ^{10}Be signature and soil mineralogy, Luquillo, CZO, Puerto Rico, EGU General Assembly 2014, Vienna, Austria.

Brocard, G., Willengring, J., Scatena, F., 2014a. Long-term increase in local relief enforced by forest competition: detrital ^{10}Be and LiDar topographic evidence in the tropical rainforest of Puerto Rico, Luquillo, CZO, EGU General Assembly 2014, Vienna, Austria.

Brown, E.T., Stallard, R.F., Larsen, M.C., Bourlés, D., Raisbeck, G.M., Yiou, F., 1998. Determination of predevelopment denudation rates of an agricultural watersheds (Cayaguás River, Puerto Rico) using in-situ produced ^{10}Be in river-borne quartz. Earth and Planetary Science Letters, 160, 723-728.

Brown, E.T., Stallard, R.F., Larsen, M.C., Raisbeck, G.M., Yiou, F., 1995. Denudation rates determined from the accumulation of in-situ produced ^{10}Be in the Luquillo Experimental Forest, Puerto Rico. Earth and Planetary Science Letters, 129, 193-202.

Brown, L., Pavich, M.J., Hickman, R.E., Klein, J., Middleton, R., 1988. Erosion of the Eastern United States observed with ^{10}Be. Earth Surface Processes and Landforms, 13, 441-457.

Burchfiel, B.C., Chen, L., Wang, E., Swanson, E., 2008. Preliminary investigation into the complexities of the Ailao Shan and Day Nui Con Voi shear zones of SE Yunnan and Vietnam. Geological Society of America Special Paper, 444(45-58).

Burchfiel, B.C., Chen, Z., 2012a. Lhasa Unit. In: K. Condie, F.E. Harvey (Eds.), Tectonics of the Southeastern Tibetan Plateau and its adjacent foreland. The Geological Society of America, Boulder, CO, pp. 117-126.

Burchfiel, B.C., Chen, Z., 2012b. Qiangtang Unit. In: K. Condie, F.E. Harvey (Eds.), Tectonics of the Southeastern Tibetan Plateau and its adjacent foreland. The Geological Society of America, Boulder, CO, pp. 77-96.

Campforts, B., Vanacker, V., Vanderborght, J., Baken, S., Smolders, E., Govers, G., 2016. Simulating the mobility of meteoric ^{10}Be in the landscape through a coupled soil-hillslope (Be2D). Earth and Planetary Science Letters, 439, 143-157.

Chen, J., Chen, J., Liao, A., Cao, X., Chen, L., He, C., Han, G., Peng, S., Lu, M., Zhang, W., Tong, X., Mills, J., 2015. Global land cover mapping at 30 m resolution: A POK-based operational approach. ISPRS Journal of Photogrammetry and Remote Sensing, 103, 7-27.

Cherem, L.F.S., Varajão, C.A.C., Braucher, R., Bourlés, D., Salgado, A.A.R., Varajão, A.C., 2012b. Long-term evolution of denudational escarpments in southeastern Brazil. Geomorphology, 173-174, 118-127.

Cherem, L.F.S., Varajão, C.A.C., Salgado, A.A.R., Varajão, A.F.D.C., Braucher, R., Bourlés, D., Magalhães Jr., A.P., Nalini Jr, H., 2012a. Denudação química e rebaixamento do relevo em bordas interplanálticas com substrato granítico: dois exemplos no se de Minas Gerais. Revista Brasileira de Geomorfologia, 13(1), 73-84.

Clapp, E.M., Bierman, P.R., Schick, A., P., Lekach, J., Enzel, Y., Caffee, M.W., 2000. Sediment yield exceeds sediment production in arid region drainage basins. Geology 28(11), 995-998.

Corbett, L.B., Bierman, P.R., Rood, D.H., 2016. An approach for optimizing *in situ* cosmogenic ^{10}Be sample preparation. Quaternary Geology, 33, 24-34.

Cox, R., Bierman, P., Jungers, Matthew C., Rakotondrazafy, A.F.M., 2009. Erosion Rates and Sediment Sources in Madagascar Inferred from ^{10}Be Analysis of Lavaka, Slope, and River Sediment. The Journal of Geology, 117(4), 363-376.

Cyr, A.J., Granger, D.E., 2008. Dynamic equilibrium among erosion, river incision, and coastal uplift in the northern and central Apennines, Italy. Geology 36(2), 103-106.

de Sherbinin, A., Hogan, D., 2011. Climate Proofing in Rio de Janeiro, Brazil. Cambridge University Press, New York, USA.

Dedkov, A.P., Moszherin, V.I., 1992. Erosion and sediment yield in mountain regions of the world, Proceedings of the Chengdu Symposium. IAHS Publications, Chengdu, China.

DiBiase, R.A., Whipple, K.X., Heimsath, A.M., Ouimet, W.B., 2010. Landscape form and millennial erosion rates in the San Gabriel Mountains, CA. Earth and Planetary Science Letters, 289, 134-144.

Dominguez, J.M.L., 2009. The coastal zone of Brazil. In: S. Dillenburg, P. Hesp (Eds.), Geology and geomorphology of Holocene coastal barriers of Brazil. Springer, Berlin, Germany.

Dunai, T.J., Lifton, N.A., 2014. The Nuts and Bolts of Cosmogenic Nuclide Production. Elements, 10(5), 347-350.

Duxbury, J., Bierman, P.R., Portenga, E.W., Pavich, M., Southworth, S., Freeman, S.P., 2015. Erosion rates in and around Shenandoah National Park, Virginia, determined using analysis of cosmogenic ^{10}Be. American Journal of Science, 315(1), 46-76.

Elmore, D., Phillips, F.M., 1987. Accelerator mass spectrometry for measurement of long-lived radioisotopes. Science, 236(4801), 543-550.

Enters, T., 1998. Methods for the economic assessment of the on- and off-site impacts of soil erosion, International Board of Soil Research and Management, Bangkok.

Fang, J., Xie, Z., 1994. Deforestation in preindustrial China: The Loess plateau region as an example. Chemosphere, 29(5), 983-999.

FAO, 2015. Georeferenced dams database. In: F.a.A.O.o.t.U. Nations (Ed.).

Fernandes, N.F., Tupinambá, M., Mello, C.L., de Peixoto, M.N.O., 2010. Rio de Janeiro: A Metropolis between granite-gneiss massifs. In: M. Migon (Ed.), Great Geomorphological Landscapes of the World, New York, USA, pp. 89-100.

Ferraro, P.J., Pattanayak, S.K., 2006. Money for Nothing? A call for empirical evaluation of biodiversity conservation investments. PLoS Biology, 4(4), 0482-0488.

Gallagher, K., Hawkesworth, C.J., Mantovani, M.S.M., 1995. Denudation, fission track analysis and the long-term evolution of passive margin topography: ana pplication to the southeast Brazilian margin. Journal of South American Earth Sciences, 8(1), 65-77.

Gellis, A.C., Pavich, M.J., Bierman, P.R., Clapp, E.M., Ellevein, A., Aby, S., 2004. Modern sediment yield compared to geologic rates of sediment production in a semi-arid basin, New Mexico: Assessing the human impact. Earth Surface Processes and Landforms, 29, 1359-1372.

Giardini, D., 1999. The Global Seismic Hazard Assessment Program (GSHAP) - 1992/1999. Annals of Geophysics, 42(6), 957-974.

Graly, J.A., Bierman, P.R., Reusser, L.J., Pavich, M.J., 2010. Meteoric ^{10}Be in soil profiles - A global meta-analysis. Geochimica et Cosmochimica Acta, 74, 6814-6829.

Graly, J.A., Reusser, L.J., Bierman, P.R., 2011. Short and long-term delivery rates of meteoric ^{10}Be to terrestrial soils. Earth and Planetary Science Letters, 302(3-4), 329-336.

Granger, D.E., Kirchner, J.W., Finkel, R.C., 1996. Spatially averaged long-term erosion rates measured from in-situ produced cosmogenic nuclides in alluvial sediment. The Journal of Geology, 104, 249-257.

Granger, D.E., Riebe, C.S., 2007. Cosmogenic nuclides in weathering and erosion. In: J.I. Drever (Ed.), Treatise on geochemistry. Elsevier, London, UK.

Guedes, E.; Heilbron, M.; Vasconcelos, P.; Valeriano, C.; Almeida, J.; Teixeira, W.; Thomaz Filho, A., 2005. K-Ar and Ar-Ar ages of dikes emplaced in the onshore basement of Santos Basin, Resende Area, SE, Brazil: Implications for the South Atlantic opening and a tertiary reactivation. Journal of South American Earth Sciences, 18(3), 371-382.

Hackspacher, P.C., Ribeiro, L.F.B., Ribeiro, M.C.S., Fetter, A.H., Hadler Neto, J.C., Tello, C.E.S., Dantas, E.L., 2004. Consolidation and Break-up of the South American

Platform in Southeastern Brazil: Tectonothermal and Denudation Histories. Gondwana Research 7(1), 91-101.
Harden, C.P., 2006. Human impacts on headwater fluvial systems in the northern and central Andes. Geomorphology, 79(3-4), 249-263.
He, F., Li, S., Zhang, X., 2015. A spatially explicity reconstruction of forest cover in China over 1700-2000. Global and Planetary Change, 131, 73-81.
Heilbron M., Machado, N., 2003. Timing of terrane accretion in the Neoproterozoic-Eopaleozoic Ribeira Orogen (SE Brazil). Precambrian Research, 125, 87–112.
Heilbron, M., Valeriano, C.M., Tassinari, C.C.G., Almeida, J.C.H., Tupinambá, M., Siga Jr., O., Truow, R.A.J., 2008. Correlation of Neoproterozoic terranes between the Ribeira Belt, SE Brazil and its african counterpart: comparative tectonic evolution and open questions. Geological Society Special Publications, 294, 211-237.
Heimsath, A.M., Chappell, J., Finkel, R.C., Fifield, K., Alimanovic, A., 2006. Escarpment erosion and landscape evolution in southeastern Australia. Geological Society of America, Special Paper 398, 173-190.
Heimsath, A.M., Fink, D., Hancock, G.R., 2009. The 'humped' soil production function: eroding Arnhem Land, Australia. Earth Surface Processes and Landforms, 34(12), 1674-1684.
Henck, A.C., Huntington, K.W., Stone, J.O., Montgomery, D.R., Hallet, B., 2011. Spatial controls on erosion in the Three Rivers Region, southeastern Tibet and southwestern China. Earth and Planetary Science Letters, 303, 71-83.
Henck, A.C., Montgomery, D.R., Huntington, K.W., Liang, C., 2010. Monsoon control of effective discharge, Yunnan and Tibet. Geology, 38(11), 975-978.
Hewawasam, T., von Blanckenburg, F., Schaller, M., Kubik, P.W., 2003. Increase of human over natural erosion rates in tropical highlands constrained by cosmogenic nuclides. Geology, 31(7), 597-600.
Heyman, J., Stroeven, A.P., Harbor, J.M., Caffee, M.W., 2011. Too young or too old: Evaluating cosmogenic exposure dating based on an analysis of compiled boulder exposure ages. Earth and Planetary Science Letters, 203, 71-80.
Hijmans, R.J., Cameron, S.E., Parra, J.L., Jones, P.G., Jarvis, A., 2005. Very high resolution interpolated climate surfaces for global land areas. International Journal of Climatology, 25(15), 1965-1978.
Hinderer, M., Pflanz, D., Schneider, S., 2013. Chemical Denudation Rates in the Humid Tropics of East Africa and Comparison with ^{10}Be-Derived Erosion Rates. Procedia Earth and Planetary Science, 7, 360-364.
Hooke, R.L., 1994. On the efficacy of the humans as geomorphic agents. GSA Today, 4(9), 217, 224-225.
Hooke, R.L., 2000. On the history of humans as geomorphic agents. Geology, 28(9), 843-846.
Hui, F., Jinming, H., Daming, H., 2013. Trends in precipitation over the low latitude highlands of Yunnan, China. Journal of Geographical Sciences, 23(6), 1107-1122.
Humphreys, G.S., Tomkins, K.M., Wilkinson, M.T., Fink, D., Shakesby, R.A., Doerr, S.H., Walbrink, P.J., Blake, W.H., 2006. Longer-term and contemporary denudation

rates, and the role of extreme events along a passive margin, Australia, Goldschmidt Conference Melbourne, Australia.

Insel, N., Ehlers, T.A., Schaller, M., Barnes, J.B., Tawackoli, S., Poulsen, C.J., 2010. Spatial and temporal variability in denudation across the Bolivian Andes from multiple geochronometers. Geomorphology, 122, 65-77.

Jungers, M.C., Bierman, P.R., Matmon, A., Nichols, K., Larsen, J., Finkel, R.C., 2009. Tracing hillslope sediment production and transport with insitu and meteoric ^{10}Be. Journal of Geophysical Research, 114, F04020.

Kirchner, J.W., Finkel, R., C., Riebe, C.S., Granger, D.E., Clayton, J.L., King, J.G., Megahan, W.F., 2001. Mountain erosion over 10 yr, 10 k.y., and 10 m.y. time scales. Geology 29(7), 591-594.

Kohl, C.P., Nishiizumi, K., 1992. Chemical isolation of quartz for measurement of in-situ produced cosmogenic nuclides. Geochimica et Cosmochimica Acta, 56, 3583-3587.

Kummu, M., Lu, X.X., Wang, J.J., Varis, O., 2010. Basin-wide sediment trapping efficiency of emerging reservoirs along the Mekong. Geomorphology, 119, 181-197.

Kummu, M., Varis, O., 2007. Sediment-related impacts due to upstream reservoir trapping, the Lower Mekong River. Geomorphology, 85, 275-293.

Lal, D., 1991. Cosmic ray labeling of erosion surfaces: in situ nuclide production rates and erosion models. Earth and Planetary Science Letters, 104, 424-439.

Lal, D., 2000. Cosmogenic ^{10}Be: A critical view on its widespread dominion in geosciences. Journal of Earth System Science, 109(1), 181-186.

Lal, D., Peters, B., 1967. Cosmic-ray produced radioactivity on the earth. In: K. Sitte (Ed.), Handuch der Physik. Springer-Verlag, New York, pp. 551-612.

Lal, R., Fifield, L.K., Tims, S.G., Wasson, R.J., Howe, D., 2012. A study of soil formation rates using ^{10}Be in the wet-dry tropics of northern Australia. EPJ Web of Conferences, 35, 01001.

Leloup, P.H., Lacassin, R., Tapponnier, P., Schärer, U., Dalai, Z., Xiaohan, L., Liangshang, Z., Schaocheng, J., Trinh, P.T., 1995. The Ailao Shan-Red River shear zone (Yunnan, China), Tertiary transform boundary of Indochina. Tectonophysics, 251, 3-84.

Lu, X.X., Siew, R.Y., 2006. Water discharge and sediment flux changes over the past decades in the Lower Mekong River: possible impacts of the Chinese dams. Hydrology and Earth System Sciences, 10, 181-195.

Lupker, M., Blard, P.-H., Lavé, J., France-Lanord, C., Leanni, L., Puchol, N., Charreau, J., Bourlès, D., 2012. ^{10}Be-derived Himalayan denudation rates and sediment budgets in the Ganga basin. Earth and Planetary Science Letters, 333-334, 146-156.

Mackey, B.H., Scheingross, J.S., Lamb, M.P., Farley, K.A., 2014. Knickpoint formation, rapid propagation, and landscape response following coastal cliff retreat at the last interglacial sea-level highstand: Kaua'i, Hawai'i. Geological Society of America Bulletin, 126(7-8), 925-942.

Magee, D., 2006. Powershed politics: hydropower and interprovincial relations under Great Western Development. The China Quarterly, 185, 23-41.

Matmon, A., Bierman, P.R., Larsen, J., Southworth, S., Pavich, M., Finkel, R., Caffee, M., 2003. Erosion of an ancient mountain range, the Great Smoky Mountains, North Carolina and Tennessee. American Journal of Science, 303, 817-855.

McHargue, L.R., Damon, P.E., 1991. The global Beryllium 10 cycle. Reviews of Geophysics, 29(2), 141-158.

McKean, J.A., Dietrich, W.E., Finkel, R.C., Southon, J.R., Caffee, M.W., 1993. Quantification of soil production and downslope creep rates from cosmogenic ^{10}Be accumulations on a hillslope profile. Geology, 21, 343-346.

Milliman, J.D., Syvitski, P.M., 1992. Geomorphic/tectonic control of sediment discharge to the ocean: the importance of small mountainous rivers. The Journal of Geology, 100, 525-544Monaghan, M.C., McKean, J.A., Dietrich, W.E., Klein, J., 1992. ^{10}Be chronometry of bedrock-to-toil conversion rates. Earth and Planetary Science Letters, 111, 483-492.

Montgomery, D.R., Balco, G., Willett, S.D., 2001. Climate, tectonics and the morphology of the Andes. Geology, 29(7), 579-582. NASA LP-DAAC, 2012. ASTER GDEM.

Neilson, T., 2015. Using long- and short-lived sediment-associated isotopes to track erosion and sediment movement through rivers in Yunnan, SW China. Master of Science, University of Vermont, Burlington, VT, 176 pp.

Nichols, K., Bierman, P.R., Rood, D.H., 2014. ^{10}Be constrains the sediment sources and sediment yields to the Great Barrier Reef from the tropical Barron River catchment, Queenslad, Australia. Geomorphology, 224, 102-110.

Nichols, K.K., Bierman, P., Finkel, R., C., Larsen, J., 2005. Long-term sediment generation rates for the Upper Río Chagres Basin: Evidence from cosmogenic ^{10}Be. In: R.S. Harmon (Ed.), The Río Chagres, Panama: A multidisciplinary profile of a tropical watershed. Springer, The Netherlands.

Niemi, N.A., Oskin, M., Burbank, D.W., Heimsath, A.M., Gabet, E.J., 2005. Effects of bedrock landslides on cosmogenically determined erosion rates. Earth and Planetary Science Letters, 237, 480-498.

Nishiizumi, K., Imamura, M., Caffee, M.W., Southon, J.R., Finkel, R.C., McAninch, J., 2007. Absolute calibration of ^{10}Be AMS standards. Nuclear Instruments and Methods B, 258(2), 403-413.

Nishiizumi, K., Kohl, C.P., Arnold, J.R., Dorn, R., Klein, J., Fink, D., Middleton, R., Lal, D., 1993. Role of *in situ* cosmogenic nuclides ^{10}Be and ^{26}Al in the study of diverse geomorphic processes. Earth Surface Processes and Landforms, 18(5), 407-425.

Nunes, L.H., Vicente, A.K., Candido, D.H., 2009. Clima da Região Sudeste do Brasil. In: I.F.A. Cavalcanti, N.J. Ferreira, M.G.A.J. Silva, M.A.F.S. Dias, (Eds.), Tempo e Clima no Brasil. Oficina de Textos, São Paulo, pp. 243-259.

Ollier, C., 2004. The evolution of mountains on passive continental margins. In: P.N. Owens, O. Slaymaker (Eds.), Mountain Geomorphology. Arnold, New York, USA.

Ouimet, W.B., Whipple, K.X., Granger, D.E., 2009. Beyond threshold hillslopes: Channel adjustment to base-level fall in tectonically active mountain ranges. Geology, 37(7), 579-582.

Ouyang, W., Skidmore, A.K., Hao, F., Wang, T., 2010. Soil erosion dynamics response to landscape pattern. Science of the Total Environment, 208, 1358-1366.

Owens, P.N., Batalla, R.J., Collins, A.J., Gomez, B., Hicks, D.M., Horowitz, A.J., Kondolf, G.M., Marden, M., Page, M.J., Peacock, D.H., Petticrew, E.L., Salomons, W., Trustrum, N.A., 2005. Fine-grained sediment in river systems: environmental significance and management issues. River Research and Applications, 21(7), 693-717.

Pavich, M.J., Brown, L., Klein, J., Middleton, R., 1984. ^{10}Be accumulation in a soil chronosequence. Earth and Planetary Science Letters, 68, 198-204.

Pavich, M.J., Brown, L., Valette-Silver, J.N., Klein, J., Middleton, R., 1985. ^{10}Be analysis of a Quaternary weathering profile in the Virginia Piedmont. Geology, 13, 39-41.

Pfaff, A., Robalino, J.A., Sanchez-Azofeiga, G.A., 2008. Payment for environmental services: empirical analysis for Costa Rica, Terry Sanford Institute of Public Policy, Duke University

Pimentel, D., 2006. Soil Erosion: A Food and Environmental Threat. Environment, Development and Sustainability, 8(1), 119-137.

Pimentel, D., Harvey, C., Resosudarmo, P., Sinclair, K., Kurz, D., McNair, M., Crist, S., Shpritz, L., Fitton, L., Saffouri, R., Blair, R., 1995. Environmental and economic costs of soil erosion and conservation benefits. Science, 267(5201), 1117-1123.

Portenga, E., Bierman, P.R., 2011. Understanding Earth's eroding surface with ^{10}Be. Geology, 21(8), 4-10.

Portenga, E.W., Bierman, P.R., Duncan, C., Corbett, L.B., Kehrwald, N.M., Rood, D.H., 2015. Erosion rate of the Bhutanese Himalaya determined using *in situ*-produced ^{10}Be. Geomorphology, 233, 112-126.

Pullin, A.S., Knight, T.M., 2001. Effectiveness in conservation practice: pointers from medicine to public health. Conservation Biology, 15(1), 50-54.

Reusser, L.J., Bierman, P.R., 2010. Using meteoric ^{10}Be to track fluvial sand through the Waipaoa River basin, New Zealand. Geology, 38(1), 47-50.

Reusser, L.J., Bierman, P.R., Rood, D., 2014. Quantifying human impacts on rates of erosion and sediment transport at a landscape scale. Geology, 43(2), 171-174.

Rezende, E.A., Salgado, A.A.R., da Silva, J.R., Bourlés, D., Leánni, L., 2013. Factores controladores da evolução do relevo no flanco NNW do rift continental do sudeste do Brasil: Uma análise baseada na mensuração dos processos denudacionais de longo-termo. Revista Brasileira de Geomorfologia, 14(2), 221-234.

Riebe, C.S., Kirchner, J.W., Finkel, R., 2003. Long-term rates of chemical weathering and physical erosion from cosmogenic nuclides and geochemical mass balance. Geochimica et Cosmochimica Acta, 67(22), 4411-4427.

Riebe, C.S., Kirchner, J.W., Granger, D.E., Finkel, R., 2001. Minimal climatic control on erosion rates in the Sierra Nevada, California. Geology, 29(5), 447-450.

Ritter, D.F., Kochel, R.C., Miller, J.R., 1995. Process Geomorphology. Brown Pubishers, Dubuque, IA.

Rozelle, S., Huang, J., Zhang, L., 1997. Poverty, population and environmental degradation in China. Food Policy, 22(3), 229-251.

Safran, E.B., Bierman, P.R., Aalto, R., Dunne, T., Whipple, K.X., Caffee, M.W., 2005. Erosion rates driven by channel network incision in the Bolivian Andes. Earth Surface Processes and Landforms, 30, 1007-1024.

Salgado, A., Varajão, C., Colin, F., Braucher, R., Varajão, A., Nalini Jr, H., 2007. Study of the erosion rates in the upper Maracujá Basin (Quadrilátero Ferrífero/MG, Brazil) by the in situ produced cosmogenic ^{10}Be method. Earth Surface Processes and Landforms, 32(6), 905-911.

Salgado, A.A.R., Braucher, R., Colin, F., Nalini, H.A., Varajão, A.F.D.C., Varajão, C.A.C., 2006. Denudation rates of the Quadrilátero Ferrífero (Minas Gerais, Brazil): Preliminary results from measurements of solute fluxes in rivers and in situ-produced cosmogenic ^{10}Be. Journal of Geochemical Exploration, 88(1-3), 313-317.

Salgado, A.A.R., Braucher, R., Varajão, A.C., Colin, F., Varajão, A.F.D.C., Nalini, J.H.A., 2008. Relief evolution of the Quadrilátero Ferrífero (Minas Gerais, Brazil) by means of (^{10}Be) cosmogenic nuclei. Zeitschrift für Geomorphologie, 52(3), 317-323.

Salgado, A.A.R., Marent, B.R., Cherem, L.F.S., Bourlès, D., Santos, L.J.C., Braucher, R., Barreto, H.N., 2013. Denudation and retreat of the Serra do Mar escarpment in southern Brazil derived from in situ-produced ^{10}Be concentration in river sediment. Earth Surface Processes and Landforms, 39(3), 311-319.

Sanjiang, Geology of, 1986. Geological map of Nujiang, Lancang, and Jinsha Rivers area. In: M.o.G.a.M. Resources (Ed.). Geological Publishing House.

Santos, G.M., Moore, R.B., Southon, J.R., Griffin, S., Hinger, E., Zhang, D., 2007. AMS ^{14}C sample preparation at the KCCAMS/UCI facility: Statys report and performance of small samples. Radiocarbon, 49(2), 255-269.

Schaller, M., von Blanckenburg, F., Veldkamp, A., Tebbens, L.A., Hovius, N., Kubik, P.W., 2002. A 30 000 yr record of erosion rates from cosmogenic ^{10}Be in Middle European river terraes. Earth and Planetary Science Letters, 204, 307-320.

Schmidt, A.H., Montgomery, D.R., Huntington, K.W., Liang, C., 2011. The question of communist land degradation: New evidence from local erosion and basin-wide sediment yield in Southwest China and Southeast Tibet. Annals of the Association of American Geographers, 101(3), 1-20.

Schoenbohm, L.M., Whipple, K.X., Burchfiel, B.C., Chen, L., 2004. Geomorphic constraints on surface uplift, exhumation, and plateau growth in Red River region, Yunnan Province, China. GSA Bulletin, 116(7/8), 895-909.

Shapiro, J., 2008. Mao's war against Nature: Politics and the Environment in Revolutionary China. Studies in Environment and History. Cambridge University Press, Cambridge, UK.

Silva, T.M., Ferrari, A.L., Tupinambá, M., Fernandes, L.A.D., 2015. The Guanabara Bay. In: B.C. Vieira, A.A.R. Salgado, L.J.C. Santos (Eds.), Lanscapes and landforms of Brazil. Springer, New York, USA, pp. 1-16.

Sosa-Gonzalez, V., 2012. Determining long-term erosion rates in Panama: An application of ^{10}Be. M.Sc., University of Vermont, Burlington, VT, USA, 114 pp.

Stevens, N., Willmott, W., 1996. The Main Range. In: Q.D. Geological Society of Australia (Ed.).

Stone, J., 1998. A rapid fusion method for separation of beryllium-10 from soils and silicates. Geochimica et Cosmochimica Acta, 62(3), 555-561.

Stone, J.O., 2000. Air pressure and cosmogenic isotope production. Journal of Geophysical Research, 105(B10), 23,573-523,579.

Strobl, M., Hetzel, R., Niedermann, S., Ding, L., Zhang, L., 2012. Landscape evolution of a bedrock peneplain on the southern Tibetan Plateau revealed by in situ-produced cosmogenic ^{10}Be and ^{21}Ne. Geomorphology, 153-154, 192-204.

Sullivan, C.L., 2007. ^{10}Be erosion rates and landscape evolution of the Blue Ridge Escarpment, southern Appalachian Mountains. M.Sc., University of Vermont, Burlington, VT, 76 pp.

Sültenfuβ, J., Purtschert, R., Führböter, J.E., 2010. Age structure and recharge conditions of a coastal aquifer (northern Germany) investigated with ^{39}Ar, ^{14}C, ^{3}H, He, isotopes and Ne. Hydrogeology Journal, 19, 221-236.

Summerfield, M.A., Hulton, N.J., 1994. Natural controls of fluvial denudation rates in major world drainage basins. Journal of Geophysical Research, 99(B7), 13,871 - 813,883.

Sutherland, W.J., Pullin, A.S., Dolman, P.M., Knight, T.M., 2004. The need for evidence-based conservation. TRENDS in Ecology and Evolution, 19(6), 305-308.

Trac, C.J., Harrell, S., Hinckley, T.M., Henck, A.C., 2007. Reforestation programs in Southwest China: Reported success, observed failures, and the reasons why. Journal of Mountain Science, 4(4), 275-292.

Trac, C.J., Schmidt, A.H., Harrell, S., Hinckley, T.M., 2013. Is the returning farmland to forest program a success? Three case studies from Sichuan. Environmental Practice, 15(3), 350-366.

Turekian, K.K., Cochran, J.K., Krishnaswami, S., Lanford, W.A., Parker, P.D., Bauer, K.A., 1979. The measurement of ^{10}Be in manganese nodules using a tandem Van de Graaff accelerator. Geophysical Research Letters, 6(5), 417-420.

USGS, 2000. Geologic Provinces of the Far East.

Vanacker, V., Von Blanckenburg, F., Govers, G., Molina, A., Campforts, B., Kubik, P., 2015. Transient river response, captured by channel steepness and its concavity. Geomorphology, 228, 234-243.

Vanacker, V., Von Blanckenburg, F., Govers, G., Molina, A., Poesen, J., Deckers, J., Kubik, P., 2007. Restoring dense vegetation can slow mountain erosion to near natural benchmark levels. Geology 35(4), 303-306.

Vanacker, V., von Blanckenburg, F., Hewawasam, T., Kubik, P.W., 2007. Constraining landscape development of the Sri Lankan escarpment with cosmogenic nuclides in river sediment. Earth and Planetary Science Letters, 253(3-4), 402-414.

von Blanckenburg, F., 2005. The control mechanisms of erosion and weathering at basin scale from cosmogenic nuclides in river sediment. Earth and Planetary Science Letters, 237(3-4), 462-479.

von Blanckenburg, F., Hewawasam, T., Kubik, P.W., 2004. Cosmogenic nuclide evidence for low weathering and denudation in the wet, tropical highlands of Sri Lanka. Journal of Geophysical Research, 109(F3).

von Blanckenburg, F., Willenbring, J.K., 2014. Cosmogenic Nuclides: Dates and Rates of Earth-Surface Change. Elements, 10(5), 341-346.

West, N., Kirby, E., Bierman, P., Rood, D., 2011. Preliminary estimates of regolith generation and mobility in the Susquehanna Shale Hills Critical Zone Observatory, Pennsylvania, using meteoric ^{10}Be. Applied Geochemistry, 26, S146-S148.

West, N., Kirby, E., Bierman, P., Slingerland, R., Ma, L., Rood, D., Brantley, S., 2013. Regolith production and transport at the Susquehanna Shale Hills Critizal Zone Observatory, Part 2: Insights from meteoric ^{10}Be. Journal of Geophysical Research, 118(3), 1877-1896.

West, N., Kirby, E., Bierman, P., Clarke, B.A., 2014. Aspect-dependent variations in regolith creep revealed by meteoric ^{10}Be. Geology, 42(6), 507-510.

Weyerhaeuser, H., Wilkes, A., Kahrl, F., 2005. Local impacts and responses to regional forest conservation and rehabilitation programs in China's northwest Yunnan province. Agricultural Systems, 85, 234-253.

Willenbring, J.K., von Blanckenburg, F., 2010. Meteoric cosmogenic Beryllium-10 adsorbed to river sediment and soil: Applications for Earth-surface dynamics. Earth-Science Reviews, 98(1-2), 105-122.

Williams, L., 1962. South Brazil: its vegetation, natural resources, research centers,a nd other economic aspects. Economic Botany, 16(3), 143-160.

Wittmann, H., von Blanckenburg, F., 2009b. Cosmogenic nuclide budgeting of floodplain sediment transfer. Geomorphology, 109(3-4), 246-256.

Wittmann, H., von Blanckenburg, F., Guyot, J.L., Maurice, L., Kubik, P.W., 2009a. From source to sink: Preserving the cosmogenic ^{10}Be-derived denudation rate signal of the Bolivian Andes in sediment of the Beni and Mamoré foreland basins. Earth and Planetary Science Letters, 288, 463-474.

Wittmann, H., von Blanckenburg, F., Guyot, J.L., Maurice, L., Kubik, P.W., 2011c. Quantifying sediment discharge from the Bolivian Andes into the Beni foreland basin from cosmogenic ^{10}Be-derived denudation rates. Brazilian Journal of Geology, 41(4), 629-641.

Wittmann, H., von Blanckenburg, F., Maurice, L., Guyot, J.L., Filizola, N., Kubik, P.W., 2011a. Sediment production and delivery in the Amazon River basin quantified by in situ-produced cosmogenic nuclides and recent river loads. Geological Society of America Bulletin, 123(5-6), 934-950.

Wittmann, H., von Blanckenburg, F., Maurice, L., Guyot, J.L., Kubik, P.W., 2011b. Recycling of Amazon floodplain sediment quantified by cosmogenic ^{26}Al and ^{10}Be. Geology, 39(5), 467-470.

Wobus, C., Whipple, K.X., Kirby, E., Snyder, N., Johnson, J., Spyropolou, K., Crosby, B., Sheehan, D., 2006. Tectonics from topography: Procedures, promise and pitfalls. Geological Society of America Special Paper, 398(55-74).

Xu, J., Yin, R., Li, Z., Liu, C., 2006. China's ecological rehabilitation: Unprecedented efforts, dramatic impacts, and requisite policies. Ecological Economics, 57, 595-607.

Xu, S., Dougans, A.B., Freeman, S.P.H.T., Schnabel, C., Wilcken, K.M., 2010. Improved Be-10 and Al-26 AMS with a 5 MV spectrometer. Nuclear Instruments and Methods B, 268(736-738).

Yatagai, A., Kamiguchi, K., Arakawa, O., Hamada, A., Yasutomi, N., Kitoh, A., 2012. APHRODITE: Constructing a long-term daily gridded precipitation dataset for Asia based on a dense network of rain gauges. Bulleting of the American Meteorological Society, 39(9), 1401-1415.

Young, R.P., Hazzard, J.F., Pettitt, W.S., 2000. Seismic and micromechanical studies of rock fracture. Geophysical Research Letters, 27(12), 1767-1770.

Zalan P.V., Oliveira J.A.B., 2005. Origem e evolução estrutural do Sistema de Riftes Cenozóicos do Sudeste do Brasil. Boletim de Geociências da Petrobrás, 13(2), 269-300.

Zhang, J., Pham, T., Kalacska, M., Turner, S., 2014. Using Landsat Thematic Mapper records to map land cover change and the impacts of reforestation programmes in the borderlands of southeast Yunnan, China: 1990-2010. International Journal of Applied Earth Observation and Geoinformation, 31, 25-36.

Zisheng, Y., Longfei, Y., Bosheng, Z., 2010. Soil erosion and its basinc characteristics at karst rocky-desertified land consolidation area: a case study at Muzhe Village of Xichou couny in Southeast Yunnan, China. Journal of Mountain Science, 7(1), 55-72.

Appendix 1 – Brazil Supplementary Material

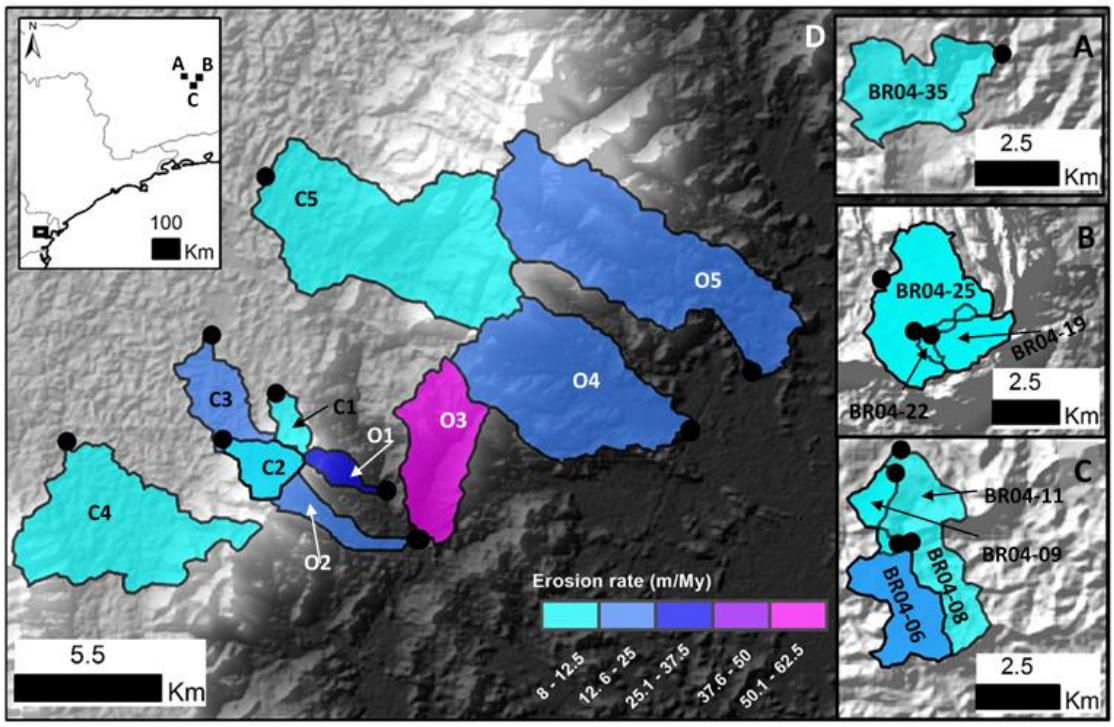

Figure DR1: Watersheds sampled for Salgado et al. 2006, 2007, 2008 and 2013 publications. Watersheds are shown imposed over a Digital Elevation Model (DEM) background. DEM data from Instituto Nacional de Pesquisas Espaciais. Published sampling location and watershed delineation were confirmed with the corresponding author.

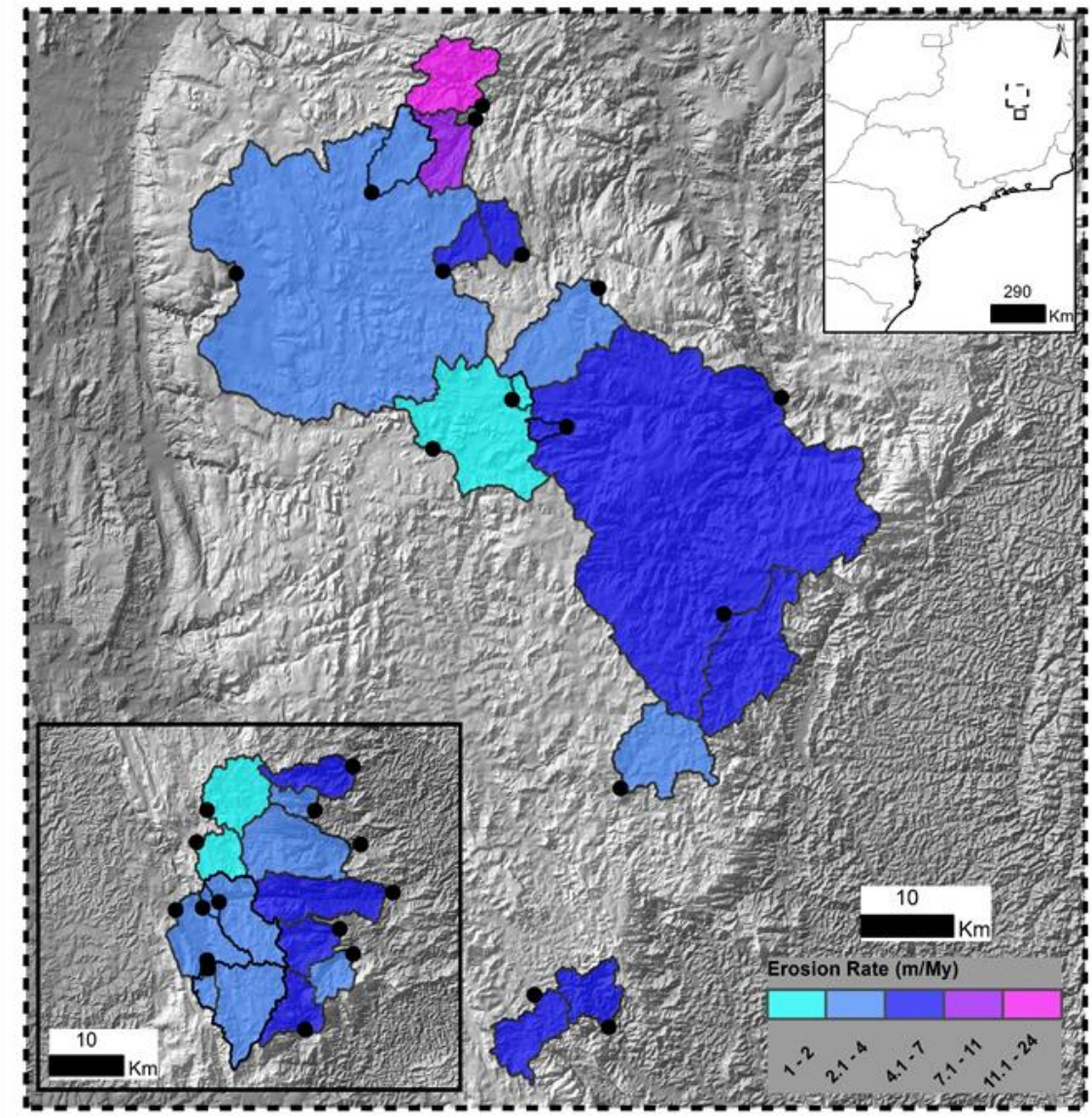

Figure DR2: Watersheds sampled for Barreto et al. 2013, 2014 publications, imposed over a DEM. DEM data from Instituto Nacional de Pesquisas Espaciais. Sampling location was confirmed by one of the authors.

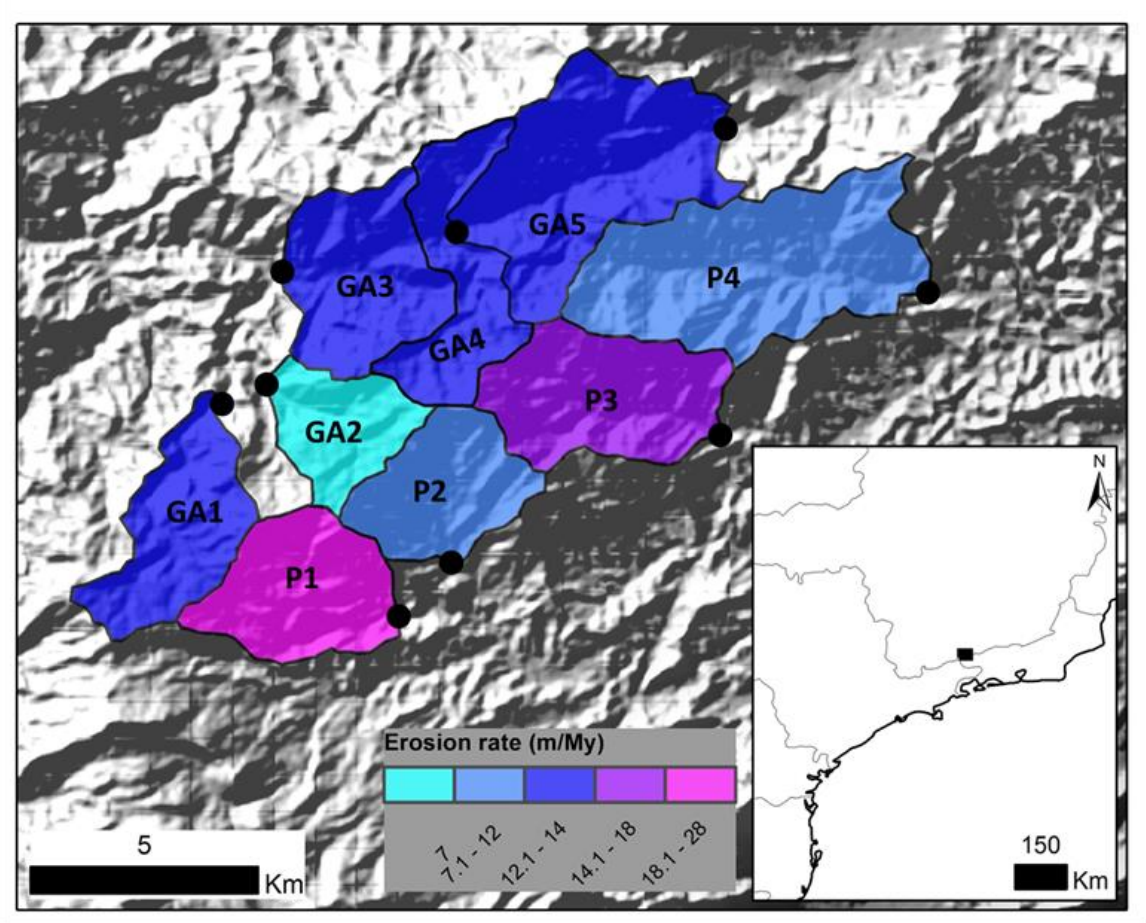

Figure DR3: Watersheds sampled for Rezende et al 2013 publication. Watersheds are shown imposed over a DEM background. DEM data from Instituto Nacional de Pesquisas Espaciais. Published sampling location and watershed delineation were confirmed with the corresponding author.

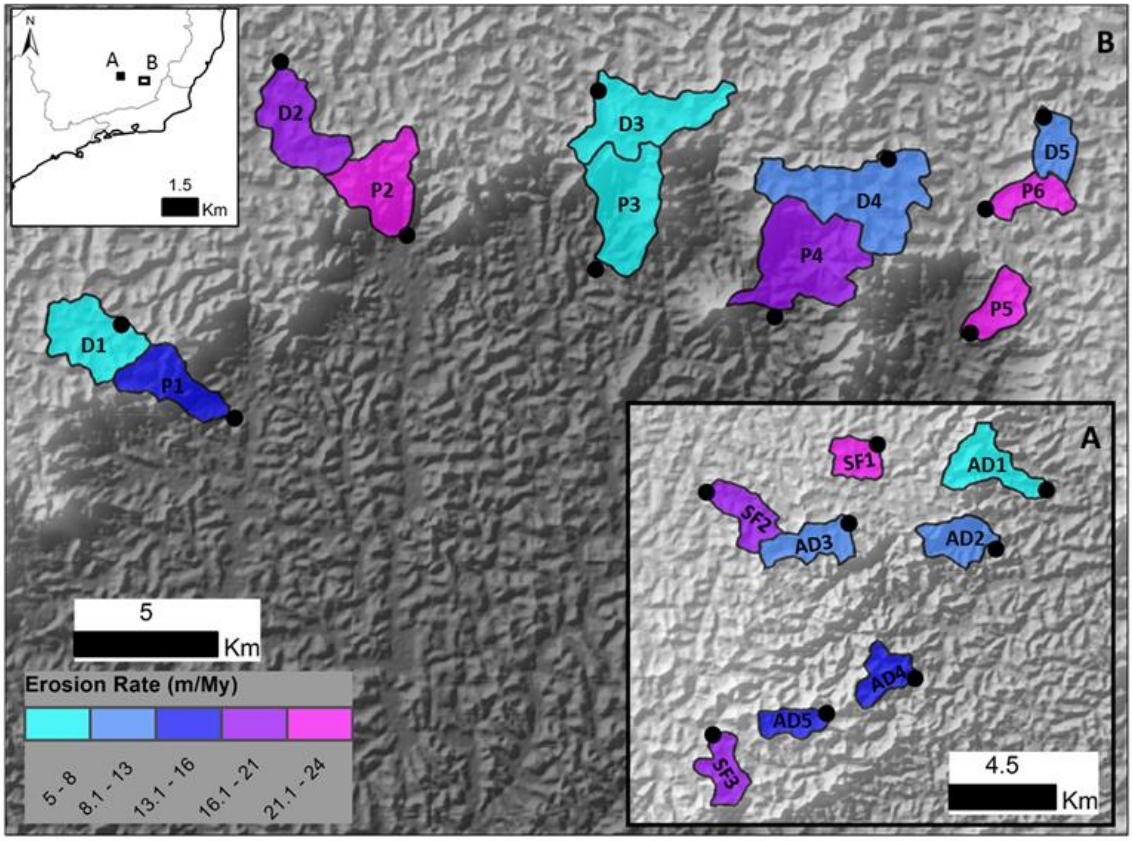

Figure DR4: Watersheds sampled for Cherem et al. 2012 publication. Watersheds are shown imposed over a DEM background. DEM data from Instituto Nacional de Pesquisas Espaciais. Published sampling location does not align perfectly with the delineated watersheds provided by the corresponding author. We adopted the author's delineation for our analysis

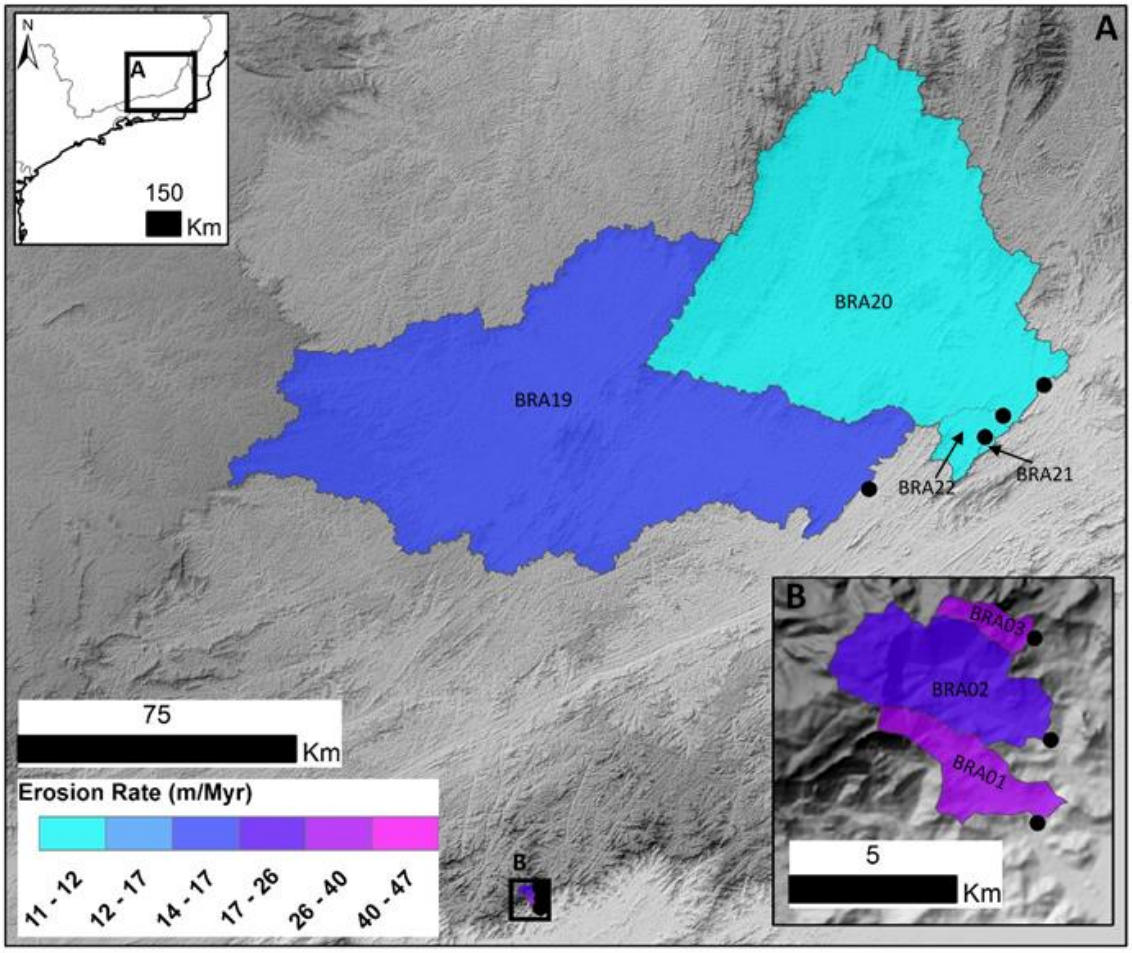

Figure DR5: Spatial distribution of erosion rates in our Rio de Janeiro watersheds. Highest erosion rates are observed in watersheds draining the Serra do Mantiqueria (inset B). Watersheds are delineated over a Digital Elevation Model (DEM) background. DEM data from Instituto Nacional de Pesquisas Espaciais

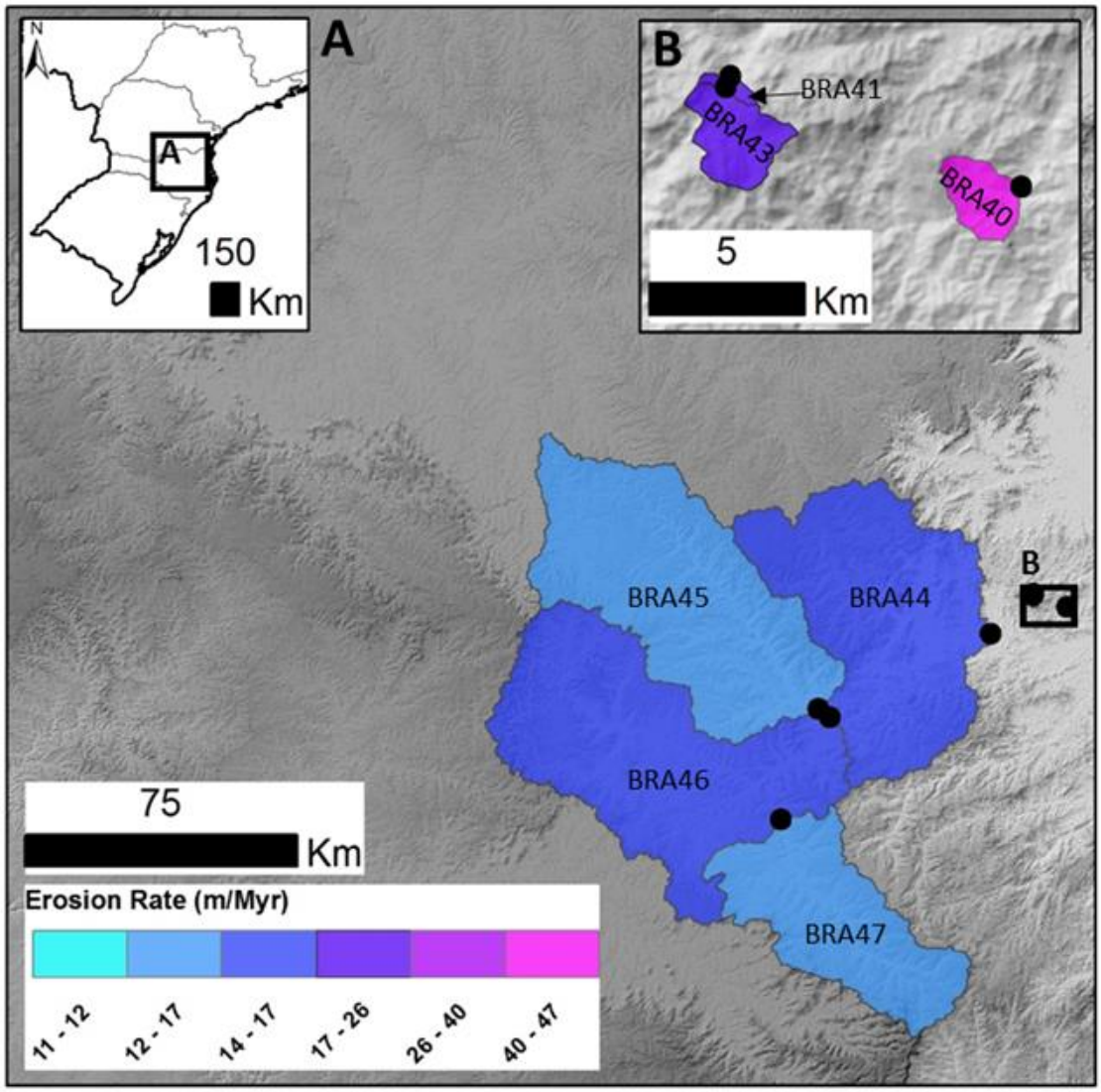

Figure DR6: Spatial distribution of erosion rates measured in Santa Catarina watersheds. Watersheds are imposed over a DEM background. DEM data from Instituto Nacional de Pesquisas Espaciais

Table Data Repository 1: CRONUS input data for all Brazilian cosmogenic studies

Publication	Sample name	Latitude[1] (DD)	Longitude[1] (DD)	Elevation (m)	Elv/pressure flag	Thickness (cm)	Density (g cm-2)	Shielding correction	[Be-10] atoms g-1	+/- atoms g-1	Be standardization	[Al-26] atoms g-1	+/- atoms g-1	Al standardization
Sosa et al., 2015	BRA01	-22.5163	-43.0006	530	std	0.1	2.7	1	83656	3012	NIST_27900	0	0	KNSTD
	BRA02	-22.4934	-42.9979	1009	std	0.1	2.7	1	121863	3199	NIST_27900	0	0	KNSTD
	BRA03	-22.4666	-43.0027	1570	std	0.1	2.7	1	86662	3885	NIST_27900	0	0	KNSTD
	BRA09	-22.3752	-42.9967	1004	std	0.1	2.7	1	336395	124591	NIST_27900	0	0	KNSTD
	BRA18	-22.2592	-42.7382	1330	std	0.1	2.7	1	484759	179540	NIST_27900	0	0	KNSTD
	BRA19	-21.5062	-42.2034	592	std	0.1	2.7	1	184702	5024	NIST_27900	0	0	KNSTD
	BRA20	-21.2550	-41.7809	555	std	0.1	2.7	1	249317	6467	NIST_27900	0	0	KNSTD
	BRA21	-21.3296	-41.8803	200	std	0.1	2.7	1	241198	4815	NIST_27900	0	0	KNSTD
	BRA22	-21.3803	-41.9238	156	std	0.1	2.7	1	241924	5782	NIST_27900	0	0	KNSTD
	BRA40	-26.8077	-48.9074	288	std	0.1	2.7	1	75607	2861	NIST_27900	0	0	KNSTD
	BRA41	-26.7753	-48.9920	283	std	0.1	2.7	1	143802	4880	NIST_27900	0	0	KNSTD
	BRA42	-26.7756	-48.9923	283	std	0.1	2.7	1	413670	153211	NIST_27900	0	0	KNSTD
	BRA43	-26.7785	-48.9929	273	std	0.1	2.7	1	146235	4422	NIST_27900	0	0	KNSTD
	BRA44	-26.8810	-49.0990	612	std	0.1	2.7	1	196183	4864	NIST_27900	0	0	KNSTD
	BRA45	-27.0608	-49.5267	553	std	0.1	2.7	1	226490	6291	NIST_27900	0	0	KNSTD
	BRA46	-27.0801	-49.4977	451	std	0.1	2.7	1	214439	5016	NIST_27900	0	0	KNSTD
	BRA47	-27.3343	-49.6195	560	std	0.1	2.7	1	237767	4802	NIST_27900	0	0	KNSTD
Barreto et al., 2013[2]	D01	-19.4677	-43.4710	1109	std	0.1	2.65	1	902000	27000	NIST_27900	0	0	KNSTD
	D02	-19.4279	-43.4262	881	std	0.1	2.7	1	1200000	40000	NIST_27900	0	0	KNSTD
	D03	-19.3882	-43.4561	1195	std	0.1	2.65	1	1030000	30000	NIST_27900	0	0	KNSTD
	D04	-19.3337	-43.4456	688	std	0.1	2.66	1	752000	20000	NIST_27900	0	0	KNSTD
	D05	-19.2727	-43.4751	995	std	0.1	2.66	1	1020000	30000	NIST_27900	0	0	KNSTD
	D06	-19.2157	-43.4701	1035	std	0.1	2.65	1	1000000	30000	NIST_27900	0	0	KNSTD
	D07	-19.1872	-43.4449	722	std	0.1	2.68	1	654000	19000	NIST_27900	0	0	KNSTD
	D08	-18.8619	-43.6268	859	std	0.1	2.72	1	704000	22000	NIST_27900	0	0	KNSTD
	J01	-18.5365	-43.4734	961	std	0.1	2.65	1	867000	29000	NIST_27900	0	0	KNSTD
	J02	-18.3174	-43.6720	1314	std	0.1	2.66	1	1600000	60000	NIST_27900	0	0	KNSTD
	J03	-18.3858	-43.5330	1026	std	0.1	2.65	1	917000	40000	NIST_27900	0	0	KNSTD
	J04	-18.2285	-43.6549	1330	std	0.1	2.67	1	1390000	40000	NIST_27900	0	0	KNSTD
	J05	-18.1258	-43.7136	1094	std	0.1	2.67	1	831000	40000	NIST_27900	0	0	KNSTD
	SF01	-19.4451	-43.5780	1291	std	0.1	2.65	1	990000	29000	NIST_27900	0	0	KNSTD
	SF02	-19.4584	-43.5360	1314	std	0.1	2.69	1	1940000	60000	NIST_27900	0	0	KNSTD
	SF03	-19.4579	-43.5365	1310	std	0.1	2.67	1	1520000	40000	NIST_27900	0	0	KNSTD
	SF04	-19.3597	-43.5303	1283	std	0.1	2.71	1	1360000	40000	NIST_27900	0	0	KNSTD
	SF05	-19.3577	-43.5344	1135	std	0.1	2.72	1	1230000	40000	NIST_27900	0	0	KNSTD
	SF06	-19.4070	-43.5487	1333	std	0.1	2.67	1	909000	28000	NIST_27900	0	0	KNSTD
	SF07	-19.2821	-43.5608	1130	std	0.1	2.67	1	2360000	70000	NIST_27900	0	0	KNSTD
	SF08	-19.2071	-43.5411	1361	std	0.1	2.65	1	1990000	50000	NIST_27900	0	0	KNSTD
	SF09	-18.9010	-43.6860	1079	std	0.1	2.65	1	951000	29000	NIST_27900	0	0	KNSTD
	SF10	-18.6286	-43.5580	1237	std	0.1	2.69	1	1120000	30000	NIST_27900	0	0	KNSTD
	SF11	-18.3149	-43.7349	1212	std	0.1	2.65	1	1810000	60000	NIST_27900	0	0	KNSTD
	SF12	-18.2816	-43.6947	1361	std	0.1	2.68	1	1420000	40000	NIST_27900	0	0	KNSTD
	SF13	-18.1400	-43.7493	1161	std	0.1	2.65	1	926000	29000	NIST_27900	0	0	KNSTD
	SF15	-18.1695	-43.8714	1293	std	0.1	2.66	1	1040000	30000	NIST_27900	0	0	KNSTD

Cont. Table Data Repository 1: CRONUS input data for all Brazilian cosmogenic studies

Publication	Sample name	Latitude[1] (DD)	Longitude[1] (DD)	Elevation (m)	Elv/pressure flag	Thickness (cm)	Density (g cm-2)	Shielding correction	[Be-10] atoms g-1	+/- atoms g-1	Be standardization	[Al-26] atoms g-1	+/- atoms g-1	Al standardization
Barreto et al., 2014[2]	Of2	-18.0509	-43.8115	1244	std	0.1	2.7	1	795000	71550	NIST_27900	0	0	KNSTD
	Oj1	-17.9770	-43.7618	1088	std	0.1	2.7	1	226000	20340	NIST_27900	0	0	KNSTD
	Oj3	-18.0481	-43.7686	1169	std	0.1	2.7	1	477000	42930	NIST_27900	0	0	KNSTD
Cherem et al., 2012[3]	AD1	-20.7264	-20.7264	883	std	0.1	2.6	1	788000	23000	NIST_27900	0	0	KNSTD
	AD2	-20.7537	-20.7537	820	std	0.1	2.6	1	455000	14000	NIST_27900	0	0	KNSTD
	AD3	-20.7556	-20.7556	1016	std	0.1	2.6	1	606000	20000	NIST_27900	0	0	KNSTD
	AD4	-20.8045	-20.8045	938	std	0.1	2.6	1	289000	10000	NIST_27900	0	0	KNSTD
	AD5	-20.8227	-20.8227	1006	std	0.1	2.6	1	320000	15000	NIST_27900	0	0	KNSTD
	D1	-20.9335	-20.9335	794	std	0.1	2.6	1	702000	22000	NIST_27900	0	0	KNSTD
	D2	-20.8718	-20.8718	775	std	0.1	2.6	1	248000	8000	NIST_27900	0	0	KNSTD
	D3	-20.8692	-20.8692	767	std	0.1	2.6	1	534000	16000	NIST_27900	0	0	KNSTD
	D4	-20.8928	-20.8928	773	std	0.1	2.6	1	343000	11000	NIST_27900	0	0	KNSTD
	D5	-20.8774	-20.8774	843	std	0.1	2.6	1	392000	12000	NIST_27900	0	0	KNSTD
	P1	-20.9463	-20.9463	729	std	0.1	2.6	1	280000	9000	NIST_27900	0	0	KNSTD
	P2	-20.8891	-20.8891	706	std	0.1	2.6	1	207000	7000	NIST_27900	0	0	KNSTD
	P3	-20.9066	-20.9066	436	std	0.1	2.6	1	426000	19000	NIST_27900	0	0	KNSTD
	P4	-20.9101	-20.9101	444	std	0.1	2.6	1	183000	8000	NIST_27900	0	0	KNSTD
	P5	-20.9314	-20.9314	392	std	0.1	2.6	1	162000	15000	NIST_27900	0	0	KNSTD
	P6	-20.8919	-20.8919	852	std	0.1	2.6	1	205000	16000	NIST_27900	0	0	KNSTD
	SF1	-20.7234	-20.7234	1007	std	0.1	2.6	1	248000	12000	NIST_27900	0	0	KNSTD
	SF2	-20.7363	-20.7363	744	std	0.1	2.6	1	237000	17000	NIST_27900	0	0	KNSTD
	SF3	-20.8412	-20.8412	1086	std	0.1	2.6	1	312000	21000	NIST_27900	0	0	KNSTD
Rezende et al., 2013[4]	GA1	-22.2980	-22.2980	1911	std	0.1	2.68	1	581000	21000	NIST_Certified	0	0	KNSTD
	GA2	-22.2779	-22.2779	1855	std	0.1	2.68	1	1065000	36000	NIST_Certified	0	0	KNSTD
	GA3	-22.2486	-22.2486	1512	std	0.1	2.68	1	497000	16000	NIST_Certified	0	0	KNSTD
	GA4	-22.2487	-22.2487	1766	std	0.1	2.68	1	781000	24000	NIST_Certified	0	0	KNSTD
	GA5	-22.2349	-22.2349	1471	std	0.1	2.68	1	475000	18000	NIST_Certified	0	0	KNSTD
	P1	-22.3102	-22.3102	1772	std	0.1	2.68	1	288000	9000	NIST_Certified	0	0	KNSTD
	P2	-22.2901	-22.2901	1623	std	0.1	2.68	1	575000	19000	NIST_Certified	0	0	KNSTD
	P3	-22.2718	-22.2718	1599	std	0.1	2.68	1	391000	13000	NIST_Certified	0	0	KNSTD
	P4	-22.2464	-22.2464	1267	std	0.1	2.68	1	488000	15000	NIST_Certified	0	0	KNSTD
Salgado et al., 2008[4]	BR04-06	-20.4072	-43.6629	1234	std	0.1	2.81	1	660183	148944	NIST_30600	0	0	KNSTD
	BR04-08	-20.4082	-43.6626	1238	std	0.1	2.81	1	423934	59604	NIST_30600	0	0	KNSTD
	BR04-09	-20.3784	-43.6700	1087	std	0.1	2.73	1	460137	174462	NIST_30600	0	0	KNSTD
	BR04-11	-20.3962	-43.6590	1190	std	0.1	2.73	1	1300733	461531	NIST_30600	0	0	KNSTD
	BR04-19	-20.1252	-43.4518	1602	std	0.1	2.57	1	5185124	409841	NIST_30600	0	0	KNSTD
	BR04-22	-20.1245	-43.4543	1561	std	0.1	2.57	1	2922000	759000	NIST_30600	0	0	KNSTD
	BR04-25	-20.1155	-43.4652	1364	std	0.1	2.57	1	2206537	129380	NIST_30600	0	0	KNSTD
	BR04-35	-20.0736	-43.9754	1333	std	0.1	2.7	1	714125	104243	NIST_30600	0	0	KNSTD

Cont. Table Data Repository 1: CRONUS input data for all Brazilian cosmogenic studies

Publication	Sample name	Latitude[1] (DD)	Longitude[1] (DD)	Elevation (m)	Elv/pressure flag	Thickness (cm)	Density (g cm-2)	Shielding correction	[Be-10] atoms g-1	+/- atoms g-1	Be standardization	[Al-26] atoms g-1	+/- atoms g-1	Al standardization
Salgado et al., 2013[4]	C1	-25.3404	-48.9089	1061	std	0.1	2.68	1	656000	32800	NIST_27900	0	0	KNSTD
	C2	-25.3547	-48.9174	1054	std	0.1	2.68	1	688000	34400	NIST_27900	0	0	KNSTD
	C3	-25.3405	-48.9268	896	std	0.1	2.68	1	397000	19850	NIST_27900	0	0	KNSTD
	C4	-25.3756	-48.9678	834	std	0.1	2.68	1	410000	20500	NIST_27900	0	0	KNSTD
	C5	-25.2532	-48.9019	837	std	0.1	2.68	1	409000	20450	NIST_27900	0	0	KNSTD
	O1	-25.3256	-48.8826	635	std	0.1	2.68	1	153000	7650	NIST_27900	0	0	KNSTD
	O2	-25.3393	-48.8774	675	std	0.1	2.68	1	266000	13300	NIST_27900	0	0	KNSTD
	O3	-25.3392	-48.8775	675	std	0.1	2.68	1	81800	4090	NIST_27900	0	0	KNSTD
	O4	-25.3278	-48.8156	231	std	0.1	2.68	1	197000	9850	NIST_27900	0	0	KNSTD
	O5	-25.2833	-48.7913	443	std	0.1	2.68	1	218000	10900	NIST_27900	0	0	KNSTD

[1] Coordinates of the watershed centroid

[2] Sampling location confirmed by one of the authors

[3] Published sampling locations do not align perfectly with delineated watersheds provided by author. We adopted the author's delineated watersheds for our analysis

[4] Sampling location and watershed delineation confirmed with corresponding author

Table Data Repository 2: Topographic variables for all cosmogenic studies in Brazil

Sample name	Publication	Sampling Location		Erosion Rate	Sample type	Area	Slope	Precipitation	Lithology
		Latitude	Longitude	(m/Myr)		(km^2)	(degrees)	(mm)	
BRA01	Sosa et al., 2015	-22.5163	-43.0006	53	Escarpment	8	24	1744	Gra
BRA02	Sosa et al., 2015	-22.4934	-42.9979	46	Escarpment	18	26	1824	Gra
BRA03	Sosa et al., 2015	-22.4666	-43.0027	90	Escarpment	3	29	1808	Gra
BRA19	Sosa et al., 2015	-21.5062	-42.2034	23	Highland	9169	12	1376	Gr, Gn
BRA20	Sosa et al., 2015	-21.2550	-41.7809	16	Highland	7243	14	1292	Gr, Gn
BRA21	Sosa et al., 2015	-21.3296	-41.8803	13	Highland	247	13	1223	Gra
BRA22	Sosa et al., 2015	-21.3803	-41.9238	13	Highland	15	15	1215	Gra
BRA40	Sosa et al., 2015	-26.8077	-48.9074	55	Highland	5	16	1649	Gr, Gn
BRA41	Sosa et al., 2015	-26.7753	-48.9920	27	Highland	9	17	1646	Gr, Gn
BRA43	Sosa et al., 2015	-26.7785	-48.9929	27	Highland	8	17	1644	Gr, Gn
BRA44	Sosa et al., 2015	-26.8810	-49.0990	24	Highland	14987	12	1533	C.S.[a]
BRA45	Sosa et al., 2015	-27.0608	-49.5267	20	Highland	4167	12	1484	C.S.[b]
BRA46	Sosa et al., 2015	-27.0801	-49.4977	20	Highland	6931	11	1543	C.S.[a]
BRA47	Sosa et al., 2015	-27.3343	-49.6195	19	Highland	2335	12	1578	C.S.[a]
D01	Barreto et al., 2013	-19.5042	-43.4599	5	Escarpment	48	14	1581	Q
D02	Barreto et al., 2013	-19.4016	-43.4004	3	Escarpment	32	15	1575	Q
D03	Barreto et al., 2013	-19.3713	-43.4157	5	Escarpment	47	13	1588	Q
D04	Barreto et al., 2013	-19.3272	-43.3526	5	Escarpment	98	14	1569	Q
D05	Barreto et al., 2013	-19.2689	-43.3907	4	Escarpment	111	12	1589	Q
D06	Barreto et al., 2013	-19.2279	-43.4462	4	Escarpment	22	14	1600	Q
D07	Barreto et al., 2013	-19.1747	-43.4000	6	Escarpment	46	13	1615	Q
D08	Barreto et al., 2013	-18.8955	-43.6103	6	Escarpment	36	14	1518	Gr, Gn
J01	Barreto et al., 2013	-18.4965	-43.4982	5	Escarpment	107	10	1472	Q
J02	Barreto et al., 2013	-18.3156	-43.6503	3	Escarpment	7	8	1479	S, P
J03	Barreto et al., 2013	-18.2879	-43.4421	5	Escarpment	901	10	1436	Q
J04	Barreto et al., 2013	-18.1816	-43.6202	4	Escarpment	87	6	1474	Q
J05	Barreto et al., 2013	-18.1492	-43.6934	6	Escarpment	25	7	1412	Q
Of2	Barreto et al., 2014	-18.0892	-43.8391	7	Escarpment	41	5	1415	N.A.
Oj1	Barreto et al., 2014	-18.0057	-43.7324	24	Escarpment	59	10	1381	N.A.
Oj3	Barreto et al., 2014	-18.0189	-43.7380	11	Escarpment	39	10	1408	N.A.

Cont. Table Data Repository 2: Topographic variables for all cosmogenic studies in Brazil

Sample name	Publication	Sampling Location		Erosion Rate	Sample type	Area	Slope	Precipitation	Lithology
		Latitude	Longitude	(m/Myr)		(km^2)	(degrees)	(mm)	
SF01	Barreto et al., 2013	-19.4188	-43.5761	4	Escarpment	13	12	1578	Q
SF02	Barreto et al., 2013	-19.4176	-43.5757	2	Escarpment	109	10	1607	Q
SF03	Barreto et al., 2013	-19.4090	-43.5765	2	Escarpment	110	16	1523	Q
SF04	Barreto et al., 2013	-19.3385	-43.5624	3	Escarpment	73	11	1599	Q
SF05	Barreto et al., 2013	-19.3460	-43.5907	3	Escarpment	81	15	1541	Q
SF06	Barreto et al., 2013	-19.3409	-43.6296	4	Escarpment	262	11	1547	Q
SF07	Barreto et al., 2013	-19.2660	-43.5897	1	Escarpment	38	9	1588	S, P
SF08	Barreto et al., 2013	-19.2276	-43.5769	2	Escarpment	73	7	1599	Q
SF09	Barreto et al., 2013	-18.8636	-43.6808	5	Escarpment	45	9	1514	Q
SF10	Barreto et al., 2013	-18.6648	-43.5983	4	Escarpment	75	8	1493	Q
SF11	Barreto et al., 2013	-18.3362	-43.7801	2	Escarpment	153	7	1445	Q
SF12	Barreto et al., 2013	-18.2889	-43.7033	4	Escarpment	7	6	1482	S, P
SF13	Barreto et al., 2013	-18.1649	-43.7700	5	Escarpment	21	6	1406	Q
SF15	Barreto et al., 2013	-18.1674	-43.9708	4	Escarpment	772	7	1381	Q
AD1	Cherem et al., 2012	-20.7353	-43.6516	5	Escarpment	7	13	1424	N.A.
AD2	Cherem et al., 2012	-20.7552	-43.6699	10	Escarpment	5	15	1414	N.A.
AD3	Cherem et al., 2012	-20.7473	-43.7265	8	Highland	5	9	1463	N.A.
AD4	Cherem et al., 2012	-20.8060	-43.7008	17	Escarpment	4	15	1434	N.A.
AD5	Cherem et al., 2012	-20.8191	-43.7349	16	Highland	3	11	1468	N.A.
D1	Cherem et al., 2012	-20.9304	-42.9233	6	Highland	7	12	1345	N.A.
D2	Cherem et al., 2012	-20.8525	-42.8752	19	Highland	7	11	1304	N.A.
D3	Cherem et al., 2012	-20.8606	-42.7745	8	Highland	9	11	1304	N.A.
D4	Cherem et al., 2012	-20.8812	-42.6840	13	Highland	10	13	1317	N.A.
D5	Cherem et al., 2012	-20.8686	-42.6348	12	Highland	3	12	1332	N.A.
P1	Cherem et al., 2012	-20.9556	-42.8901	16	Escarpment	5	15	1311	N.A.
P2	Cherem et al., 2012	-20.9029	-42.8351	22	Escarpment	5	15	1268	N.A.
P3	Cherem et al., 2012	-20.9132	-42.7767	8	Escarpment	5	14	1240	N.A.
P4	Cherem et al., 2012	-20.9281	-42.7195	21	Escarpment	11	17	1264	N.A.
P5	Cherem et al., 2012	-20.9327	-42.6588	24	Escarpment	1	12	1248	N.A.
P6	Cherem et al., 2012	-20.8949	-42.6543	24	Highland	3	12	1332	N.A.
SF1	Cherem et al., 2012	-20.7180	-43.7160	21	Highland	3	7	1456	N.A.
SF2	Cherem et al., 2012	-20.7358	-42.7794	19	Highland	4	13	1274	N.A.
SF3	Cherem et al., 2012	-20.8265	-43.7768	18	Highland	4	10	1473	N.A.

Cont. Table Data Repository 2: Topographic variables for all cosmogenic studies in Brazil

Sample name	Publication	Sampling Location		Erosion Rate	Sample type	Area	Slope	Precipitation	Lithology
		Latitude	Longitude	(m/Myr)		(km^2)	(degrees)	(mm)	
GA1	Rezende et al., 2013	-22.2670	-44.6430	14	Escarpment	11	14	2068	N.A.
GA2	Rezende et al., 2013	-22.2689	-44.6359	7	Escarpment	8	15	2043	N.A.
GA3	Rezende et al., 2013	-22.2466	-44.6328	13	Escarpment	13	18	1916	N.A.
GA4	Rezende et al., 2013	-22.2346	-44.5859	10	Escarpment	10	16	2057	N.A.
GA5	Rezende et al., 2013	-22.2174	-44.5395	14	Escarpment	31	20	1873	N.A.
P1	Rezende et al., 2013	-22.3145	-44.6039	28	Escarpment	12	18	1991	N.A.
P2	Rezende et al., 2013	-22.3066	-44.5962	12	Escarpment	10	19	1991	N.A.
P3	Rezende et al., 2013	-22.2782	-44.5389	18	Escarpment	14	21	1880	N.A.
P4	Rezende et al., 2013	-22.2515	-44.4965	12	Escarpment	24	19	1783	N.A.
BR04-06	Salgado et al., 2008	-20.3913	-43.6640	9	Highland	7	16	1591	S, P
BR04-08	Salgado et al., 2008	-20.3916	-43.6636	14	Highland	6	8	1591	S, P
BR04-09	Salgado et al., 2008	-20.3716	-43.6644	12	Highland	2	5	1534	Gr, Gn
BR04-11	Salgado et al., 2008	-20.3656	-43.6620	4	Highland	18	10	1570	Gr, Gn
BR04-19	Salgado et al., 2008	-20.1236	-43.4655	1	Highland	4	13	1712	Q
BR04-22	Salgado et al., 2008	-20.1242	-43.4716	2	Highland	6	15	1570	Q, Md
BR04-25	Salgado et al., 2008	-20.1041	-43.4822	3	Highland	22	19	1660	Q, Md
BR04-35	Salgado et al., 2008	-20.0664	-43.9512	9	Highland	10	11	1554	S, P
C1	Salgado et al., 2013	-25.3305	-48.9132	9	Escarpment	3	13	1813	Gr
C2	Salgado et al., 2013	-25.3459	-48.9313	8	Escarpment	5	17	1851	Gr
C3	Salgado et al., 2013	-25.3109	-48.9351	13	Escarpment	13	7	1733	Gr, M
C4	Salgado et al., 2013	-25.3467	-48.9840	12	Escarpment	30	10	1744	Gr, M
C5	Salgado et al., 2013	-25.2576	-48.9129	12	Escarpment	3	10	1692	Gr, M
O1	Salgado et al., 2013	-25.3653	-48.8752	31	Escarpment	37	15	1783	Gr
O2	Salgado et al., 2013	-25.3830	-48.8651	17	Escarpment	64	8	1824	Gr
O3	Salgado et al., 2013	-25.3809	-48.8643	62	Escarpment	63	17	1867	Gr, Gn
O4	Salgado et al., 2013	-25.3435	-48.7730	18	Escarpment	35	15	1940	Gr, M, Gn
O5	Salgado et al., 2013	-25.3235	-48.7522	19	Escarpment	47	18	1919	Gr, M

Notes: Samples published in Barreto et al., 2014 are from the same locations as Barreto et al., 2013. with the exception of three samples. We report the 2013 and only the new 2014 samples to avoid duplicates. Since sample ID differs in both publications, we use the ID from the 2013 publication. Samples published in Salgado et al., 2006, 2007, and 2008 are from the same locations. We report the samples in the 2008 publication, which includes all samples

Dominant lithology is reported for each watershed: Quartzite (Q), Granite (Gr), Gneiss (Gn), Schist (S), Phyllite (P), Mafic dikes (Md), Migmatites (M), Granitoid (Gra), Consolidated Sedimentary (C. For watersheds were the data is not available, we report N.A.

[a] Consolidated sedimentary sequences composed of sandy, silty conglomerates.

[b] Consolidated sedimentary sequences of eolian origin

Appendix 2 – China Supplementary Material

Table Data Repository 3: Isotopic data of all samples included in this study

Sample ID	Year sampled	Sample type	Sample location[1]		Quartz mass	SUERC ID[2]	^{9}Be Carrier	Measured ^{10}Be/^{9}Be ratio[3]			In situ ^{10}Be concentration		
			Latitude	Longitude	(g)		(µg)	($x10^{-13}$ atoms)			($x10^{5}$ atoms/g)		
CH-001[4,5]	2013	Station 35 - in channel	27.156	99.321	8.086	b7722	218.5	1.06	±	0.04	1.92	±	0.07
CH-002[4]	2013	Station 35 - overbank	27.156	99.321	5.92	b7676	246.4	1.12	±	0.03	3.11	±	0.10
CH-002(A)[4,6]	2013	Station 35 - overbank	27.156	99.321	11.93	b7723	222.5	2.63	±	0.11	3.28	±	0.14
CH-005[5]	2013	No station - in channel	27.064	99.351	12.04	b7691	219.7	2.13	±	0.07	2.60	±	0.08
CH-008[7]	2013	Terrace sample by CH-005 site	27.064	99.351	16.89	b7693	220.8	1.52	±	0.05	1.32	±	0.05
CH-017[5,7]	2013	No station - in channel	27.131	99.406	19.99	b7698	221.6	7.72	±	0.24	5.72	±	0.18
CH-018[7]	2013	Terrace sample by CH-017 site	27.131	99.406	5.79	b7699	221.9	3.00	±	0.06	7.68	±	0.15
CH-019[7]	2013	Terrace sample by CH-017 site	27.131	99.406	9.37	b7728	222.2	3.92	±	0.09	6.21	±	0.14
CH-022[7]	2013	Terrace sample by CH-023 site	27.123	99.347	10.52	b7663	249.3	12.70	±	0.16	20.20	±	0.26
CH-023[5,7]	2013	No station - in channel	27.121	99.353	19.50	b7705	223.2	12.40	±	0.15	9.47	±	0.12
CH-037[5,7]	2013	No station - in channel	24.060	100.808	19.91	b7711	223.1	1.25	±	0.05	0.93	±	0.04
CH-038[7]	2013	Terrace sample by CH-037 site	24.060	100.808	14.60	b7679	248.1	0.79	±	0.03	0.89	±	0.03
CH-039[5,7]	2013	No station - in channel	23.980	100.799	19.08	b7118	248.3	0.94	±	0.03	0.81	±	0.03
CH-040[7]	2013	Terrace sample by CH-039 site	23.980	100.799	20.13	b7682	247.8	0.97	±	0.03	0.80	±	0.03
CH-043	2013	No station - in channel	23.695	100.634	20.01	b7121	248.2	1.96	±	0.04	1.60	±	0.04
CH-044[5,7]	2013	Station 49 - in channel	23.557	100.710	17.57	b7730	220.4	0.96	±	0.03	0.81	±	0.03
CH-050[5,7]	2013	No station - in channel	23.726	100.830	13.73	b7684	247.7	0.60	±	0.03	0.72	±	0.03
CH-051[7]	2013	Terrace sample by CH-050	23.726	100.830	20.07	b7715	222.4	1.25	±	0.04	0.93	±	0.03
CH-056	2013	No station - in channel	23.700	100.816	19.97	b7672	248.2	0.72	±	0.03	0.58	±	0.03
CH-058	2013	No station - in channel	23.692	100.814	19.98	b7685	247.8	0.84	±	0.03	0.67	±	0.02
CH-060[8]	2013	Station 49 - overbank	23.557	100.710	11.02	b7732	221.3	0.54	±	0.02	0.72	±	0.03
CH-070	2013	No station - in channel	21.794	100.367	20.25	b7138	248.9	1.47	±	0.06	1.19	±	0.05
CH-071	2013	No station - in channel	21.944	100.341	16.48	b7139	249.5	1.73	±	0.05	1.73	±	0.06
CH-073[5,7]	2013	Station 6 - in channel	21.846	100.980	20.20	b9141	260.3	0.86	±	0.03	0.74	±	0.03
CH-074[8]	2013	Station 6 - overbank	21.846	100.980	19.87	b9142	258.6	0.95	±	0.03	0.83	±	0.03
CH-075[5,7]	2013	Station 11 - in channel	21.952	100.425	20.00	b7735	221.3	2.04	±	0.05	1.51	±	0.04
CH-076[8]	2013	Station 11 - overbank	21.952	100.425	20.01	b7736	221.6	2.33	±	0.05	1.72	±	0.04
CH-101	2014	Station 91 - in channel	22.969	104.818	10.42	b9313	300.9	0.53	±	0.03	1.03	±	0.06
CH-102	2014	Station 91 - overbank	22.969	104.818	20.43	b9003	333.38	1.16	±	0.05	1.27	±	0.06
CH-103	2014	Station 90 - in channel	23.134	104.507	12.48	b9455	315.19	1.55	±	0.04	2.61	±	0.07
CH-104	2014	Station 90 - overbank	23.134	104.507	12.62	b9456	274.01	1.92	±	0.05	2.79	±	0.07
CH-105	2014	Station 108 - in channel	23.284	103.724	8.69	b9155	269.11	2.52	±	0.06	5.21	±	0.13
CH-106	2014	Station 108 - overbank	23.284	103.724	13.91	b9156	258.71	3.82	±	0.12	4.74	±	0.15
CH-107	2014	Station 106 - in channel	22.852	103.580	19.12	b9457	353.88	0.45	±	0.03	0.55	±	0.03
CH-108	2014	Station 106 - overbank	22.852	103.580	15.05	b9458	505.98	0.28	±	0.03	0.62	±	0.06
CH-109	2014	Station 103 - in channel	23.547	102.073	19.88	b9312	259.14	0.82	±	0.04	0.72	±	0.04
CH-110	2014	Station 103 - overbank	23.547	102.073	15.84	b9145	259.51	1.14	±	0.04	1.25	±	0.04

Cont. Table Data Repository 3: Isotopic data of all samples included in this study

Sample ID	Year sampled	Sample type	Sample location[1]		Quartz mass	SUERC ID[2]	^{9}Be Carrier	Measured ^{10}Be/^{9}Be ratio[3]			In situ ^{10}Be concentration		
			Latitude	Longitude	(g)		(µg)	(x10^{-13} atoms)			(x10^{5} atoms/g)		
CH-111	2014	No station - in channel	23.545	102.086	26.05	b9017	263.60	1.37	±	0.04	0.93	±	0.03
CH-112	2014	No station - overbank	23.545	102.086	10.14	b9461	259.57	0.74	±	0.04	1.26	±	0.06
CH-113	2014	Station 87 - in channel	23.352	101.502	17.90	b9021	259.02	0.59	±	0.04	0.57	±	0.04
CH-114	2014	Resample CH-056	23.700	100.816	19.61	b9022	261.66	0.91	±	0.07	0.81	±	0.06
CH-115	2014	Resample CH-058	23.694	100.818	19.37	b9146	259.02	0.91	±	0.04	0.82	±	0.03
CH-116	2014	Resample CH-043	23.696	100.630	20.09	b9004	258.62	1.32	±	0.04	1.14	±	0.04
CH-117[8]	2014	Resample CH-044	23.557	100.710	18.02	b9005	258.04	0.81	±	0.03	0.77	±	0.03
CH-118[8]	2014	Resample CH-060	23.557	100.710	19.94	b9008	254.20	0.84	±	0.04	0.71	±	0.03
CH-119[8]	2014	Resample CH-073	21.846	100.980	20.32	b9009	257.85	0.95	±	0.04	0.81	±	0.03
CH-120[8]	2014	Resample CH-074	21.846	100.980	20.01	b9010	258.99	1.04	±	0.04	0.90	±	0.03
CH-121	2014	Resample CH-070	21.794	100.366	20.02	b9012	258.74	1.24	±	0.05	1.07	±	0.04
CH-122	2014	Resample CH-071	21.794	100.366	20.07	b9014	253.74	1.46	±	0.04	1.23	±	0.04
CH-123	2014	Terrace sand + charcoal at CH-071 location	21.942	100.341	17.01	b9147	258.87	1.37	±	0.05	1.39	±	0.05
CH-124	2014	Terrace sand + charcoal at CH-071 location	21.942	100.341	14.21	b9148	258.47	1.00	±	0.04	1.22	±	0.04
CH-125	2014	Charcoal at CH-074 location	21.942	100.341	NOT APLICABLE						NOT APPLICABLE		
CH-126[8]	2014	Resample CH-076	21.952	100.421	20.18	b9159	260.56	2.07	±	0.05	1.79	±	0.05
CH-127[8]	2014	Resample CH-075	21.952	100.421	19.93	b9149	258.96	2.01	±	0.06	1.75	±	0.05
CH-128	2014	Station 109 - overbank	22.184	99.222	20.06	b9160	258.71	1.86	±	0.05	1.60	±	0.05
CH-129	2014	Station 109 - in channel	22.184	99.222	19.94	b9023	260.53	1.83	±	0.05	1.60	±	0.04
CH-130	2014	Station 94 - overbank	22.337	99.575	19.84	b9153	257.73	1.09	±	0.04	0.95	±	0.03
CH-131	2014	Station 94 - in channel	22.337	99.575	17.86	b9024	259.17	1.01	±	0.04	0.98	±	0.04
CH-132	2014	Station 32 - overbank	23.365	99.447	16.81	b9154	257.95	1.33	±	0.04	1.36	±	0.04
CH-133	2014	Station 32 - in channel	23.365	99.447	20.13	b9161	258.22	1.36	±	0.05	1.16	±	0.04
CH-134	2014	Station 93 - overbank	23.677	99.237	18.16	b9205	260.49	0.52	±	0.03	0.50	±	0.03
CH-135	2014	Station 93 - in channel	23.677	99.237	17.17	b9162	258.25	0.41	±	0.03	0.41	±	0.03
CH-136	2014	No station - overbank	23.526	98.971	20.13	b9166	258.25	0.63	±	0.03	0.54	±	0.03
CH-137	2014	No station - in channel	23.526	98.971	20.18	b9167	258.84	1.07	±	0.04	0.92	±	0.03
CH-137(A)[6]	2014	No station - in channel	23.526	98.971	20.28	b9169	265.58	0.58	±	0.03	0.51	±	0.03
CH-138	2014	No station - overbank	23.531	98.988	20.07	b9206	259.51	0.55	±	0.03	0.48	±	0.03
CH-139	2014	No station - in channel	23.531	98.988	21.86	b9015	257.36	0.60	±	0.03	0.48	±	0.03
CH-140	2014	Station 99 - overbank	24.052	97.975	20.02	b9207	263.85	0.73	±	0.35	0.65	±	0.03
CH-141	2014	Station 99 - in channel	24.052	97.975	20.03	b9016	258.54	0.67	±	0.03	0.58	±	0.03
CH-142	2014	Station 85 - overbank	24.487	97.726	19.20	b9025	260.59	0.59	±	0.03	0.53	±	0.03
CH-143	2014	Station 85 - in channel	24.487	97.726	20.02	b9027	257.70	0.63	±	0.03	0.54	±	0.03
CH-144	2014	Station 84 - overbank	24.622	97.868	19.98	b9029	263.63	0.75	±	0.04	0.66	±	0.03
CH-145	2014	Station 84 - in channel	24.622	97.868	18.61	b9030	256.99	0.70	±	0.03	0.65	±	0.03
CH-146	2014	Station 100 - overbank	24.671	98.651	20.12	b9226	258.90	1.01	±	0.04	0.87	±	0.04

Cont. Table Data Repository 3: Isotopic data of all samples included in this study

Sample ID	Year sampled	Sample type	Sample location[1]		Quartz mass	SUERC ID[2]	^{9}Be Carrier	Measured ^{10}Be/^{9}Be ratio[3]			In situ ^{10}Be concentration		
			Latitude	Longitude	(g)		(µg)	(x10^{-13} atoms)			(x10^{5} atoms/g)		
CH-147	2014	Station 15 - in channel	25.102	98.839	9.86	b9208	273.16	0.59	±	0.03	1.08	±	0.06
CH-148	2014	Station 15 - overbank	25.102	98.839	20.16	b9462	298.24	2.33	±	0.12	2.31	±	0.12
CH-148(A)[6]	2014	Station 15 - overbank	25.102	98.839	15.23	b9463	285.88	1.69	±	0.05	2.12	±	0.07
CH-149	2014	Resample TRR 13b - in channel	25.866	98.850	11.29	b9211	259.52	0.69	±	0.03	1.06	±	0.05
CH-150	2014	Resample TRR 13b - overbank	25.866	98.850	20.70	b9464	286.59	1.30	±	0.04	1.21	±	0.04
CH-153	2014	Resample TRR 14b - in channel	25.441	99.286	10.27	b9467	258.78	0.16	±	0.02	0.27	±	0.04
CH-154	2014	Resample TRR 14b - overbank	25.441	99.286	12.02	b9468	256.29	0.34	±	0.03	0.48	±	0.04
CH-155	2014	Station 86 - in channel	25.418	100.007	15.01	b9303	260.25	0.69	±	0.08	0.80	±	0.09
CH-156	2014	Station 86 - overbank	25.418	100.007	17.94	b9031	253.65	0.76	±	0.04	0.72	±	0.04
CH-157	2014	Station 97 - in channel	24.434	100.118	17.10	b9227	258.99	1.05	±	0.05	1.06	±	0.05
CH-158	2014	Station 97 - overbank	24.434	100.118	13.09	b9228	258.78	0.67	±	0.03	0.89	±	0.04
CH-159	2014	Station 101 - in channel	25.064	100.541	18.93	b9212	260.83	1.38	±	0.04	1.27	±	0.04
CH-160	2014	Station 101 - overbank	25.064	100.541	17.55	b9213	261.33	1.16	±	0.04	1.15	±	0.04
CH-161	2014	Resample TRR 9 - in channel	28.026	98.632	9.40	b9214	260.53	1.10	±	0.04	2.05	±	0.07
CH-162	2014	Resample TRR 9 - overbank	28.026	98.632	9.02	b9231	259.78	1.11	±	0.05	2.14	±	0.09
CH-166	2014	Resample TRR 10 - overbank	27.583	98.793	9.75	b9305	283.03	0.84	±	0.04	1.62	±	0.08
CH-167	2014	Resample TRR 10 - in channel	27.583	98.793	14.41	b9306	344.78	0.79	±	0.04	1.26	±	0.06
CH-168	2014	Resample TRR 11a (tributary) - in channel	27.228	98.892	20.03	b9232	285.58	1.20	±	0.05	1.14	±	0.05
CH-169	2014	Resample TRR 11b (main channel) - in channel sample	27.228	98.892	8.06	b9308	262.50	0.68	±	0.04	1.47	±	0.08
CH-170	2014	Resample TRR 11b (main channel) - overbank sample	27.228	98.892	8.56	b9233	256.81	1.02	±	0.05	2.05	±	0.09
CH-171	2014	Resample TRR 12 (in channel)	26.483	98.898	10.34	b9309	258.71	0.91	±	0.05	1.52	±	0.08
CH-172	2014	Resample TRR 12 (overbank)	26.483	98.898	4.93	b9311	258.50	0.38	±	0.03	1.33	±	0.10
Y13-01-DM[9]	2013	Station 87 - in channel	23.327	101.510	20.23	b9218	259.42	0.70	±	0.03	0.60	±	0.03
TRR-9	2005	No station - overbank	28.022	98.630	20.17	582	252.40	6.25	±	0.14	5.19	±	0.12
TRR-10	2005	No station - overbank	27.583	98.793	19.96	847	250.90	5.15	±	0.14	4.28	±	0.12
TRR-11b	2005	No station - overbank	31.279	94.429	10.02	848	255.20	3.18	±	1.00	5.32	±	0.18
TRR-12	2005	No station - overbank	26.477	98.896	20.52	232	253.00	4.93	±	1.84	4.02	±	0.16
TRR-13b	2005	No station - overbank	25.846	98.861	10.22	737	252.200				2.94	±	0.12
TRR-14b	2005	No station - overbank	25.429	99.291			NOT MEASURED				NOT MEASURED		
TRR-14b(A)[6]	2005	No station - overbank	25.429	99.291			NOT MEASURED				NOT MEASURED		

[1] Sample locations are reported in WGS84.

[2] Unique sample ID assigned at the Scottish Universities Environmental Research Centre (SUERC) Accelerator Mass Spectrometry Laboratory

[3] Ratios have been blank corrected

[4] Samples used only for in-channel and overbank comparison; not included in any other statistical analysis.

[5] Data from Neilson et al., 2015 (in review)

[6] Process replicate. Error-weighted average of the isotopic concentration of the original sample and replicate was used to calculate erosion rates

[7] Samples used for temporal comparison of isotopic concentration between terrace and active channel material; not included in any other statistical analysis.

[8] Measured concentrations were used for comparisons in isotopic activities over time. Additionally, weighted-average of replicate samples from the same site were used to calculate erosion rates and assess the relationship with topography

[9] Sample collected by Devin McPhillips, about 3 Km downstream from our CH-113 sample. Sample was processed with samples for this paper. Isotopic concentration of this sample is weight-averaged with our sample, and used to calculate erosion and asses relationship with topography

Cont. Table Data Repository 3: Isotopic data of all samples included in this study

Sample ID	Year sampled	Sample mass (g)	SUERC ID[2]	^{9}Be Carrier (μg)	Measured ^{10}Be/^{9}Be ratio[3] (x10^{-13} atoms)			Meteoric ^{10}Be (x10^{7} atoms/g)			Notes
CH-001[4,5]	2013	0.501	b8221	322.6	11.50	±	0.28	4.85	±	0.16	
CH-002[4]	2013				NOT MEASURED						
CH-002(A)[4,6]	2013				NOT MEASURED						
CH-005[5]	2013	0.498	b8093	323.0	9.60	±	0.62	4.15	±	0.29	
CH-008[7]	2013				NOT MEASURED						^{14}C age: 1450 ± 20 YBP
CH-017[5,7]	2013	0.511	b8101	322.0	31.10	±	3.20	13.00	±	1.35	
CH-018[7]	2013				NOT MEASURED						^{14}C age: 340 ± 15 YBP
CH-019[7]	2013				NOT MEASURED						^{14}C age: 115 ± 15 YBP
CH-022[7]	2013				NOT MEASURED						^{14}C age: 190 ± 15 YBP
CH-023[5,7]	2013	0.495	b8106	322.3	29.10	±	1.22	12.50	±	0.54	
CH-037[5,7]	2013	0.508	b8190	320.4	5.52	±	0.13	2.23	±	0.11	
CH-038[7]	2013				NOT MEASURED						^{14}C age: 130 ± 20 YBP
CH-039[5,7]	2013	0.498	b8191	320.7	2.03	±	0.13	0.78	±	0.11	
CH-040[7]	2013				NOT MEASURED						^{14}C age: 0 ± 20 YBP (modern)
CH-043	2013	0.496	b8195	325.8	3.32	±	0.09	1.36	±	0.11	
CH-044[5,7]	2013	0.493	b8849	394.3	1.72	±	0.04	0.84	±	0.03	
CH-050[5,7]	2013	0.501	b8228	319.8	2.63	±	0.11	1.02	±	0.11	
CH-051[7]	2013				NOT MEASURED						^{14}C age: 0 ± 15 YBP (modern)
CH-056	2013	0.507	b8999	497.0	1.30	±	0.04	77.10	±	3.05	
CH-058	2013	0.572	b8909	502.0	1.76	±	0.04	95.20	±	2.97	
CH-060[8]	2013				NOT MEASURED						
CH-070	2013	0.507	b8322	320.7	6.16	±	0.15	2.51	±	0.12	
CH-071	2013	0.508	b8323	322.3	9.94	±	0.19	4.11	±	0.13	
CH-073[5,7]	2013	0.546	b8965	497.0	0.74	±	0.04	0.37	±	0.03	
CH-074[8]	2013	0.513	b8966	499.0	0.86	±	0.03	0.48	±	0.03	
CH-075[5,7]	2013	0.504	b8324	322.3	14.40	±	0.24	6.07	±	0.14	
CH-076[8]	2013				NOT MEASURED						
CH-101	2014	0.525	b8868	495.1	3.21	±	0.09	1.94	±	0.06	
CH-102	2014	0.546	b8930	485.2	1.81	±	0.04	0.99	±	0.03	
CH-103	2014	0.500	b8869	495.1	11.00	±	0.14	7.21	±	0.10	
CH-104	2014	0.515	b8870	495.1	12.20	±	0.17	7.74	±	0.11	
CH-105	2014	0.506	b8871	493.1	13.90	±	0.21	9.00	±	0.14	
CH-106	2014	0.524	b8874	498.0	14.60	±	0.31	9.21	±	0.20	
CH-107	2014	0.580	b8913	498.0	3.56	±	0.08	1.96	±	0.05	
CH-108	2014	0.570	b8932	497.0	6.99	±	0.12	3.99	±	0.07	
CH-109	2014	0.516	b8914	499.0	1.27	±	0.03	0.74	±	0.03	
CH-110	2014	0.553	b8875	498.0	2.14	±	0.05	1.21	±	0.03	

Cont. Table Data Repository 3: Isotopic data of all samples included in this study

Sample ID	Year sampled	Sample mass (g)	SUERC ID[2]	^{9}Be Carrier (µg)	Measured ^{10}Be/^{9}Be ratio[3] ($x10^{-13}$ atoms)			Meteoric ^{10}Be ($x10^{7}$ atoms/g)			Notes
CH-111	2014	0.518	b8876	494.1	1.67	±	0.04	0.98	±	0.03	
CH-112	2014	0.550	b8877	497.0	2.38	±	0.05	1.36	±	0.04	
CH-113	2014	0.533	b8934	498.0	1.35	±	0.04	0.76	±	0.03	
CH-114	2014	0.507	b8915	501.0	1.47	±	0.04	0.89	±	0.03	
CH-115	2014	0.553	b8935	501.0	1.56	±	0.04	0.86	±	0.03	
CH-116	2014	0.516	b8916	500.0	1.91	±	0.06	1.15	±	0.04	
CH-117[8]	2014	0.506	b8936	498.0	1.09	±	0.03	0.64	±	0.03	
CH-118[8]	2014	0.525	b8878	497.0	1.21	±	0.03	0.68	±	0.03	
CH-119[8]	2014	0.531	b8917	499.0	1.00	±	0.03	0.55	±	0.03	
CH-120[8]	2014	0.503	b8880	494.1	1.39	±	0.03	0.83	±	0.03	
CH-121	2014	0.548	b8881	505.9	3.55	±	0.08	2.11	±	0.05	
CH-122	2014	0.498	b8882	496.0	4.67	±	0.09	3.03	±	0.06	
CH-123	2014				NOT MEASURED						^{14}C age: 1630 ± 15 YBP
CH-124	2014				NOT MEASURED						^{14}C age: 2570 ± 20 YBP
CH-125	2014				NOT APPLICABLE						
CH-126[8]	2014	0.513	b8884	493.1	11.00		0.09	6.96	±	0.19	
CH-127[8]	2014	0.537	b8887	500.0	10.90	±	0.04	6.68	±	0.17	
CH-128	2014	0.529	b8939	500.0	2.93	±	0.14	1.77	±	0.05	
CH-129	2014	0.533	b8888	497.0	3.03	±	0.17	1.81	±	0.05	
CH-130	2014	0.544	b8940	495.1	2.88	±	0.21	1.67	±	0.06	
CH-131	2014	0.520	b8941	496.0	3.70	±	0.31	2.28	±	0.05	
CH-132	2014	0.539	b8890	495.1	4.18	±	0.08	2.48	±	0.06	
CH-133	2014	0.527	b8919	498.0	4.42	±	0.12	2.71	±	0.06	
CH-134	2014	0.522	b8891	499.0	1.70	±	0.03	1.00	±	0.03	
CH-135	2014	0.511	b8920	497.0	1.47	±	0.05	0.88	±	0.03	
CH-136	2014	0.500	b8942	514.8	1.70	±	0.04	1.09	±	0.05	
CH-137	2014	0.522	b8893	497.0	3.93	±	0.05	2.42	±	0.11	
CH-137(A)[6]	2014	0.523	b9001	499.0	3.76	±	0.04	2.32	±	0.06	
CH-138	2014	0.537	b8943	500.0	0.76	±	0.04	0.40	±	0.03	
CH-139	2014	0.511	b8945	498.0	0.70	±	0.04	0.38	±	0.03	
CH-140	2014	0.518	b8946	499.0	2.37	±	0.06	1.45	±	0.04	
CH-141	2014	0.491	b8894	499.0	1.10	±	0.03	0.66	±	0.03	
CH-142	2014	0.499	b8895	498.0	1.34	±	0.03	0.81	±	0.03	
CH-143	2014	0.522	b8921	501.0	1.26	±	0.03	0.72	±	0.03	
CH-144	2014	0.516	b8896	496.0	1.19	±	0.03	0.68	±	0.03	
CH-145	2014	0.528	b8947	498.0	1.15	±	0.08	0.64	±	0.03	
CH-146	2014	0.528	b8922	496.0	2.31	±	0.09	1.37	±	0.04	

Cont. Table Data Repository 3: Isotopic data of all samples included in this study

Sample ID	Year sampled	Sample mass (g)	SUERC ID[2]	^{9}Be Carrier (µg)	Measured ^{10}Be/^{9}Be ratio[3] (x10^{-13} atoms)			Meteoric ^{10}Be (x10^{7} atoms/g)			Notes
CH-147	2014	0.562	b8897	494.1	4.20	±	0.09	2.39	±	0.06	
CH-148	2014	0.523	b8900	495.1	2.59	±	0.05	1.56	±	0.04	
CH-148(A)[6]	2014				NOT MEASURED						
CH-149	2014	0.552	b8901	494.1	3.78	±	0.09	2.18	±	0.05	
CH-150	2014	0.572	b8983	497.0	1.06	±	0.03	0.53	±	0.03	
CH-153	2014	0.538	b8903	497.0	1.90	±	0.05	1.09	±	0.03	
CH-154	2014	0.558	b8906	500.0	3.32	±	0.07	1.91	±	0.05	
CH-155	2014	0.560	b8923	499.0	1.63	±	0.04	0.89	±	0.03	
CH-156	2014	0.530	b8926	498.0	1.70	±	0.04	0.99	±	0.03	
CH-157	2014	0.540	b8928	497.0	2.59	±	0.06	1.51	±	0.04	
CH-158	2014	0.515	b8907	497.0	2.41	±	0.05	1.47	±	0.04	
CH-159	2014	0.577	b8908	501.0	4.00	±	0.09	2.24	±	0.06	
CH-160	2014	0.545	b8929	498.0	4.21	±	0.10	2.49	±	0.06	
CH-161	2014	0.517	b8949	501.0	0.63	±	0.03	0.32	±	0.02	
CH-162	2014	0.529	b8952	495.1	0.58	±	0.02	0.28	±	0.02	
CH-166	2014	0.516	b8953	501.0	1.28	±	0.03	0.75	±	0.03	
CH-167	2014	0.577	b8955	494.1	0.60	±	0.02	0.26	±	0.02	
CH-168	2014	0.536	b8956	502.0	8.40	±	0.15	5.17	±	0.09	
CH-169	2014	0.521	b8958	497.0	1.25	±	0.03	0.72	±	0.03	
CH-170	2014	0.564	b8959	496.0	1.63	±	0.04	0.88	±	0.03	
CH-171	2014	0.511	b8960	500.0	1.49	±	0.04	0.90	±	0.03	
CH-172	2014	0.511	b8961	499.0	1.02	±	0.03	0.58	±	0.03	
Y13-01-DM[9]	2013	0.515	b8962	500.0	1.36	±	0.03	0.80	±	0.03	
TRR-9	2005	0.511	b8989	497.0	0.82	±	0.03	0.45	±	0.03	
TRR-10	2005	0.510	b8990	491.1	0.80	±	0.03	0.43	±	0.03	
TRR-11b	2005	0.535	b8991	496.0	1.48	±	0.04	0.84	±	0.03	
TRR-12	2005	0.514	b8992	500.0	1.17	±	0.03	0.68	±	0.03	
TRR-13b	2005	0.513	b8995	497.0	1.42	±	0.06	0.84	±	0.04	
TRR-14b	2005	0.563	b8996	500.0	4.68	±	0.09	2.69	±	0.06	
TRR-14b(A)[6]	2005	0.547	b8968	503.0	4.57	±	0.11	2.73	±	0.07	

Cont. Table Data Repository 3: Isotopic data of all samples included in this study

Sample ID	Year sampled	Analyses						
		Erosion and topography	Sediment yields	Erosion Index	Temporal replicate - 6 months	Temporal replicate - in channel and overbank	Temporal replicate - Decade	Temporal replicate - Millenia
CH-001[4,5]	2013					X		
CH-002[4]	2013					X		
CH-002(A)[4,6]	2013					X		
CH-005[5]	2013							X
CH-008[7]	2013							X
CH-017[5,7]	2013							X
CH-018[7]	2013							X
CH-019[7]	2013							X
CH-022[7]	2013							X
CH-023[5,7]	2013							X
CH-037[5,7]	2013							X
CH-038[7]	2013							X
CH-039[5,7]	2013							X
CH-040[7]	2013							X
CH-043	2013				X			
CH-044[5,7]	2013				X	X		
CH-050[5,7]	2013							X
CH-051[7]	2013							X
CH-056	2013				X			
CH-058	2013				X			
CH-060[8]	2013				X	X		
CH-070	2013				X			
CH-071	2013				X			
CH-073[5,7]	2013				X	X		
CH-074[8]	2013				X	X		
CH-075[5,7]	2013				X	X		
CH-076[8]	2013				X	X		
CH-101	2014	X	X			X		
CH-102	2014	X	X			X		
CH-103	2014	X	X	X		X		
CH-104	2014	X	X	X		X		
CH-105	2014	X	X	X		X		
CH-106	2014	X				X		
CH-107	2014	X	X	X		X		
CH-108	2014	X				X		
CH-109	2014	X	X	X		X		
CH-110	2014	X				X		

Cont. Table Data Repository 3: Isotopic data of all samples included in this study

Sample ID	Year sampled	Analyses						
		Erosion and topography	Sediment yields	Erosion Index	Temporal replicate - 6 months	Temporal replicate - in channel and overbank	Temporal replicate - Decade	Temporal replicate - Millenia
CH-110	2014	X				X		
CH-111	2014	X				X		
CH-112	2014	X				X		
CH-113	2014	X	X	X				
CH-114	2014	X			X			
CH-115	2014	X			X			
CH-116	2014	X			X			
CH-117[8]	2014	X	X		X	X		
CH-118[8]	2014	X			X	X		
CH-119[8]	2014	X	X	X	X	X		
CH-120[8]	2014	X			X	X		
CH-121	2014	X			X			
CH-122	2014	X			X			X
CH-123	2014							X
CH-124	2014							X
CH-125	2014							X
CH-126[8]	2014	X			X	X		
CH-127[8]	2014	X			X	X		
CH-128	2014	X				X		
CH-129	2014	X	X	X		X		
CH-130	2014	X				X		
CH-131	2014	X	X	X		X		
CH-132	2014	X				X		
CH-133	2014	X				X		
CH-134	2014	X				X		
CH-135	2014	X	X	X		X		
CH-136	2014	X				X		
CH-137	2014	X				X		
CH-137(A)[6]	2014	X				X		
CH-138	2014	X				X		
CH-139	2014	X				X		
CH-140	2014	X				X		
CH-141	2014	X	X	X		X		
CH-142	2014	X				X		
CH-143	2014	X	X	X		X		
CH-144	2014	X				X		
CH-145	2014	X	X	X		X		
CH-146	2014	X	X	X				

Cont. Table Data Repository 3: Isotopic data of all samples included in this study

Sample ID	Year sampled	Analyses						
		Erosion and topography	Sediment yields	Erosion Index	Temporal replicate - 6 months	Temporal replicate - in channel and overbank	Temporal replicate - Decade	Temporal replicate - Millenia
CH-147	2014	X	X	X		X		
CH-148	2014	X				X		
CH-148(A)[6]	2014	X				X		
CH-149	2014	X				X		
CH-150	2014	X				X	X	
CH-153	2014	X				X		
CH-154	2014	X				X	X	
CH-155	2014	X	X	X		X		
CH-156	2014	X				X		
CH-157	2014	X	X	X		X		
CH-158	2014	X				X		
CH-159	2014	X	X	X		X		
CH-160	2014	X	X					
CH-161	2014	X				X		
CH-162	2014	X				X	X	
CH-166	2014	X				X	X	
CH-167	2014	X				X	X	
CH-168	2014	X					X	
CH-169	2014	X				X		
CH-170	2014	X				X	X	
CH-171	2014	X				X		
CH-172	2014	X				X	X	
Y13-01-DM[9]	2013	X						
TRR-9	2005						X	
TRR-10	2005						X	
TRR-11b	2005						X	X
TRR-12	2005						X	
TRR-13b	2005						X	
TRR-14b	2005						X	
TRR-14b(A)[6]	2005						X	

Table Data Repository 4: Radiocarbon information of charcoal samples

Charcoal sample ID	Sediment sample ID	Location[1]		14C Age	UCIAMS ID[2]
		Latitude	Longitude	(yr BP)	
CH-008	CH-005	27.06397	99.35139	1450 ± 20	136307
CH-018	CH-017	27.1312	99.40647	340 ± 15	136308
CH-019	CH-017	27.1312	99.40647	115 ± 15	136309
CH-022	CH-023	27.1227	99.34739	190 ± 15	136310
CH-038	CH-037	24.06035	100.8075	130 ± 20	136314
CH-040	CH-039	23.97972	100.7989	-5 ± 20	136315
CH-051	CH-050	23.72601	100.8299	-1170 ± 15	136316
CH-125	CH-074	21.94219	100.3407	1245 ± 15	136319

[1] Sample locations are reported in WGS84

[2] Unique sample ID assigned at the W.M. Keck Carbon Cycle Accelerator Mass Spectrometry Laboratory

Table Data Repository 5: CRONUS input data for samples considered in this study

Sample name	Latitude (DD)	Longitude (DD)	Elevation (m)	Elv/pressure flag	Thickness (cm)	Density (g cm-2)	Shielding correction	[Be-10][1] atoms g-1	+/- atoms g-1	Be standardization	[Al-26] atoms g-1	+/- atoms g-1	Al standardization
CH-001	27.1200	99.3600	2931	std	0.1	2.7	1	250827.913	5383.562	NIST_27900	0.00E+00	0.00E+00	KNSTD
CH-101	23.3912	104.2044	1539	std	0.1	2.7	1	116195.490	4156.932	NIST_27900	0.00E+00	0.00E+00	KNSTD
CH-103	23.4892	104.0484	1605	std	0.1	2.7	1	269352.173	4822.640	NIST_27900	0.00E+00	0.00E+00	KNSTD
CH-105	23.3343	103.6554	1751	std	0.1	2.7	1	500393.994	9903.974	NIST_27900	0.00E+00	0.00E+00	KNSTD
CH-107	24.2913	101.8461	1739	std	0.1	2.7	1	57077.794	2945.696	NIST_27900	0.00E+00	0.00E+00	KNSTD
CH-109	24.6829	101.4641	1832	std	0.1	2.7	1	92202.842	2748.978	NIST_27900	0.00E+00	0.00E+00	KNSTD
CH-111	24.6791	101.4659	1830	std	0.1	2.7	1	99119.322	2642.619	NIST_27900	0.00E+00	0.00E+00	KNSTD
CH-113	23.8724	101.3593	1581	std	0.1	2.7	1	58832.638	2304.478	NIST_27900	0.00E+00	0.00E+00	KNSTD
CH-114	23.9756	100.8231	1644	std	0.1	2.7	1	80985.198	6387.855	NIST_27900	0.00E+00	0.00E+00	KNSTD
CH-115	23.9298	100.8373	1653	std	0.1	2.7	1	81639.392	3138.092	NIST_27900	0.00E+00	0.00E+00	KNSTD
CH-116	23.6763	100.6005	1748	std	0.1	2.7	1	113911.360	3524.884	NIST_27900	0.00E+00	0.00E+00	KNSTD
CH-117	23.8739	100.7848	1646	std	0.1	2.7	1	81836.817	1694.457	NIST_27900	0.00E+00	0.00E+00	KNSTD
CH-119	28.5588	98.0423	3806	std	0.1	2.7	1	81778.566	1520.874	NIST_27900	0.00E+00	0.00E+00	KNSTD
CH-121	21.7525	100.3624	1551	std	0.1	2.7	1	107356.019	4464.946	NIST_27900	0.00E+00	0.00E+00	KNSTD
CH-127	21.8944	100.3392	1434	std	0.1	2.7	1	166733.098	2060.005	NIST_27900	0.00E+00	0.00E+00	KNSTD
CH-129	22.1919	99.3722	1439	std	0.1	2.7	1	160211.711	3135.742	NIST_27900	0.00E+00	0.00E+00	KNSTD
CH-131	22.4716	99.6442	1388	std	0.1	2.7	1	96079.377	2430.265	NIST_27900	0.00E+00	0.00E+00	KNSTD
CH-133	23.1966	99.4989	1659	std	0.1	2.7	1	124351.612	2757.172	NIST_27900	0.00E+00	0.00E+00	KNSTD
CH-135	23.9474	99.8065	1723	std	0.1	2.7	1	45016.229	2050.405	NIST_27900	0.00E+00	0.00E+00	KNSTD
CH-137	23.8516	99.6602	1631	std	0.1	2.7	1	62389.437	1619.929	NIST_27900	0.00E+00	0.00E+00	KNSTD
CH-139	23.4020	99.0540	1257	std	0.1	2.7	1	47507.761	1873.170	NIST_27900	0.00E+00	0.00E+00	KNSTD
CH-141	24.8531	98.4669	1745	std	0.1	2.7	1	60681.159	2079.218	NIST_27900	0.00E+00	0.00E+00	KNSTD
CH-143	24.9857	98.1636	1806	std	0.1	2.7	1	53667.398	2066.316	NIST_27900	0.00E+00	0.00E+00	KNSTD
CH-145	24.5773	97.9037	1459	std	0.1	2.7	1	65307.658	2149.297	NIST_27900	0.00E+00	0.00E+00	KNSTD
CH-146	25.3533	98.5934	2096	std	0.1	2.7	1	87069.636	3548.439	NIST_27900	0.00E+00	0.00E+00	KNSTD
CH-147	30.6623	90.0862	4571	std	0.1	2.7	1	164673.195	4284.813	NIST_27900	0.00E+00	0.00E+00	KNSTD
CH-150	30.8288	94.9607	4616	std	0.1	2.7	1	115371.078	3121.699	NIST_27900	0.00E+00	0.00E+00	KNSTD
CH-153	25.5394	99.1583	2457	std	0.1	2.7	1	37159.635	2802.411	NIST_27900	0.00E+00	0.00E+00	KNSTD
CH-155	25.9968	99.8758	2520	std	0.1	2.7	1	73001.318	3287.917	NIST_27900	0.00E+00	0.00E+00	KNSTD
CH-157	24.5146	99.8169	1927	std	0.1	2.7	1	97005.831	3225.518	NIST_27900	0.00E+00	0.00E+00	KNSTD
CH-159	25.1924	100.3208	2062	std	0.1	2.7	1	121416.516	2932.998	NIST_27900	0.00E+00	0.00E+00	KNSTD
CH-161	31.0905	94.6990	4699	std	0.1	2.7	1	208357.315	5656.026	NIST_27900	0.00E+00	0.00E+00	KNSTD
CH-167	31.0351	94.7649	4678	std	0.1	2.7	1	138333.268	4804.762	NIST_27900	0.00E+00	0.00E+00	KNSTD
CH-169	30.9995	94.8059	4667	std	0.1	2.7	1	172499.087	6237.454	NIST_27900	0.00E+00	0.00E+00	KNSTD
CH-171	30.9154	94.8873	4641	std	0.1	2.7	1	145007.159	6088.102	NIST_27900	0.00E+00	0.00E+00	KNSTD

[1] Isotopic concentration used for erosion calculations is the weighted-averge of the in-channel and overbank samples at each site, where both data are available.

Table Data Repository 6: Erosion rates and topography variables for studied watersheds

Sample ID	River	Erosion rate (mm/yr)			Area (km^2)	Mean basin slope (°)	Mean basin relief (m)	Mean annual rainfall(mm)	KSN	PGA
CH-101	Red	0.07	±	0.01	6499	11	637	1180	70	1.13
CH-103	Red	0.03	±	0.00	4781	10	503	1134	46	1.19
CH-105	Red	0.02	±	0.00	136	12	614	1190	66	2.82
CH-107	Red	0.16	±	0.01	39499	17	1126	937	120	4.31
CH-109	Red	0.10	±	0.01	26842	17	1049	874	107	4.45
CH-111	Red	0.10	±	0.01	26936	17	1050	874	107	4.45
CH-113	Red	0.14	±	0.01	4213	18	1100	1023	100	1.89
CH-114	Mekong	0.10	±	0.01	1722	17	975	1029	79	2.08
CH-115	Mekong	0.10	±	0.01	2039	17	1003	1044	82	2.45
CH-116	Mekong	0.08	±	0.01	21	18	846	1141	101	4.12
CH-117	Mekong	0.11	±	0.01	2997	16	978	1066	79	2.76
CH-119	Mekong	0.34	±	0.03	189028	18	1126	758	120	2.36
CH-121	Mekong	0.07	±	0.01	38	11	801	1294	76	3.36
CH-127	Mekong	0.04	±	0.00	1170	9	613	1300	8085	3.95
CH-129	Salween	0.04	±	0.00	605	16	1150	1258	114	2.53
CH-131	Mekong	0.07	±	0.01	840	14	810	1349	56	2.78
CH-133	Mekong	0.07	±	0.00	917	17	1001	1287	76	4.64
CH-135	Salween	0.20	±	0.02	4647	18	1313	1086	126	2.24
CH-137	Salween	0.14	±	0.01	5884	17	1304	1124	117	2.72
CH-139	Salween	0.14	±	0.01	493	19	1286	1275	131	2.57
CH-141	Irrawaddy	0.15	±	0.01	9499	14	1033	1021	81	3.68
CH-143	Irrawaddy	0.18	±	0.01	6495	14	1086	1034	97	2.74
CH-145	Irrawaddy	0.12	±	0.01	31	16	1493	1174	13407	1.21
CH-146	Irrawaddy	0.13	±	0.01	4185	15	1119	938	89	4.65
CH-147	Salween	0.25	±	0.02	154332	19	1218	558	133	1.79
CH-150	Salween	0.37	±	0.03	150172	19	1205	546	131	1.70
CH-153	Mekong	0.37	±	0.04	677	20	1534	910	118	3.10
CH-155	Mekong	0.19	±	0.02	11418	15	1105	930	90	6.70
CH-157	Mekong	0.10	±	0.01	2261	16	1032	927	82	1.08
CH-159	Red	0.09	±	0.01	1915	15	948	907	61	9.29
CH-161	Salween	0.21	±	0.02	141722	18	1141	511	122	1.67
CH-167	Salween	0.32	±	0.03	143962	18	1158	523	124	1.64
CH-168	Salween	0.39	±	0.04	145127	18	1167	527	125	1.71
CH-169	Salween	0.26	±	0.02	145127	18	1167	527	125	1.71
CH-171	Salween	0.30	±	0.03	147736	19	1188	538	128	1.68

Table Data Repository 7: Summar of regression analyses results

	Climate			Land use			Tectonic activity			Topography					
	Rainfall			Cultivated land use			PGA			Slope			Relief		
	R^2	p	Symbol of relationship	R^2	p	Symbol of relationship	R^2	p	Symbol of relationship	R^2	p	Symbol of relationship	R^2	p	Symbol of relationship
Erosion rates - Global	0.63	<0.01	-	0.60	< 0.01	-	0.06	0.14	-	0.51	< 0.01	+	0.61	< 0.01	+
Erosion rates - Mekong	0.61	<0.01	-	0.46	0.01	-	0	0.91	-	0.35	0.04	+	0.73	< 0.01	+
Erosion rates - Salween	0.7	< 0.01	-	0.56	< 0.01	-	0.69	< 0.01	-	0.38	0.05	+	0.1	0.35	-
Erosion rates - Irrawaddy	0.07	0.74	-	0.67	0.18	-	0.01	0.89	+	0.73	0.14	-	0.44	0.34	-
Erosion rates - Red	0.43	0.08	-	0.6	0.02	-	0.06	0.57	+	0.73	< 0.01	+	0.82	< 0.01	+
$^{10}Be_m$	0.05	0.19	+	0.21	< 0.01	+	0	0.91	+	0.31	< 0.01	-	0.32	< 0.01	-

Blank cells represent variables that are not independent; no statistical analyses was performed in these cases

Cont. Table Data Repository 7: Summar of regression analyses results

	Topography								
	KSN			Area			$^{10}Be_i$		
	R^2	p	Symbol of relationship	R^2	p	Symbol of relationship	R^2	p	Symbol of relationship
Erosion rates - Global	0.55	< 0.01	+	0.6	< 0.01	+			
Erosion rates - Mekong	0.7	< 0.01	+	0.34	0.06	+			
Erosion rates - Salween	0.31	0.08	+	0.67	< 0.01	+			
Erosion rates - Irrawaddy	0.31	0.62	+	0.48	0.3	+			
Erosion rates - Red	0.68	0.01	+	0.38	0.1	+			
$^{10}Be_m$	0.01	0.5	+	0.02	0.46	-	0.51	0.01	+

Blank cells represent variables that are not independent; no statistical analyses was performed in these cases

Table DR8: Temporal replicates data

Replicate sample ID	Sample year	Sample type	$^{10}Be_m$ concentration (atoms/g)			$^{10}Be_i$ concentration (atoms/g)			Comparison type
CH-001	2013	Inchannel sediment	4.85E+07	±	1.57E+06	1.92E+05	±	7.42E+03	Paired in channel/overbank
CH-044	2013	Inchannel sediment	8.39E+06	±	2.92E+05	8.06E+04	±	2.66E+03	
CH-073	2013	Inchannel sediment	3.51E+06	±	3.01E+05	7.44E+04	±	3.00E+03	
CH-075	2013	Inchannel sediment	1.18E+08	±	2.75E+06	1.51E+05	±	3.50E+03	
CH-101	2014	Inchannel sediment	1.69E+07	±	5.23E+05	1.03E+05	±	6.27E+03	
CH-103	2014	Inchannel sediment	6.49E+07	±	8.66E+05	2.61E+05	±	6.67E+03	
CH-105	2014	Inchannel sediment	7.78E+07	±	1.22E+06	5.21E+05	±	1.32E+04	
CH-107	2014	Inchannel sediment	2.05E+07	±	5.33E+05	5.51E+04	±	3.46E+03	
CH-109	2014	Inchannel sediment	8.11E+06	±	3.22E+05	7.16E+04	±	3.51E+03	
CH-111	2014	Inchannel sediment	1.07E+07	±	3.45E+05	9.27E+04	±	2.94E+03	
CH-117	2014	Inchannel sediment	5.97E+06	±	2.66E+05	7.70E+04	±	3.29E+03	
CH-119	2014	Inchannel sediment	5.42E+06	±	2.65E+05	8.08E+04	±	3.02E+03	
CH-127	2014	Inchannel sediment	5.66E+07	±	1.47E+06	1.75E+05	±	4.79E+03	
CH-129	2014	Inchannel sediment	1.56E+07	±	3.95E+05	1.60E+05	±	4.33E+03	
CH-131	2014	Inchannel sediment	1.81E+07	±	4.05E+05	9.76E+04	±	3.59E+03	
CH-133	2014	Inchannel sediment	2.18E+07	±	5.22E+05	1.16E+05	±	3.58E+03	
CH-135	2014	Inchannel sediment	8.08E+06	±	3.16E+05	4.11E+04	±	2.79E+03	
CH-137	2014	Inchannel sediment	2.11E+07	±	7.20E+05	9.15E+04	±	3.20E+03	
CH-139	2014	Inchannel sediment	3.02E+06	±	2.07E+05	4.75E+04	±	2.52E+03	
CH-141	2014	Inchannel sediment	6.15E+06	±	3.17E+05	5.76E+04	±	2.79E+03	
CH-143	2014	Inchannel sediment	6.58E+06	±	2.65E+05	5.41E+04	±	2.98E+03	
CH-145	2014	Inchannel sediment	5.26E+06	±	2.37E+05	6.48E+04	±	3.11E+03	
CH-147	2014	Inchannel sediment	2.79E+07	±	6.78E+05	1.08E+05	±	6.18E+03	
CH-149	2014	Inchannel sediment	2.58E+07	±	6.50E+05	1.21E+05	±	3.93E+03	
CH-153	2014	Inchannel sediment	1.09E+07	±	3.40E+05	2.72E+04	±	3.89E+03	
CH-155	2014	Inchannel sediment	8.48E+06	±	2.95E+05	8.03E+04	±	8.80E+03	
CH-157	2014	Inchannel sediment	1.58E+07	±	4.28E+05	1.06E+05	±	4.69E+03	
CH-159	2014	Inchannel sediment	2.29E+07	±	5.78E+05	1.27E+05	±	4.02E+03	
CH-161	2014	Inchannel sediment	4.03E+06	±	3.03E+05	2.05E+05	±	7.33E+03	
CH-166	2014	Inchannel sediment	3.18E+06	±	2.91E+05	1.26E+05	±	5.94E+03	
CH-169	2014	Inchannel sediment	8.68E+06	±	3.46E+05	1.47E+05	±	8.29E+03	
CH-171	2014	Inchannel sediment	1.07E+07	±	3.69E+05	1.52E+05	±	7.74E+03	

Shaded isotopic concentrations represent the samples with a difference greater than 10% both isotopic measurements.

Cont. Table DR8: Temporal replicates data

Replicate sample ID	Sample year	Sample type	$^{10}Be_m$ concentration (atoms/g)			$^{10}Be_i$ concentration (atoms/g)			Comparison type
CH-114	2014	Inchannel sediment	8.88E+06	±	3.05E+05	8.10E+04	±	6.39E+03	6 months
CH-115	2014	Inchannel sediment	8.62E+06	±	2.98E+05	8.16E+04	±	3.14E+03	
CH-116	2014	Inchannel sediment	1.15E+07	±	4.13E+05	1.14E+05	±	3.52E+03	
CH-117	2014	Inchannel sediment	6.37E+06	±	2.83E+05	7.70E+04	±	3.29E+03	
CH-118	2014	Inchannel sediment	NOT MEASURED			7.12E+04	±	3.05E+03	
CH-119	2014	Inchannel sediment	5.50E+06	±	2.69E+05	8.08E+04	±	3.02E+03	
CH-120	2014	Inchannel sediment	8.33E+06	±	2.97E+05	9.04E+04	±	3.27E+03	
CH-121	2014	Inchannel sediment	2.11E+07	±	5.48E+05	1.07E+05	±	4.46E+03	
CH-122	2014	Inchannel sediment	3.03E+07	±	6.39E+05	1.73E+05	±	6.00E+03	
CH-126	2014	Inchannel sediment	NOT MEASURED			1.75E+05	±	4.79E+03	
CH-127	2014	Inchannel sediment	6.96E+07	±	1.86E+06	1.79E+05	±	4.62E+03	
CH-150	2014	Inchannel sediment	5.33E+06	±	2.76E+05	1.21E+05	±	3.93E+03	Decade
CH-154	2014	Inchannel sediment	1.91E+07	±	4.56E+05	NOT MEASURED			
CH-162	2014	Inchannel sediment	2.84E+06	±	2.39E+05	2.14E+05	±	8.90E+03	
CH-166	2014	Inchannel sediment	7.48E+06	±	2.96E+05	1.62E+05	±	8.17E+03	
CH-168	2014	Inchannel sediment	NOT MEASURED			1.14E+05	±	4.70E+03	
CH-170	2014	Inchannel sediment	8.75E+06	±	2.95E+05	2.05E+05	±	9.47E+03	
CH-172	2014	Inchannel sediment	5.84E+06	±	2.72E+05	1.33E+05	±	9.87E+03	
CH-005	2013	Inchannel sediment	NOT MEASURED			2.60E+05	±	7.95E+03	Millenia
CH-005	2013	Inchannel sediment	NOT MEASURED			2.60E+05	±	7.95E+03	
CH-005	2013	Inchannel sediment	NOT MEASURED			2.60E+05	±	7.95E+03	
CH-017	2013	Inchannel sediment	NOT MEASURED			5.72E+05	±	1.75E+04	
CH-017	2013	Inchannel sediment	NOT MEASURED			5.72E+05	±	1.75E+04	
CH-023	2013	Inchannel sediment	NOT MEASURED			9.47E+05	±	1.16E+04	
CH-037	2013	Inchannel sediment	NOT MEASURED			9.33E+04	±	3.75E+03	
CH-039	2013	Inchannel sediment	NOT MEASURED			8.14E+04	±	3.01E+03	
CH-050	2013	Inchannel sediment	NOT MEASURED			7.22E+04	±	3.18E+03	
CH-122	2014	Inchannel sediment	NOT MEASURED			1.23E+05	±	3.76E+03	
CH-122	2014	Inchannel sediment	NOT MEASURED			1.23E+05	±	3.76E+03	

Shaded isotopic concentrations represent the samples with a difference greater than 10% both isotopic measurements.

Cont. Table DR8: Temporal replicates data

Original sample ID	Sample year	Sample type	$^{10}Be_m$ concentration (atoms/g)			$^{10}Be_i$ concentration (atoms/g)			Comparison type	Notes
CH-002	2013	Overbank sediment	NOT MEASURED			3.19E+05	±	1.16E+04	Paired in channel/overbank	
CH-060	2013	Overbank sediment	NOT MEASURED			7.21E+04	±	3.05E+03		
CH-074	2013	Overbank sediment	4.56E+06	±	2.79E+05	8.28E+04	±	2.91E+03		
CH-076	2013	Overbank sediment	NOT MEASURED			1.72E+05	±	3.97E+03		
CH-102	2014	Overbank sediment	8.64E+06	±	2.68E+05	1.27E+05	±	5.55E+03		
CH-104	2014	Overbank sediment	6.96E+07	±	1.01E+06	2.79E+05	±	6.98E+03		
CH-106	2014	Overbank sediment	7.96E+07	±	1.72E+06	4.74E+05	±	1.50E+04		
CH-108	2014	Overbank sediment	4.16E+07	±	7.81E+05	6.22E+04	±	5.62E+03		
CH-110	2014	Overbank sediment	1.32E+07	±	3.67E+05	1.25E+05	±	4.43E+03		
CH-112	2014	Overbank sediment	1.48E+07	±	4.19E+05	1.26E+05	±	6.03E+03		
CH-118	2014	Overbank sediment	6.40E+06	±	2.63E+05	7.12E+04	±	3.05E+03		
CH-120	2014	Overbank sediment	8.21E+06	±	2.93E+05	9.04E+04	±	3.27E+03		
CH-126	2014	Overbank sediment	5.89E+07	±	1.57E+06	1.79E+05	±	4.62E+03		
CH-128	2014	Overbank sediment	1.53E+07	±	4.32E+05	1.60E+05	±	4.54E+03		
CH-130	2014	Overbank sediment	1.33E+07	±	4.89E+05	9.48E+04	±	3.30E+03		
CH-132	2014	Overbank sediment	2.00E+07	±	5.08E+05	1.36E+05	±	4.33E+03		
CH-134	2014	Overbank sediment	9.22E+06	±	2.97E+05	4.97E+04	±	3.03E+03		
CH-136	2014	Overbank sediment	9.71E+06	±	4.29E+05	5.39E+04	±	2.74E+03		
CH-138	2014	Overbank sediment	3.17E+06	±	2.04E+05	4.75E+04	±	2.80E+03		
CH-140	2014	Overbank sediment	1.34E+07	±	3.80E+05	6.45E+04	±	3.12E+03		
CH-142	2014	Overbank sediment	7.36E+06	±	2.62E+05	5.33E+04	±	2.87E+03		
CH-144	2014	Overbank sediment	5.61E+06	±	2.27E+05	6.58E+04	±	2.97E+03		
CH-148	2014	Overbank sediment	1.82E+07	±	4.35E+05	2.31E+05	±	1.21E+04		
CH-150	2014	Overbank sediment	6.31E+06	±	3.27E+05	1.06E+05	±	5.14E+03		
CH-154	2014	Overbank sediment	1.91E+07	±	4.55E+05	4.79E+04	±	4.04E+03		
CH-156	2014	Overbank sediment	9.38E+06	±	2.97E+05	7.18E+04	±	3.54E+03		
CH-158	2014	Overbank sediment	1.53E+07	±	3.71E+05	8.89E+04	±	4.44E+03		
CH-160	2014	Overbank sediment	2.55E+07	±	6.28E+05	1.15E+05	±	4.29E+03		
CH-162	2014	Overbank sediment	3.53E+06	±	2.97E+05	2.14E+05	±	8.90E+03		
CH-167	2014	Overbank sediment	9.14E+06	±	3.62E+05	1.62E+05	±	8.17E+03		
CH-170	2014	Overbank sediment	1.06E+07	±	3.58E+05	2.05E+05	±	9.47E+03		
CH-172	2014	Overbank sediment	6.97E+06	±	3.25E+05	1.33E+05	±	9.87E+03		

Cont. Table DR8: Temporal replicates data

Original sample ID	Sample year	Sample type	$^{10}Be_m$ concentration (atoms/g)			$^{10}Be_i$ concentration (atoms/g)			Comparison type	Notes
CH-056	2013	Inchannel sediment	7.71E+06	±	3.05E+05	5.78E+04	±	2.52E+03	6 months	
CH-058	2013	Inchannel sediment	9.52E+06	±	2.97E+05	6.72E+04	±	2.39E+03		
CH-043	2013	Inchannel sediment	1.36E+07	±	1.09E+06	1.60E+05	±	3.70E+03		
CH-044	2013	Inchannel sediment	8.39E+06	±	2.92E+05	8.06E+04	±	2.66E+03		
CH-060	2013	Inchannel sediment	NOT MEASURED			7.21E+04	±	3.05E+03		
CH-073	2013	Inchannel sediment	3.67E+06	±	3.16E+05	7.44E+04	±	3.00E+03		
CH-074	2013	Inchannel sediment	4.78E+06	±	2.92E+05	8.28E+04	±	2.91E+03		
CH-070	2013	Inchannel sediment	2.51E+07	±	1.16E+06	1.19E+05	±	5.17E+03		
CH-071	2013	Inchannel sediment	4.11E+07	±	1.27E+06	1.73E+05	±	5.59E+03		
CH-076	2013	Inchannel sediment	NOT MEASURED			1.72E+05	±	3.97E+03		
CH-075	2013	Inchannel sediment	6.07E+07	±	1.42E+06	1.51E+05	±	3.50E+03		
TRR-13b	2005	Inchannel sediment	8.40E+06	±	4.07E+05	2.94E+05	±	1.22E+04	Decade	TRR-13b published by Henck et al., 2011 as 05-3R-13b-SAL
TRR-14b	2005	Inchannel sediment	2.69E+07	±	6.14E+05	NOT MEASURED				TRR-14b published by Henck et al., 2011 as 05-3R-14b-MEK
TRR-9	2005	Inchannel sediment	4.52E+06	±	2.64E+05	5.19E+05	±	1.23E+04		TRR-9 published by Henck et al., 2011 as 05-3R-09-SAL
TRR-10	2005	Inchannel sediment	4.31E+06	±	2.65E+05	4.28E+05	±	1.19E+04		TRR-10 published by Henck et al., 2011 as 05-3R-10-SAL
TRR-11a	2005	Inchannel sediment	NOT MEASURED			1.61E+05	±	7.13E+03		TRR-11a published by Henck et al., 2011 as 05-3R-11a-SAL
TRR-11b	2005	Inchannel sediment	8.39E+06	±	3.00E+05	5.32E+05	±	1.82E+04		TRR-11b published by Henck et al., 2011 as 05-3R-11b-SAL
TRR-12	2005	Inchannel sediment	6.81E+06	±	2.84E+05	4.02E+05	±	1.55E+04		TRR-12 published by Henck et al., 2011 as 05-3R-12-SAL
CH-006	2013	Terrace sediment	NOT MEASURED			1.37E+05	±	3.46E+03	Millenia	Terrace age: Not measured
CH-007	2013	Terrace sediment	NOT MEASURED			1.16E+05	±	6.08E+03		Terrace age: Not measured
CH-008	2013	Terrace sediment	NOT MEASURED			1.32E+05	±	4.61E+03		Terrace age: 1450 ± 20 ybp
CH-018	2013	Terrace sediment	NOT MEASURED			7.68E+05	±	1.45E+04		Terrace age: 340 ± 15 ybp
CH-019	2013	Terrace sediment	NOT MEASURED			6.21E+05	±	1.42E+04		Terrace age: 115 ± 15 ybp
CH-022	2013	Terrace sediment	NOT MEASURED			2.02E+06	±	2.62E+04		Terrace age: 190 ± 15 ybp
CH-038	2013	Terrace sediment	NOT MEASURED			8.92E+04	±	3.26E+03		Terrace age: 130 ±20 ybp
CH-040	2013	Terrace sediment	NOT MEASURED			7.95E+04	±	2.56E+03		Terrace age: 0 ±20 ybp
CH-051	2013	Terrace sediment	NOT MEASURED			9.27E+04	±	2.98E+03		Terrace age: 0 ± 15 ybp
CH-123	2014	Terrace sediment	NOT MEASURED			1.39E+05	±	4.63E+03		Terrace age: 1630 ± 15 ybp
CH-124	2014	Terrace sediment	NOT MEASURED			1.22E+05	±	4.41E+03		Terrace age: 2570 ± 20 ybp

Table Data Repository 9: Long-term and contemporary sediment yield for gauged rivers

Sample ID	River	Hydrology Station[1]	Years of data	Long-term erosion rate (mm/yr)			Long-term sediment yield (tons $km^{-2}yr^{-1}$)	Modern sediment yield (tons $km^{-2}yr^{-1}$)	Modern/long-term sediment yield ratio
CH-103	Red	90	27	0.03	±	0.00	79	252	3.19
CH-105	Red	108	7	0.02	±	0.00	45	90	2.02
CH-107	Red	106	25	0.16	±	0.01	427	1038	2.43
CH-109	Red	103	21	0.10	±	0.01	277	1076	3.88
CH-113	Red	87	17	0.14	±	0.01	377	1790	4.75
CH-117	Mekong	49	20	0.11	±	0.01	310	1196	3.86
CH-119	Mekong	6	22	0.34	±	0.03	930	566	0.61
CH-121	Mekong	11	23	0.07	±	0.01	193	113	0.58
CH-129	Salween	109	18	0.04	±	0.00	121	2879	23.85
CH-131	Mekong	94	16	0.07	±	0.01	200	593	2.96
CH-133[2]	Mekong	32	5	0.07	±	0.00	181	21919	121.17
CH-135	Salween	93	20	0.20	±	0.02	536	1624	3.03
CH-141	Irrawaddy	99	6	0.15	±	0.01	407	476	1.17
CH-143	Irrawaddy	85	17	0.18	±	0.01	479	1074	2.24
CH-145	Irrawaddy	84	6	0.12	±	0.01	322	589	1.83
CH-146	Irrawaddy	100	18	0.13	±	0.01	344	507	1.47
CH-147	Salween	15	23	0.25	±	0.02	681	212	0.31
CH-155	Mekong	86	12	0.19	±	0.02	519	395	0.76
CH-157	Mekong	97	17	0.10	±	0.01	276	709	2.56
CH-159	Red	101	23	0.09	±	0.01	239	1139	4.76

[1] Hydrology station number assigned by Schmidt et al., 2011

[2] This outlier is not included in our analyses

Table Data Repository 10: Erosion Index

Sample ID	q (atoms cm^{-2} yr^{-1})[1]	Long term sediment yield (g/y)	Modern sediment yield (g/y)	Area (cm^2)	Modern Erosion Index
CH-103	9.77E+05	3.77E+11	1.20E+12	4.78E+13	1.92
CH-105	1.02E+06	6.12E+09	1.23E+10	1.36E+12	0.80
CH-107	8.42E+05	1.65E+13	4.10E+13	3.95E+14	2.42
CH-109	8.03E+05	7.54E+12	2.89E+13	2.68E+14	0.99
CH-113	8.99E+05	1.64E+12	7.54E+12	4.21E+13	1.52
CH-119	8.92E+05	1.69E+14	1.07E+14	1.89E+15	0.35
CH-121	1.03E+06	7.32E+09	4.28E+09	3.79E+11	0.23
CH-129	1.02E+06	7.30E+10	1.74E+12	6.05E+12	5.11
CH-131	1.11E+06	1.68E+11	4.98E+11	8.40E+12	1.22
CH-133[2]	1.09E+06	1.64E+11	2.01E+13	9.17E+12	54.39
CH-135	9.58E+05	2.49E+12	7.55E+12	4.65E+13	1.49
CH-141	9.49E+05	3.86E+12	4.52E+12	9.50E+13	0.33
CH-143	9.68E+05	3.11E+12	6.98E+12	6.50E+13	0.80
CH-145	1.07E+06	9.84E+09	1.80E+10	3.05E+11	0.35
CH-146	8.97E+05	1.44E+12	2.12E+12	4.18E+13	0.77
CH-147	7.51E+05	1.05E+14	3.27E+13	1.54E+15	0.67
CH-155	9.25E+05	5.70E+12	4.51E+12	1.14E+14	0.38
CH-157	8.44E+05	6.27E+11	1.60E+12	2.26E+13	1.27
CH-159	8.59E+05	4.61E+11	2.18E+12	1.91E+13	2.97

[1] Calculated as per Graly et al., 2011

[2] Outlier not used for analyses

Appendix 3 – Brazil Sample catalog

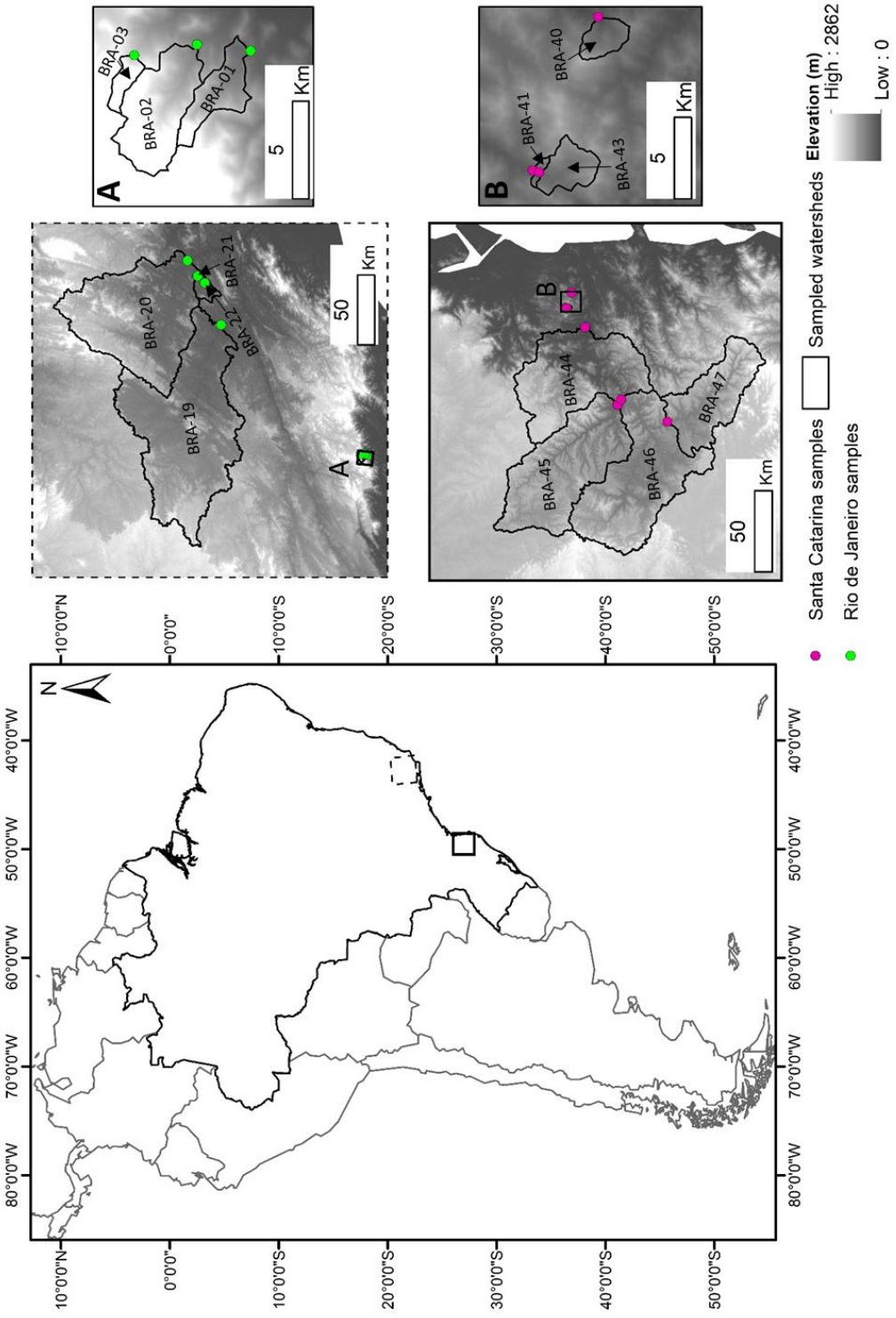

BRA-01

Field Area: Rio de Janeiro, Brazil
Collection Date: September 2011
Latitude: -22.500 **Longitude:** -43.019
Site description: This sample is from a watershed draining Serra dos Órgãos escarpment. At this site, we sampled river sand (sample ID: BRA-01S) and river clasts (sample ID: BRA-01).

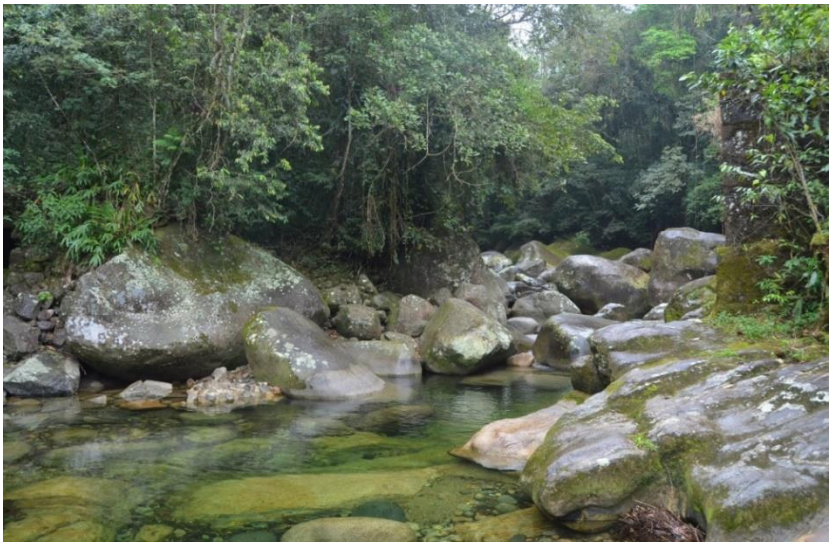

BRA-02

Field Area: Rio de Janeiro, Brazil
Collection Date: September 2011
Latitude: -22.476 **Longitude:** -43.028
Site description: This sample is from a watershed draining Serra dos Órgãos escarpment. At this site, we sampled river sand (sample ID: BRA-02S) and river clasts (sample ID: BRA-02).

BRA-03

Field Area: Rio de Janeiro, Brazil
Collection Date: September 2011
Latitude: -22.464 **Longitude:** -43.016
Site description: Sample taken at a small watershed draining the Serra dos Órgãos escarpment. We sampled river sand (BRA-03S) and clasts (BRA-03) at this site.

BRA-19

Field Area: Rio de Janeiro, Brazil
Collection Date: September 2011
Latitude: -21.498 **Longitude:** -42.204
Site description: Wide channel, with dense vegetation on both river banks

BRA-20
Field Area: Rio de Janeiro, Brazil
Collection Date: September 2011
Latitude: -21.247 **Longitude:** -41.781
Site description:

BRA-21
Field Area: Rio de Janeiro, Brazil
Collection Date: September 2011
Latitude: -21.321 **Longitude:** -41.880
Site description:

BRA-22

Field Area: Rio de Janeiro, Brazil
Collection Date: September 2011
Latitude: -21.371 **Longitude:** -41.924
Site description:

BRA-40

Field Area: Santa Catarina, Brazil
Collection Date: May 2012
Latitude: -26.808 **Longitude:** -48.907
Site description: Narrow channel, low flow, big cobbles in the river. Banana plantations on both sides of the river, and on the steeps slopes around the channel.

BRA-41

Field Area: Santa Catarina, Brazil
Collection Date: May 2012
Latitude: -26.775 **Longitude:** -48.992
Site description: narrow channel, with multiple boulders and cobbles on the channel. Redish sediment.

BRA-43

Field Area: Santa Catarina, Brazil
Collection Date: May 2012
Latitude: -26.779 **Longitude**: -48.993
Site description: Narrow, boulder dominated channel. Some vegetation on both sides (vines). We sampled under a bridge.

BRA-44

Field Area: Santa Catarina, Brazil
Collection Date: May 2012
Latitude: -26.881 **Longitude:** -49.099
Site description: Wide channel, with fine sands on the shore and river bed

BRA-45

Field Area: Santa Catarina, Brazil
Collection Date: May 2012
Latitude: -27.061 **Longitude:** -49.527
Site description: Wide, deep channel, with many large boulders. Sand is buried under boulders.

BRA-46

Field Area: Santa Catarina, Brazil
Collection Date: May 2012
Latitude: -27.080 **Longitude:** -49.498
Site description: Wide, rocky boulder. Low water flow. Sample taken on the right bank of the river.

BRA-47

Field Area: Santa Catarina, Brazil
Collection Date: May 2012
Latitude: -27.334 **Longitude:** -49.620
Site description: Sample taken at the left bank, by the collapsed bridge, not from the active channel.

Appendix 4 – China Sample catalog

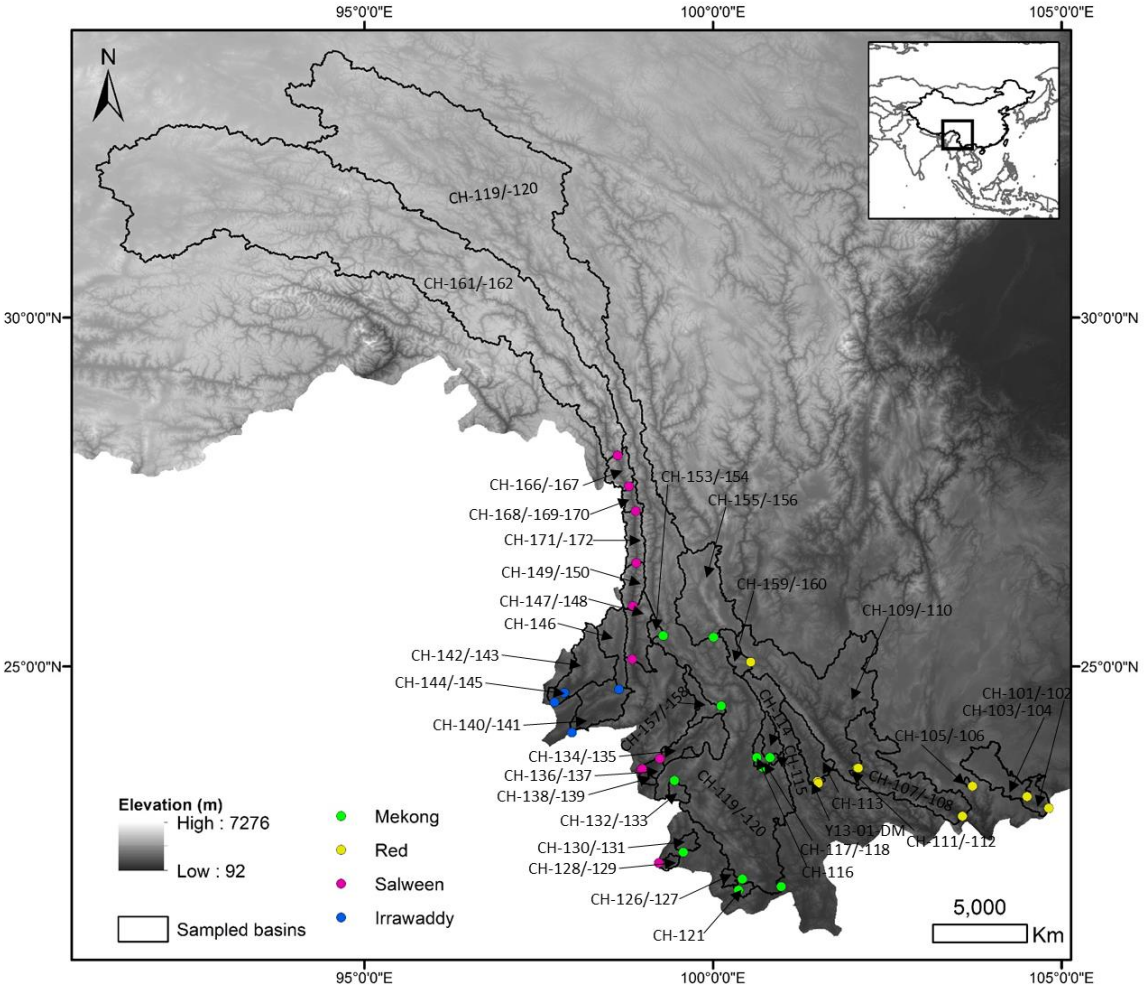

CH-101 (IC)/-102 (OB)

Field Area: Yunnan, China
Collection Date: 1/5/2014
Latitude: 22.969 **Longitude:** 104.818
Site description: Station 91, in channel/overbank. Wide channel upstream of station, downstream of sand mining, but sample from river sediments. Banana plantations, but generally low agriculture in watershed. Cement factories in the headwaters.

CH-103 (IC)/-104(OB)
Field Area: Yunnan, China
Collection Date: 1/5/2014
Latitude: 23.134 **Longitude:** 104.507
Site description: Station 90, in channel/overbank. 2 dams upstream of sampling site. Not sure if more down. Deep gorge. Mostly limestone, bedrock at sample site surrounded by terraced. Sample on right bank. Downstream of station but we didn't see station.

CH-105 (IC)/-106 (OB)

Field Area: Yunnan, China
Collection Date: 1/6/2014
Latitude: 23.284 **Longitude:** 103.724
Site description: Station 108, in channel/overbank. Sample taken under bridge. Tiny check dam at bridge. Fast flowing channel. Unsorted sediments. About 1 km upstream of sampling site, there is cement block manufacturing off the river (we don't know if there is mining on the river). There is also limestone mining off the side of the mountain on the right bank, about 1 km upstream of the sample site.

CH-107 (IC)/-108 (OB)

Field Area: Yunnan, China
Collection Date: 1/7/2014
Latitude: 22.852 **Longitude:** 103.580

Site description: Station 106 in channel/overbank. Downstream of tributary, steep slopes on both sides of the river, with agriculture going to the base of mountain (just about 50m above river, there are tree plantations). Samples taken at a sand bar in the river that has been mined (or is currently being mined?)

CH-109 (IC)/-110 (OB)

Field Area: Yunnan, China
Collection Date: 1/8/2014
Latitude: 23.547 **Longitude:** 102.073
Site description: Station 103 in channel/overbank. Steep slopes on both sides of the river, banana plantation all the way to the river on the left bank, mostly brushes and bar land on the right bank. About 5 km upstream there is a big mining operation in the river. Sample taken higher upstream than GIS point (there may be a tributary coming in, before guessed location of station).

CH-111 (IC)/-112 (OB)

Field Area: Yunnan, China
Collection Date: 1/8/2014
Latitude: 23.545 **Longitude:** 102.086
Site description: 2 km downstream of previous sample (below confluence with tributary). Wide deep channel. Wide floodplain on both banks, and steep slopes on the mountains around. Up above on road cut there is big fluvial material with layers of laminated fine material above, possible dam existed here? Angular limestone gravel, everything else sub-rounded. Sample taken at tributary delta, there is no water coming out, delta is forested (about 40 year old trees). Deep seated landslides upstream of sampling spot. Debris-flow (old one) stops at the floodplain (tall vegetation) growing on it, so not recent. The tributary hasn't entered the river at another point in a while. It doesn't cross river elsewhere and delta is forested.

CH-113 (IC)

Field Area: Yunnan, China
Collection Date: 1/8/2014
Latitude: 23.352 **Longitude:** 101.502
Site description: Station 87, in channel. Gravel mining site. Sample taken late at night, no pictures of the site. Collected a bulk sample to be lab-sieved. No over bank sample.

CH-114 (IC)

Field Area: Yunnan, China
Collection Date: 1/9/2014
Latitude: 23.700 **Longitude:** 100.816
Site description: Resample CH-056. Attempted to resample CH-057 but terrace was totally eroded away, interesting. Immediately downstream of a bridge, of on point bars upstream. Left bank: sand and boulders. Agriculture on the left bank, road and forested low on right bank, bananas higher.

CH-115 (IC)

Field Area: Yunnan, China
Collection Date: 1/9/2014
Latitude: 23.694 **Longitude:** 100.818
Site description: Resample of CH-058. Downstream of gravel mining and junction of two tributaries. We are upstream of CH-058, but nothing comes in.

CH-116 (IC)

Field Area: Yunnan, China
Collection Date: 1/9/2014
Latitude: 23.696 **Longitude:** 100.630
Site description: Resample of CH-043 (a bit downstream of previous GIS point). Headwater of the west branch. Floodplain on both sides along forested slopes.

CH-117 (IC)/-118 (OB)

Field Area: Yunnan, China
Collection Date: 1/9/2014
Latitude: 23.557 **Longitude:** 100.710
Site description: Resample of CH-060 and CH-044. Left bank: ag field with sugar cane. Gravel/sand mining both up and downstream, wide channel with steep slope to the right

CH-119 (IC)/-120 (OB)

Field Area: Yunnan, China
Collection Date: 1/10/2014
Latitude: 21.846 **Longitude:** 100.980
Site description: Resample of CH-073 and CH-074. Wide channel with big floodplains, samples collected at right bank. Agriculture field. Jetties structures immediately upstream. Outlet suspected, hydrostation 2 km upstream

CH-121 (IC)

Field Area: Yunnan, China
Collection Date: 1/11/2014
Latitude: 21.794 **Longitude:** 100.366
Site description: Resample of CH-070. High water level (higher than base flow) but low. Large crystalline boulders on the river. Headwater stream. Left side of the bank has agricultural fields right next to river (about 1/2 meter above the water), forested river

banks. Moderate slopes around river (not too steep), micas (lots of), sample taken on right bank, water relatively low (dry season)

CH-122 (IC)
Field Area: Yunnan, China
Collection Date: 1/11/2014
Latitude: 21.794 **Longitude:** 100.366
Site description: Resample of CH-071. Downstream of a factory (sugar cane processing?), left bank dips into river at slight angle, small fields on the bank (~10 ft above the water), left bank is incised (cuts through) in a terrace. Sugar cane plantations on right bank (ranges from 5 to about 15 feet above the river)

CH-123/-124/-125
Field Area: Yunnan, China
Collection Date: 1/11/2014
Latitude: 21.942 **Longitude:** 100.341
Site description: Terrace on the side of the river (right bank) where CH-122 was collected. Terrace is under the sugar cane field, and goes up to about 3 or 4 meters above the river. CH-123 and 124 have sand for insitu, CH-125 is just the charcoal, no insitu. Sand at bottom (charcoal extracted from there) from bottom: coarse sand, reduced gray clay (also has charcoal). Reduced gray interbedded with med. sand, small pack of gray clay, mid-size sand, then gravel, then clay above.

CH-126 (OB)/-127 (IC)

Field Area: Yunnan, China
Collection Date: 1/11/2014
Latitude: 21.952 **Longitude:** 100.421
Site description: Resample of CH-075 and CH-076. Wide channel (turbid water). Sample taken on left bank. Mostly flat area surrounding agricultural fields (chinese greens, onions, lettuce) on the elf bank all the way to the river (about 20 feet above the fields), right bank is steep and right against the wall of a bus station and houses.

CH-128 (OB)/-129 (IC)

Field Area: Yunnan, China
Collection Date: 1/12/2014
Latitude: 22.184 **Longitude:** 99.222
Site description: Station 109 in channel/overbank. Upstream of town. Not sure where station is. Left bank of channel, upstream of bridge, forested hillslopes (maybe

plantations-rubber?) very close to Myanmar border. Unsorted sediments (very fine mud to boulders (rounded). Upstream channel seems too big for river.

CH-130 (OB)/-131 (IC)

Field Area: Yunnan, China
Collection Date: 1/12/2014
Latitude: 22.337 **Longitude:** 99.575
Site description: Station 94 in channel/overbank. Station is downstream of us in town, just upstream of bridge. Totally channelized river with small dam. We are on a point bar below retaining wall/rip rap. Forested park on right bank, road on left bank. Sample on left bank. Bedrock outcrops upstream and downstream. Channelization ends just upstream of us and our sample. Channel is bedrock and forested slopes upstream.

CH-132 (OB)/-133 (IC)

Field Area: Yunnan, China

Collection Date: 1/13/2014
Latitude: 23.365 **Longitude:** 99.447
Site description: Station 32 in channel/overbank. Sample taken at a gravel mining operation, but there are laminations in the sediment close to the river. We are pretty certain that it's overbank and not material falling from mining, and debris above it. Downstream of a big factory (we don't know what kind), moderate slopes around the channel, the right bank comes into the channel at steep angle, and it is mostly planted with sugar cane, left bank is the mining operation.

CH-134 (OB)/-135 (IC)
Field Area: Yunnan, China
Collection Date: 1/13/2014
Latitude: 23.677 **Longitude:** 99.237
Site description: Station 93 in channel/overbank. Sample taken at hydrostation but GPS says we are 1 hr away from our sampling site. Wide channel (about 150 m wide) with a mid-channel bar about 20 m wide and another one 10 m wide next to the right bank, sample taken at left. Station may not be operating? Water flow is low. Steep slopes around us, right bank looks forested with some small fields on bank. River is incising both banks.

CH-136 (OB)/-137 (IC)

Field Area: Yunnan, China
Collection Date: 1/13/2014
Latitude: 23.526 **Longitude:** 98.971
Site description: We collected two bulk samples for overbank and two for in-channel. Sample collected at the river and overbank at the bottom of a mining operation, there is a part that looks like it is river deposits and not mining, there is debris on it. Sample taken below junction of a tributary with the main stem of river.

.

CH-138/-139

Field Area: Yunnan, China
Collection Date: 1/13/2014
Latitude: 23.531 **Longitude:** 98.988
Site description: Sample taken after sunset, too dark to sieve or take notes. Two bulk samples collected for overbank and two for in-channel. Sample collected at main stem before junction with tributary (see previous sampling spot). There are agricultural fields on the floodplain (as far as we could see driving by earlier, and with moonlight)

CH-140 (OB)/-141 (IC)

Field Area: Yunnan, China
Collection Date: 1/14/2014
Latitude: 24.052 **Longitude:** 97.975
Site description: Station 99 in channel/overbank. 20 km upstream of projected point. Left bank of the river. Immediately adjacent to a gigantic sand mining factory, unclear

whether our collected sample is contaminated by the factory sand pile. Right bank looks vegetated, with clumps of sugar cane plot.

CH-142 (OB)/-143 (IC)

Field Area: Yunnan, China
Collection Date: 1/15/2014
Latitude: 24.487 **Longitude:** 97.726
Site description: Station 85 in channel/overbank. Wide calm channel, about 700m wide, high quartz content on sandbars, samples collected at left bank, upstream of a dam. Wide, flat floodplains, extending at least 50 m. Left bank vegetated; along the track were some boulder-sized angular metamorphic rocks (carbonate and igneous in origin), right bank looks vegetated in part, mostly terraced.

CH-144 (OB)/-145 (IC)

Field Area: Yunnan, China
Collection Date: 1/15/2014
Latitude: 24.622 **Longitude:** 97.868
Site description: Station 84 in channel/overbank. Extremely wide and braided channel, samples at left bank. Right bank has field burning when we were sampling, left bank is barren, show signs of tillage and possibly burned as well. 20km upstream of previous site.

CH-146 (OB)

Field Area: Yunnan, China
Collection Date: 1/16/2014
Latitude: 24.671 **Longitude:** 98.651
Site description: Station 100 overbank. Sample taken at the hydrostation. We think it may still be in use. Looks a bit run down but someone made a path through the gravelly

point bar to the river along all the stage markers. Maybe just stage in off season? Sample directly under old (2012-12-05 out of use) bridge. At head of reservoir would probably be submerged in rainy season and just downstream of another dam. This is the same river as we sampled in Ruili. Left bank sample 200m wide channel (active) but only about 50m wetted. Cannot get an in channel sample because no sand accessible. Upstream river is calmer but pool is really deep.

CH-147 (IC)/-148 (OB)

Field Area: Yunnan, China
Collection Date: 1/16/2014
Latitude: 25.102 **Longitude:** 98.839
Site description: Station 15 inchannel/overbank. Right bank on fine sandy beach. Downslope of reinforcements to protect road, but beach clearly river deposits. Deep river but not fast flowing. Alluvial fan coming in across channel. Boulders on that side of channel likely from fan, not from channel. River sand goes all the way to the bottom of the concrete wall (around the big rocks). Couldn't sieve anything coarse for 500-850 or 250-850 in channel or 500-850 overbank. Note:

CH-149 (OB)/-150 (IC)

Field Area: Yunnan, China
Collection Date:
Latitude: 25.866 **Longitude:** 98.850
Site description: Just bulk sample collected at mining site. Sampling after sunset, dark out, no site pictures Overbank (CH-149) collected from sand imbricated with rocks. In-channel (CH-150) sample (bulk) collected from sand mine called "river sand"

CH-153 (IC)/-154 (OB)

Field Area: Yunnan, China
Collection Date: 1/17/2014
Latitude: 25.441 **Longitude:** 99.286
Site description: TRR 14b resample in channel/overbank. Resample of TRR 14b, a tributary that joins Mekong River. Nasty brown/tan colored river, big boulders in the channel. Active mining immediately downstream. Samples (bulk) taken at left bank. Steep slope at right bank (forested). Right by a highway.

CH-155 (IC)/-156 (OB)

Field Area: Yunnan, China
Collection Date:
Latitude: 25.418 **Longitude:** 100.007
Site description: Station 86 in channel/overbank. Narrow steep valley. Lots of limestone on drive in. Downslope of dam, upstream of station. Dam releases irregularly. Sample from bottom of dirt road at a gravel/sand mine. Confident in overbank not recycled because below trimline for dam releases. Right bank across from dry tributary/small fan
No site pictures

CH-157 (IC)/-158 (OB)

Field Area: Yunnan, China
Collection Date: 1/18/2014
Latitude: 24.434 **Longitude:** 100.118
Site description: Station 97 in channel/overbank. Right bank, overbank collected at a clean quartz sandy pile. **Speculate that it's from mining upstream (in channel) and deposited last monsoon. A ton of mining upstream and downstream, and construction. Turbid slow flowing river. Entire stretch is channelized.

CH-159 (IC)/-160 (OB)

Field Area: Yunnan, China
Collection Date:
Latitude: 25.064 **Longitude:** 100.541
Site description: Station 101 in channel/overbank. Late at night. Downstream of town. Right bank 2+bulk in overbank. Gravel mine, construction zone. Seems convincingly overbank/in channel.
No site pictures

CH-161 (IC)/-162 (OB)

Field Area: Yunnan, China
Collection Date: 1/20/2014
Latitude: 28.026 **Longitude:** 98.632
Site description: Resample TRR 9 in channel/overbank. 3+bulk bags. Beautiful site upstream of town and very minor tributaries (dry?) Sand mine from point bar. Right bank. Pretty sedimentary structures in overbank sand.

CH-166 (OB)/-167 (IC)

Field Area: Yunnan, China
Collection Date: 1/20/2014
Latitude: 27.583 **Longitude:** 98.793
Site description: Resample TRR 10 in channel/overbank. Bulk only. Probably same spot as TRR 10. Right bank. Big channel. Bedrock. Low quartz content. Fine sands.

CH-168/-169/-170

Field Area: Yunnan, China
Collection Date: 1/20/2014
Latitude: 27.228 **Longitude:** 98.892
Site description: Resample TRR11a (tributary) in channel. Resample TRR11b in channel/overbank. CH-168 tiny tributary into Salween. Teeny tiny. CH-169, 170 are in main stream downstream of tributary. Sample at sand mine (small). Mining sand bar. Left bank sample at spot with road to river. Valley a little broader, no bedrock along channel. Agriculture close to channel but not high up. Tributary sampled in channel only CH-168.

CH-171/-172

Field Area: Yunnan, China
Collection Date:
Latitude: 26.483 **Longitude:** 98.898
Site description: TRR 12 resample. No pictures because we were sampling in the dark. Nice sandy beach, downhill of a construction pile of sand but collected samples are definitely not from the construction. Downstream of a bridge. The overbank sample is a resample of TRR12.